Mulugeta Genanu

"BUILDING ETHIOPIA'S WATER FUTURE TOGETHER"

Addis Ababa University

P.O.Box 1176, Addis Ababa, Ethiopia
T +251-11-1239 768
F +251-11-1239 752
I www.aau.edu.et

Ethiopian Institute of Water Resources

P.O.Box 150461, Addis Ababa, Ethiopia
T +251-11-1223 344
F +251-11-1239 480
E info@eiwr.org
I www.eiwr.org

MSc Thesis on: Remote Sensing Based Estimation of Evapo-Transpiration Using Selected Algorithms; the Case of Wonji Shoa Sugar Cane Estate

Prepared By:

Mulugeta Genanu Kebede

Supervised By:

Tena Alamirew (Ph.D), EIWR (AAU), Ethiopia
Gabriel Senay (Ph.D), USGS, USA
Mekonnen Gebremichael (Ph.D), University of Connecticut, USA

Submitted on:

June, 2013
Addis Ababa, Ethiopia.

ABSTRACT

The goal of every grower is to practice irrigation management to fulfill water needs profitably, safely, and in an environmentally responsible way. For this, accurate knowledge of the amount of evapotranspiration (ET) is critical. The focus of this study was to estimate and compare the actual evapotranspiration (ET_a) of the Wonji Shoa Sugarcane Estate using different remote sensing algorithms. The daily ET_a of the sugarcane was estimated and thematically mapped pixel-by-pixel using Surface Energy Balance Algorithm for Land (SEBAL), Simplified Surface Energy Balance (SSEB) and Operational Simplified Surface Energy Balance ($SSEB_{op}$) algorithms on Landsat7 ETM+ and MODIS images acquired on four days in 2002. The algorithms were based on image processing which uses spatially distributed spectral satellite data (visible, near infrared and thermal infrared) and ground meteorological data to derive the surface energy balance components. The results obtained revealed that the ranges of the daily ET_a estimated on January 25, February 26, September 06 and October 08, 2002 using SEBAL were 0.0 - 6.85, 0.0 – 9.36, 0.0 – 3.61, 0.0 – 6.83 mm/day; using SSEB 0.0 - 6.78, 0.0 – 7.81, 0.0 – 3.65, 0.0 – 6.46 mm/day, and $SSEB_{op}$ were 0.05 - 8.25, 0.0 – 8.82, 0.2 – 4.0, 0.0 – 7.40 mm/day, respectively. The Root Mean Square Error (RMSE) values between SSEB and SEBAL, $SSEB_{op}$ and SEBAL, and SSEB and SSEBop were 0.548, 0.548, and 0.99 for January 25, 2002; 0.739, 0.753, and 0.994 for February 26, 2002;0.847, 0.846, and 0.999 for September 06, 2002; 0.573, 0.573, and 1.00 for October 08, 2002, respectively. The standard deviation of ET_a over the sugarcane estate showed high spatio-temporal variability perhaps due to soil moisture variability and surface cover. Dry periods exhibit greater variability compared to wetter periods. Generally during the dry season, ET is limited to the well watered sugarcane fields and water storage areas only. During the peak rainy season, ET_a was high throughout the entire sugarcane estate. All the three algorithm results showed that generally well watered sugarcane fields in the mid-season growing stage of the crop and water storage areas had higher ET_a values compared with the other dry agricultural fields confirming that they consumptively use more water. The evaporation fraction (ET_rF) results also followed the same pattern as the daily ET_a over the sugarcane estate. Comparison of ET_a obtained from the MODIS Product (MOD16) with those obtained from the Landsat based algorithms resulted in a very poor correlation. The total crop and irrigation water requirement and effective rainfall estimated using the Cropwat model were 2468.8, 2061.6 and 423.8 mm/yr for January 2001 planted and 2281.9, 1851.0 and 437.8 mm/yr for March 2001planted sugarcanes, respectively. The mean annual ET_a estimated for the whole estate were 107 Mm^3, 140 Mm^3, 178 Mm^3 and 80 Mm^3 using SEBAL, SSEB, $SSEB_{op}$ and MOD16, respectively. Though the algorithms need to be validated through field observation, either of these algorithms tested in this study have potential to be used for effective irrigation water management.

Key Words: CWR, ET, IR, Landsat ETM+, MODIS, Remote Sensing, SEBAL, SSEB, $SSEB_{op}$

ACKNOWLEDGEMENT

The study was supported by the United States Agency for International Development (USAID) under the Africa-US Higher Education Initiative - HED052-9740-ETH-11-01. The author wishes to express his gratitude for the opportunity.

I am greatly indebted to my advisors Dr. Tena Alamirew, Dr. Gabriel Senay, and Dr. Mekonnen G/ Michael for their guidance and valuable comments from the preparation of the concept until the compilation of this thesis. I also thank Prof. Junming Wang for his useful comments during the thesis preparation.

I thankfully acknowledge Ethiopian Institute of Water Resources (EIWR) community for all the support I have been enjoying. I would like to express my sincere gratitude to Wonji Research and Training Center community for the support during field work.

I would like to express my deepest appreciation to my beloved mother W/ro Ateref Simegnew, my brothers and sisters, uncles and aunts for being the source of inspiration in my life. Last, but not least, I would like to extend my special and profound gratitude to my beloved uncle Ato Dinku Kebede and his family who have been very supportive since right from the start of my childhood.

DEDICATION

This thesis is dedicated to my late father and my Uncles who could not witness this achievement and event, yet always encouraged me for higher studies.

Table of Contents

List of Figures

LIST of TABLES

List of Appendix

1. INTRODUCTION

1.1 Background to the Study

Water is one of the most important limited natural resources crucial for all socio-economic and environmental needs to be managed in a sustainable way to ensure its long-term availability. Judicious management of precious land and water resources is emerging as one of the biggest challenges of the 21st century. Both water and land resources are finite, but competitive demand from other sectors is increasing. Managing water for multiple benefits and between competing demands is occupying the minds of irrigators, catchment water managers and policy-makers. Agriculture is by far the largest water user sector, accounting for about 70% of all water withdrawn worldwide from rivers and aquifers compared to the industry (20%) and municipality (10%) (CAWMA, 2007). The goal of every grower is to practice irrigation management to fulfill water needs profitably, safely, and in an environmentally responsible way. Irrigation depends on reliable supplies of fresh, clean water from surface and/or groundwater sources. Knowing how much water moves through soils and crop canopy can help growers use irrigation water more effectively with less risk to water sources.

In several developing countries, irrigation represents up to 95% of all water withdrawn, and it plays a major role in food production and food security. The use of this irrigation water plays a major role in increasing land productivity. Globally, about 40% of agricultural outputs and 60% of grain production is produced from irrigated areas which together make up only 20% of the total arable land. While irrigation has greatly increased global and regional food security, further rapid increases in agricultural production will be required to meet future food and fiber demands. This goal can be achieved either by bringing more area under irrigation or by increasing the yields of existing cropped area whilst using similar or even reduced water resources.

Efficient water use is the key for sustainable management of water resources. The major reason for non-efficient management of water resources, especially in developing countries, is non-availability of reliable hydrological information about the actual water used by different agricultural crops with in a large irrigation system or at the basin scale. Since water resources

management strategies are usually formulated on basin scale, understanding of the hydrological processes at this scale is a pre-requisite for implementation of these strategies. Increasing pressure on water resources requires a sound knowledge of where, when and how much water is used.

Irrigation is important for strengthening local and regional economy and for enhancing food security. The rate of increase in irrigated land reached a peak of about 2.2% per year in the mid-1970s which was directly related to massive investments by international financing institutions, like World Bank (Jensen, 2007), but the annual rate of increase has decreased since the mid-1990s to less than 0.5% per year at the beginning of the 21st century. This reduction has largely been the result of diminishing water supplies and increased demands from other sectors (Hoffman and Evans, 2007). In the 20th century, worldwide irrigated area experienced a huge expansion of more than 500% with an increasing from 40 million to 270 million ha of irrigated land (de Oliveira et al., 2009). Such numbers are part of the ability of humankind to produce food fast enough to meet population growth. But that remarkable ability, on the other hand, has its cost – a water crisis, characterized by water scarcity and competition, pollution and malnutrition (Molden, 2003).

Three basic approaches (supply side, conservation, and unit productivity) were pointed out by Molden (2003) to increase food production. The 'supply side' approach suggests the development of more infrastructures and more rain-fed and irrigated land to supply more water for more agriculture. The "conservation" approach establishes the importance on reducing wastage and loss of water by agriculture; and the "unit productivity" calls for increasing in the productivity of water for each drop consumed by agriculture.

The agriculture development strategies of most of the developing countries depend on the possibility of maintaining, improving and expanding irrigated agriculture (Siebert *et al.*, 2006). However, as the pressure on water resources increases, irrigation is facing growing competition from other water-use sectors and becoming a threat to the environment in an increasing number of regions. The challenges in the promotion of irrigation development, water management and water use uniformity are not easy. The nature of farmland distribution, the soil characteristics and topography are different on the potentially irrigated lands and this unable to manage properly

with the water requirement of the irrigation system which require accurate determination of remote sensing based water requirement of each crop on the farmland for appropriate water supply.

Despite the current problems and negative perceptions in many sectors of society (Hoffman and Evans, 2007), it is certain that irrigation will continue to be a necessary and important component of the world's well-being and growth. All these issues call for the implementation of sustainable irrigation in order to preserve the environment while keeping the actual levels of food production. On this, Oster and Wichelns (2003) defined sustainability as the likelihood that an irrigation system will continue to generate desirable outputs and amenities at reasonable costs in future. They pointed out that in order to reach sustainability, irrigation and drainage systems should be managed in a manner that does not degrade the quality of land, water, and other natural resources that contribute to agricultural production and environmental quality.

To make irrigation sustainable, both environmentally and economically, society will need to improve agricultural productivity, change institutional structures, modify water policies, improve delivery and on-farm systems, improve management of degraded soils, enhance water reuse, improve crop water management, and address rising energy prices (Howell, 2001; Hoffman and Evans, 2007). Integrated water management including sustainable use of irrigation water requires understanding the hydrological relationships at different scales.

Among the total population in Ethiopia, about 83.83 % lives in the rural areas depending on subsistence agriculture. Though agriculture is the dominant sector, most of Ethiopia's cultivated land is under rain-fed agriculture. Due to lack of water storage and large spatial and temporal variations in rainfall, there is no enough water for most farmers to produce more than one crop per year and hence there are frequent crop failures due to dry spells and droughts which have resulted in a chronic food shortage currently facing the country (Awulachew et al. 2005). Ethiopia has an area of 3.7 Mha potential irrigable land and only 11% (289,530 ha) of this potential irrigable land is water managed (Awulachew et al. 2007). Irrigation was an old age practice and continued to date with minimal scientific input in most parts of the country for crop production in arid and semi-arid regions where annual evapotranspiration exceeds precipitation. Efforts are being made to involve farmers progressively in various aspects of management of

small to large scale irrigation systems, starting from planning, implementation and management aspects, particularly, in water distribution and operation and maintenance to improve the performance of irrigated agriculture.

Most large-scale irrigation systems are located in the arid and semi-arid regions of the world, and water is one of the most limiting factors in increasing agricultural production (Seckler, 1996; Thenkabail et al., 2006). Therefore, further expansion in irrigated area is often limited by water availability. Thus it is important to find ways to increase agricultural production by careful evaluation of existing irrigated lands. This strategy will not only help to meet future food demands but may also ease competition with other sectors and help to ensure water availability for nature (Hamdy *et al.*, 2003). Irrigation policy makers and managers need information on the crop water consumption, irrigation performance and productivity of water at various scales to devise appropriate water management strategies, in particular considering dwindling water availability, further threats from climate change, and continually rising population and food demand. In practice it is often difficult to access sufficient water supply and use data to determine crop water consumption and irrigation performance.

Therefore, a better management of water in irrigated agriculture is necessary to enhance crop production and preserve soil and water quality. Irrigation management should focus in the adoption of practices that enhance the efficient use of water so that other sectors can have more water for economic use (CAWMA, 2007). On this, Howell (2001) suggested three paths that can be taken to improve water use efficiency on irrigated agriculture: (a) increase the output per unit of water; (b) reduce loss of water to unusable sinks and reduce water degradation; and (c) reallocate water to higher priority uses.

As stated by Hemukamara *et al*. (2003), ET which is a process governed by the energy and heat exchanges at the land surface, with the upper bound being constrained and controlled by the amount of available energy and water respectively is also an important factor for evaluating water productivity and monitoring of irrigation performance. Therefore, an estimation of spatially distributed crop water consumption is challenging, but important to determine water balance at different scales to promote efficient management of water resources. Evapotranspiration from irrigated agriculture is an important issue in arid and semi-arid regions

where it has large impact on water resources depletion and water management (Tasumi and Allen, 2007). Accurate determination of crop ET is essential for designing irrigation systems and for irrigation scheduling. Remote sensing data can resolve difficulties in determining water balance due to scientific developments in the calculation of spatially distributed actual evapotranspiration. The use of remote sensing techniques to estimate evaporation is achieved by solving the energy balance of thermodynamics fluxes at the surface of the earth and it is used for calculating the actual evapotranspiration (ET_a) based on the equilibrium between the radiation balance and the energy balance at the surface of the earth.

1.2 Statement of the Problem

The present challenge for irrigated agriculture is to improve food security through more efficient and effective use of water. Sugarcane, as the commercial crop, is expanding in Ethiopia. The consumptive use of water by crops ET_a is only part of the total irrigation water supply from a river diversion or a reservoir. Measuring the evapotranspiration is of highest importance for understanding and eventually intervening into the water cycle of natural systems, especially different critical users of water, like irrigated areas and their field crops. Understanding the amount of evaporation from water supply reservoirs and other storages is an important part of the water resource management. Accurate estimation of evapotranspiration (ET) plays an important role in quantification of the water balance at the pixel, watershed, basin and regional scale for better planning and managing water resources. Estimates of land surface evapotranspiration (ET) using remote sensing data are essential in effective planning of irrigation water use in arid and semiarid regions. It is very essential for the water managers and irrigation engineers to know the accurate ET estimations.

Satellite based measurements used in association with energy balance models can provide the spatial distribution of ET and used to derive maps of actual evapotranspiration (ET_a) with reasonable accuracy. Surface Energy Balance Algorithm for Land (SEBAL), Simplified Surface Energy Balance (SSEB) and operational Simplified Surface Energy Balance ($SSEB_{op}$) are robust remote sensing models which uses spectral radiances recorded by Landsat-7 ETM+ or other thermal infrared satellite images, plus routine weather data, to solve the energy balance at the earth's surface. Remote sensing models can generate spatial coverage of water use uniformity

and integration for different crops within agricultural areas and for various land types within river basins. This enables assessment of irrigation management practices within and among fields and improves the degree of confidence in development and interpretation of water balances at various spatial scales and identifying pumping units that lift insufficient water for potential growth of crops and identification of non-uniformity in water availability. This provides appropriate supply of irrigation water for the field based on the water requirement of the crop.

The dynamic interaction between ET and soil moisture, the loss of water in the form of ET, and the performance gap in the study area need to be diagnosed and determined to provide suitable and sustainable water management practice in the sugarcane plantation. As a result it is very important to study the loss of water in the form of ET and understand its relation with the soil water storage change in the root zone for proper and sustainable use of water for the crop growth and better yield production. The remote sensing technology application is being tested in Ethiopia, but it has rarely been applied to support crop ET, soil moisture and irrigation management practices because of the associated costs and quality of images.

There are many remote sensing algorithms for an estimation of spatially distributed actual evapotranspiration and each algorithm has its own merits and demerits. However, a review of different ET mapping algorithms shows that most Energy Balance (EB) models are complex to use and may not be suitable for operational ET remote sensing (Gowda et al., 2008). Efforts are being made to simplify procedures to estimate regional ET mainly through the scaling of reference ET. The Simplified Surface Energy Balance (SSEB) is one such method and also the Surface Energy Balance Algorithm for Land (SEBAL) is the other most promising algorithm with the minimum input of ground based variables and it has been widely applied in many countries of the world due to accurate estimation of actual evapotranspiration (Hafeez and Khan, 2002).

Hence, the general aim of this study is to produce ET_a estimates and to address some issues related to the management of irrigation water using the combination of SEBAL, SSEB and $SSEB_{op}$ algorithms with representative ground meteorological data and remotely-sensed

Landsat7 ETM+ and MODIS imagery and reference ET over Wonji Shoa irrigated sugarcane plantation.

1.3 Research Questions

The study had the following research questions.

- Can we estimate actual evapotranspiration of sugarcane using Surface Energy Balance Algorithm for Land (SEBAL), Simplified Surface Energy Balance (SSEB) and operational Simplified Surface Energy Balance ($SSEB_{op}$)?
- Which Energy Balance (EB) algorithm, (Surface Energy Balance Algorithm for Land (SEBAL) or Simplified Surface Energy Balance (SSEB)) or operational Simplified Surface Energy Balance ($SSEB_{op}$) best estimates ET for the sugarcane plantation?
- Can we accurately estimate the crop water requirement of the sugarcane plantation by using the estimated evapotranspiration at estate level?

1.4 Objective of the Study

This study had the following main objectives.

- To estimate actual ET using Surface Energy Balance Algorithm for Land (SEBAL), Simplified Surface Energy Balance (SSEB), Operational Simplified Surface Energy Balance (SSEBop); and Penman-Monteith Methods;
- To compare the actual ET results of Surface Energy Balance Algorithm for Land (SEBAL), Operational Simplified Surface Energy Balance (SSEBop) and Simplified Surface Energy Balance (SSEB) in the sugarcane estate; and
- To calculate the crop water requirement of the sugarcane plantation at the estate level

2. LITERATURE REVIEW

2.1 Theoretical Background of Evapotranspiration

Water molecules continually exchange between liquid and vapor phases by a process known as evaporation. In this process liquid water is converted into water vapor and removed from evaporating surface (Shaw 1994, Chow 1998). Water can be evaporated from a variety of surface such as water body (lakes), bare soil or soil covered with vegetation, agricultural field, forest and impervious surface. From water bodies (lakes and rivers) evaporation takes place continually and hence there is continual loss of water. Evaporation is a function of climate factors. When water evaporates from vegetation through leaves, it is called transpiration. This process also includes evaporation of rain water intercepted by vegetation. Vegetations continually pump water from the ground into the atmosphere and the rate varies depending on the type of vegetation. Transpiration is related to draws of water stored in soil pores at depth and is a function of land cover and vegetation. Practically, it is hard to differentiate between evaporation and transpiration when the ground is covered by dense vegetation because these processes occur simultaneously. Because of this, these two processes are collectively termed as evapotranspiration.

The change of state of the molecules of water from liquid to vapor requires energy input, called latent heat of vaporization. Solar radiation and the ambient temperature of the air provide this energy. The difference between vapor pressure at the evaporative surface and surrounding atmosphere is the main cause of vapor removal from evaporative surface. When water passes from liquid to vapor state, it absorbs about 590 calories of heat per gram of water from evaporative surface. Some factors affecting evapotranspiration are as follows (Maidment, 2002, 1993):

1) Solar radiation: the energy input responsible for conversion of water into vapor.
2) Wind: important factor controlling evapotranspiration which governs ability to transport vapor away from the surface.
3) Relative humidity (vapor pressure gradient): determines the ability of the air to absorb water. As humidity rises, its ability to absorb water decreases and rate of evaporation slows.
4) Temperature: evaporation proceeds if the ambient air and ground temperature is high.
5) Soil water content and its ability to conduct water;

6) Cultivation practice and extent of vegetation;
7) Environmental aspect and management;

Evapotranspiration can be actual or potential. Potential evapotranspiration refers to the rate at which evaporation occurs from an area completely and uniformly covered with short green crops containing surplus water. It depends on several surface characteristics: surface albedo which determines the net radiation, maximum leaf conductance, atmospheric conductance and presence of intercepted water as defined by Penman (Shaw 1994). Actual evapotranspiration is the loss of water dependent upon available soil moisture or water.

2.2 Estimation of Evapotranspiration

Evapotranspiration is an important parameter in water resource studies. Its accurate estimation is vital, because the difference between precipitation and evaporation determines aquifer recharge and water use. It is difficult, however, to accurately quantify evapotranspiration directly. There are multiple methods for estimating evapotranspiration for a drainage basin. The most widely used methods can be grouped into three categories, field in-situ measurement, modeling approach and remote sensing technique (Bastiaanssen et al., 2005). The methodological approaches are briefly discussed below.

In-situ measurement: most field measurements of evapotranspiration are indirect involving measuring of other water and energy balance components mostly using lysimeter, Bowen ratio and Eddy correlation methods. However, these techniques are subjected to series of errors such as measurement error, when the process is not fully understood or when too many simplifications and approximations are made and errors related to spatial and temporal variability over a landscape (Twine et al. 2000, Allen et al. 1991 as cited in Basitiaanssen 2005). For example, performance of lysimeter strongly depends on the precision of instrument installation and on the representation of the surrounding vegetation and soil moisture content. Most direct measurements of water and energy balance components often provide only point/localized phenomena and do not integrate spatial and temporal variability.

Modeling approach: Hydrological models are simplification and abstraction of known or assumed functions expressing the various components of a hydrologic cycle. They are a powerful tool for water resources studies. Spatially distributed hydrological models such as SWAT (Arnold et al., 1998) have been used to simulate hydrological parameters including runoff, interception, evapotranspiration, infiltration and climate change, over a drainage basin (Neilson, 1995; Najjar, 1999 as described in Mendoza et al., 2002). Therefore, evapotranspiration can be estimated and its relation can be assessed with respect to other relevant variables such as precipitation, infiltration and soil moisture.

Remote sensing technique: Remote sensing is, as defined and discussed by Sabins (1987), and Lillesand and Kiefer (1994), " the science and art of obtaining information about an object, area or phenomena through the analysis of data acquired by sensor that is not in direct contact with the target of investigation". Remote sensing is used for monitoring hydrological state variables and as a basis for parameter estimation in hydrological models (e.g., Schultz and Engman, 2000). Its main advantage lies on its ability to provide spatial and temporal data instead of point data. Besides, remote sensing has the following three levels of use in water resource studies (Salomonson, 1983 cited in Mendoza et al., 2002):

1. Identifying area of interest such as water body, alluvial fun,

2. Retrieving land cover data, geological and geo-morphological features through interpretation and classification, and

3. Direct estimation of precipitation, evaporation and other hydrological parameters.

2.3 Application of Remote Sensing for Estimation of Evapotranspiration

Remote sensing estimates of actual evapotranspiration (ETa) have been made in hydrology, agronomy and meteorology at a range of spatial scales. Remote Sensing data are used to derive surfaces temperature, surfaces reflectance and vegetation indices, which are combined with local meteorological observations in models to estimate AET. Irrigation has contributed significantly to poverty reduction, food security, and improving the quality of life for rural populations. However, the sustainability of irrigated agriculture is being questioned, both economically and environmentally. Remote sensing data and geographic information systems are increasingly

becoming an important tool in Hydrology and water resources development. This is due to the fact most of the data required for hydrological analysis can easily be obtained from Remote sensed images. The greatest advantage of using Remote sensed data for hydrology is its ability to generate information in spatial and temporal domain (Jagadeesha, 1999), which is very crucial for successful model analysis, prediction and validation.

The potential of remote sensing techniques in estimating evapotranspiration for irrigation and water resource management has been widely acknowledged. Environmental physics based on electromagnetic radiation and micro-hydrology has evolved in the development of quantitative algorithms to convert remotely sensed spectral radiances into useful information such as evapotranspiration, root zone soil moisture, and biomass growth. Different applications relating crop water consumption to irrigation water supply by remote sensing with developed theories are available in the electronic media with easy access. Also, in the field of geoinformatics, the software developments provide advanced techniques and modern facilities to the user. The low cost high speed personal computers can handle vast amounts of data at a time. Estimation of crop water parameters using remote sensing techniques is an expanding research field and development trends have been progressing since 1970s and the remote sensing algorithms such as SEBAL (Surface Energy Balance Algorithm for Land) by Bastiaanssen et al. (2003) and SEBS (Surface Energy Balance System) by Su (2002) are widely used approaches to estimate crop water parameters.

The scale of satellite measurements is a measure of its quality and which is associated with two parameters, namely spatial resolution and temporal resolution. The spatial resolution measures the ability of a sensor to distinguish among closely spaced objects in the terrain. One pixel is the smallest area of the terrain that can be recorded as a unique element by the sensor and Landsat-7 ETM+ satellite produce images of a more accurate shape of the ground object because of their smaller pixel size (30 m × 30 m for visible bands and 60×60 for thermal bands) and even much less than to this pixel size), compared to those of the MODIS or the NOAAAVHRR satellites which have pixels of 1000 m × 1000 m and 1100 m × 1100 m respectively (Bandara, 2006).

The mission of the Landsat Program is to provide repetitive acquisition of high-resolution multispectral data of the Earth's surface on a global basis. Landsat represents the only source of

global, calibrated, high spatial resolution measurements of the Earth's surface that can be compared to previous data records. The data from the Landsat spacecraft (every 16 days) constitute the longest record of the Earth's continental surfaces as seen from space. It is a record unmatched in quality, detail, coverage, and value. The Landsat platforms carry multiple remote sensor systems and data relay systems along with altitude-control and orbit-adjust subsystems, power supply, and receivers for ground station commands and transmitters to send the data to ground receiving stations. The ETM+ design provides for a nadir-viewing, eight-band multispectral scanning radiometer capable of providing high-resolution image information of the Earth's surface when operated from Landsat 7 ETM+, a three axis stabilized spacecraft located in a near polar, sun-synchronous and circular orbit at a 705 km nominal altitude, with an orbit inclination of 98.2 degrees. The ETM+ is designed to collect, filter and detect radiation from the Earth in a swath 185 km wide as it passes overhead and provides the necessary cross-track scanning motion while the spacecraft orbital motion provides an along-track scan.

The Moderate-resolution Imaging Spectroradiometer (MODIS) images are provided by USGS earth observing system website (http://edcimswww.cr.usgs.gov/pub/imswelcome) which is an excellent source of free downloadable MODIS data or products. MODIS is a multi-spectral imaging instrument aboard NASA's Terra (EOS AM) and Aqua (EOS PM) satellites. Terra's orbit around the Earth is timed so that it passes from north to south across the equator in the morning, while Aqua passes south to north over the equator in the afternoon. The MODIS instrument operating on both the Terra and Aqua satellites has a swath width of 2,330 km and views the entire surface of the Earth every one to two days. They acquire moderate resolution images in 36 spectral wavelength ranges between 0.405 and 14.385 μm at 250m, 500m, and 1,000m. The MOD16 ET algorithm has a good performance in generating global ET data products, providing critical information on global terrestrial water and energy cycles and environmental changes (Mu et al., 2007, 2009, 2011).

Calculation of water consumptions by remote sensing has been under high research efforts for the last 20 years, especially the energy balance models. The problem of actual ET estimation over a large area can be solved using remote sensing methods that provide ET on pixel by-pixel basis. Many researchers (Vidal and Perrier, 1989, Granger, 1989, Bastiaanssen, 1995, 2000, Bastiaanssen, et al., 1998, 2005, Tasumi, et al, 2000, Almhab et al, 2007, and Almhab & Busu,

2008) have already developed various methodologies by combining of satellite and ground data for large areas since the 1990s (Almhab and Busu, 2008). Some dedicated energy-balance models like the SEBAL, Simplified Surface Energy Balance (SSEB), Surface Energy Balance Index (SEBI), a Simple Remote Sensing Evapotranspiration Model (Sim-ReSET) and also some related models calculating evapotranspiration are also available among others not mentioned here.

In addition to this, a lot of Global Climatologic Models (GCMs) use the energy-balance process for various outputs like ET or soil moisture. For crop ET monitoring, high spatial resolution satellites are required, but the least is restricted to satellites having the capacity to calculate the surface temperature, as the latent heat flux of vaporization which is temperature driven. Some coarser spatial resolution satellites up to 1 km pixel sizes are still used for irrigation system temporal ET monitoring (Molla, 2009). Larger spatial resolution satellites, generally for meteorological purposes, even if used largely in GCMs, are not used for crop monitoring. SEBAL is one of the thermodynamically based models available, which partitions the sensible heat flux and the latent heat flux of vaporization.

Actual evapotranspiration is actually evapotranspired under the existing soil moisture supply. It is dependent on the unsaturated moisture storage properties of the soil. It is also affected by vegetated factors such as plant type and stage of growth (Freeze and Cherry, 1979). Actual evapotranspiration is the amount of evaporation that occurs under field conditions. If there is abundant moisture in the soil, the actual evapotranspiration rate is equal to potential evapotranspiration. When the moisture content in the soil is limited and vegetation unable to abstract enough water from the soil, then actual evapotranspiration becomes less than the potential evapotranspiration. Thus the relationship between ET_a and ET_o depends upon the soil moisture content. If there is no rain to replenish the water supply, the soil moisture gradually become depleted by the demands of the vegetation to produce a soil moisture deficit. As soil moisture deficit increases, the ET_a become increasingly less than ET_o. The value of soil moisture deficit and ET_a vary with soil type and vegetation (Shaw, 1988).

2.4 Surface Energy Balance Estimation of Evapotranspiration (ET)

Surface energy balance methods for ET estimation have been successfully applied by several researchers (Jackson et al., 1981; Moran et al., 1996; Bastiaanssen et al., 1998, 2005; Kustas and Norman, 2000; Roerink et al., 2000; Allen et al., 2005, 2007a, b; Su, 2002; Su et al., 2005; Anderson et al., 1997, 2007) to estimate agricultural crop water use and ET by general landscapes. A comprehensive summary of the various surface energy balance models is presented by Gowda et al. (2008) and Kalma et al. (2008). The approach of most energy balance models requires solving the energy balance (Eq. (1)) at the land surface, where the latent heat flux, comparable to ETa, is calculated as the residual of the difference between the net radiation to the surface and losses due to the sensible heat flux (energy used to heat the air) and ground heat flux (energy stored in the surface).

Land surface energy balance (EB) models, using remote sensing data from ground to airborne to satellite platforms at different spatial resolutions, have been found to be promising for mapping daily and seasonal ET at a regional scale. A detailed review of different ET algorithms was presented in Gowda et al. (2008). They reported that ET estimation accuracy varied from 67 to 97% for daily ET and above 94% for seasonal ET, indicating that remote sensing technology with appropriate algorithms has the potential to estimate regional ET accurately.

In recent years, methods for deriving surface fluxes using remote sensing data have been developed, such as SEBAL (Surface Energy Balances Algorithm for Land) (Bastiaanssen et al., 1998; Bastiaanssen, 2000; Bastiaanssen et al., 2002, 2005), SEBS (Surface Energy Balance System) (Su, 2002), TSEB (Two-Source Energy Balances) (Norman, et al., 1995) and S-SEBI (Simplified Surface Energy Balances Index) (Roerink et al., 2000) cited in (Jin, *et al*., 2008) . SEBAL is a robust remote sensing model that can be applied to estimate the different components of the energy balance of the earth surface including actual evapotranspiration (ET_a).Their approach requires solving the energy balance equation at the surface where the ET_a is calculated as the residual of the difference between the net radiation to the surface and losses due to the sensible heat flux (energy used to heat the air) and ground heat flux (energy stored in the soil and vegetation).

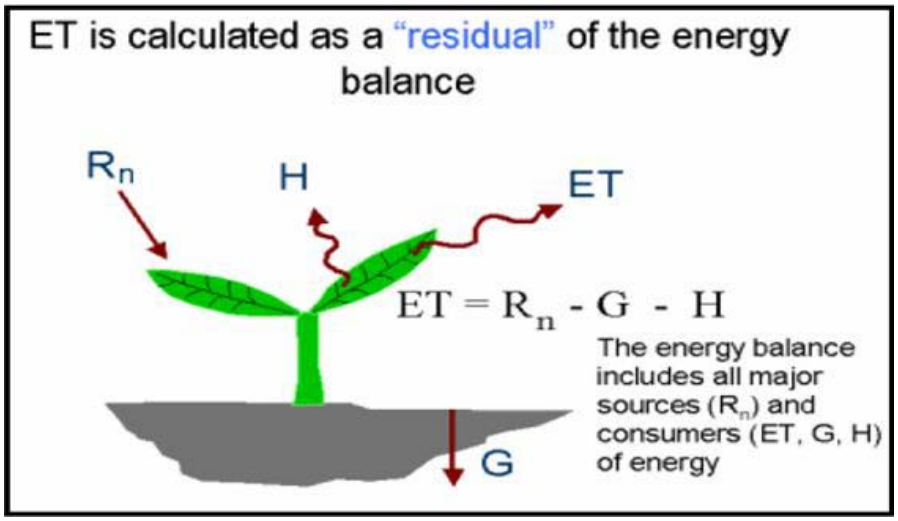

Figure 1. Diagram of the energy balance relationships that yield ET (Allen et.al, 2002)

$$ET = R_n - G - H \quad (1)$$

ET = Latent heat flux (energy consumed by evapotranspiration) (W/m^2)

R_n = Net radiation at the surface (W/m^2)

G = Ground heat flux (W/ m^2)

H = Sensible heat flux (W/ m^2)

The estimation of each of these terms from remotely sensed imagery requires high quality data sets.

Allen et al. (2005) described the several steps required to estimate actual ET using the surface energy-balance method that employs the hot and cold pixel approach of Bastiaanssen et al. (1998). In summary, for the net radiation term, data on incoming and outgoing radiation and the associated surface albedo and emissivity fractions for shortwave and long wave bands are required. The ground heat flux is estimated using surface temperature, albedo, and normalized difference vegetation index (NDVI). The sensible heat flux is estimated as a function of the temperature gradient above the surface, surface roughness, and wind speed.

Although solving the full energy-balance approach has been shown to give good results in many parts of the world, the data and skill requirements to solve for the various terms in the equation are prohibitive for operational applications where year-to-year differences and long term anomalies are more useful than absolute values. The Surface Energy Balance Algorithm for Land (SEBAL), the Simplified Surface Energy balance (SSEB) and operational application for Simplified Surface Energy balance ($SSEB_{op}$) methods were used to estimate actual ET. The SEBAL method assumes that the temperature difference between the land surface and the air (near-surface temperature difference) varies linearly with land surface temperature. It derives this relationship based on two anchor pixels known as the hot and cold pixels, representing dry and bare agricultural fields and wet and well-vegetated fields, respectively.

The latent heat flux (actual evapotranspiration) varies linearly between the hot and cold pixels and this assumption is based on the logic that the temperature difference between soil surface and air is linearly related to soil moisture (Senay et. al, 2007). Furthermore, crop soil water-balance methods estimate actual ET using a linear reduction from the potential ET depending on soil moisture. Therefore, it is possible that actual ET can be estimated by the near-surface temperature difference, which in turn is estimated from the land surface temperatures of the hot and cold pixels in the study area. In other words, while the hot pixel of a bare agricultural area experiences little ET and the cold pixel of a well-watered irrigated field experiences maximum ET, and the remaining pixels in the study area will experience ET in proportion to their land surface temperature in relation to the hot and cold pixels. This approach can be compared to the crop water stress index (CWSI) first developed by Jackson (1982). The CWSI is derived from the temperature difference between the crop canopy and the air. Dividing the current temperature difference (canopy vs air) by known upper and lower canopy air temperature difference values creates a ratio index varying between 0 and 1. The lower limiting canopy temperature is reached when the crop transpires without water shortage, and the upper limiting canopy temperature is reached when the plant transpiration is zero, owing to water shortage. In this study, the cold and hot anchor land surface temperature pixel values are the equivalent of the lower and upper limiting canopy temperatures of the CWSI method.

2.5 Theoretical Basis of SEBAL

Energy is required to change the state of the molecules of water from liquid to vapour. Direct solar radiation and, to a lesser extent, the ambient temperature of the air provide this energy. The driving force to remove water vapour from the evaporating surface is the difference between the water vapour pressure at the evaporating surface and that of the surrounding atmosphere. As evaporation proceeds, the surrounding air becomes gradually saturated and the process will slow down and might stop if the wet air is not transferred to the atmosphere. The replacement of the saturated air with drier air depends greatly on wind speed (Allen et al., 1998). According to Bastiaanssen and Chandrapala (2003), SEBAL is the currently used approaches to estimate crop water parameters.

SEBAL is a physically based multi-step model which has been designed to calculate the energy partitioning at regional scale with minimum ground data (Bastiaanssen et.al., 1998). It is a relatively new parameterization of surface heat fluxes based on spectral satellite measurements which has been formulated and developed by Bastiaanssen (1995). SEBAL uses surface temperature T_s, hemispherical surface reflectance, ρ_λ and Normalized Difference Vegetation Index (NDVI), as well as their interrelationships to infer surface fluxes on a pixel-by-pixel basis for a wide spectrum of land types. SEBAL requires spatially distributed, visible, near-infrared and thermal infrared data, which can be taken from satellite imageries. Major model components describe conversion of remotely sensed emitted and reflected radiances into surface energy balance and wetness indicator. The SEBAL parameterization is an iterative and feedback-based numerical procedure that deduces the radiation, heat and evaporation fluxes. The principle behind SEBAL model is conservation of energy.

The Surface Energy Balance Algorithm for Land (SEBAL) is an energy partitioning algorithm over the land surface, which has been developed to estimate actual evaporation from satellite images (Bastiaanssen et al., 1998a, 2000). The scheme has found applications in different basins of the world, e.g. Snake River basin in Idaho, USA (Allen et al., 2002), the lake Naivasha drainage basin in Kenya (Farah,2001), all river basins in Sri Lanka (Bastiaanssen and Chandrapala, 2003) and the irrigated Indus Basin in Pakistan (Bastiaanssen et al., 2002). In this study, a brief review of the algorithm is presented along with its assumptions, and the range of

the attainable accuracies. One distinct feature of the SEBAL algorithm is that the actual evaporation from various surface types, including different leaf coverages, soil types or groundwater table conditions can be derived. SEBAL estimates the spatial variation of the hydro meteorological parameters using satellite spectral measurements and (limited) ground-based meteorological data (Farah and Bastiaanssen, 2001). These parameters of the Soil–Vegetation–Atmosphere system are used to assess the surface energy balance terms and the latent heatflux λET is computed as the residue of the energy balance.

SEBAL uses digital imagery data collected by a remote-sensing satellite measuring visible, near infrared and thermal infrared radiation. In the SEBAL model, ET is computed from satellite images and weather data using the surface energy balance. Since the satellite image provides information for the overpass time only, SEBAL computes an instantaneous ET flux for the image time. The ET flux is calculated for each pixel of the image as a "residual" of the surface energy budget equation. The principles and steps needed to apply SEBAL to estimate evapotranspiration are described in Bastiaanssen (1995), Bastiaanssen et al. (1998).

Evapotranspiration (ET) is computed as a residual of the energy balance equation on a pixel-by pixel basis:

$$LE_{pixel} = \lambda \times ET_{pixel} = R_{npixel} - H_{pixel} - G_{pixel} \quad (1)$$

Where LE_{pixel}: latent heat flux for the pixel, ET_{pixel}: pixel ET, λ:latent heat of vaporization, and R_{npixel}, H_{pixel}, and G_{pixel} are the net radiation, sensible heat flux and soil heat flux for each pixel, respectively.

Guidelines for proper selection of both the cold and hot pixel can be found in Bastiaanssen (1995) or Trezza (2002). ET in the cold pixel (ET_{cold}) was defined using the single crop coefficient approach of FAO-56 (Allen et al., 1998):

$$ET_{cold} = ET_c = K_c \times ET_o \quad (2)$$

Where ET_c: crop evapotranspiration, ET_o: grass reference evapotranspiration, and K_c: crop coefficient.

In 1948, Penman combined the energy balance with the mass transfer method and derived an equation to compute the evaporation from an open water surface from standard climatological records of sunshine, temperature, humidity and wind speed. This so-called combination method was further developed by many researchers and extended to cropped surfaces by introducing resistance factors. The value of ET_o was calculated using the FAO Penman-Monteith equation of FAO-56 (Allen et al., 1998). The equation uses standard climatological records of solar radiation (sunshine), air temperature, humidity and wind speed. To ensure the integrity of computations, the weather measurements should be made at 2 m (or converted to that height) above an extensive surface of green grass, shading the ground and not short of water.

The hypothesis here is that the assignment of the calculated evapotranspiration (ET_c) to the cold pixel will produce a better approximation of the real ET that takes place in the study area, and serve as a self-calibration of the image. ET_c is calculated from ET_o, which incorporates the meteorological information of the site and from the crop coefficient (K_c), which is related to the actual crop that is available in cold pixel candidates inside the study area.

In summary, SEBAL is applied following these steps: **a)** calculation of R_n for each pixel from equation 4; **b)** calculation of G for each pixel from equation 29; **c)** definition of the dT function (equation. 37) using dT and Ts obtained from the two "anchor" pixels; **d)** calculation of dT for each pixel from the pixel surface temperature, using equation 37; **e)** calculation of H for each pixel from equation 30; and **f)** calculation of latent heat flux from equation 1. All energy balance fluxes (R_n, G, H, and LE) represent instantaneous fluxes corresponding to the instant when the satellite image was taken.

2.6 Extrapolation of Instantaneous ET to Daily ET Values

The values of ET derived from SEBAL represent instantaneous values corresponding to the time at which the satellite image was taken. However, instantaneous ET values are not very useful inputs for many hydrological and ecological applications where daily, monthly, and seasonal values are commonly needed. To estimate the 24 hour ET for the day of the image, SEBAL uses an approach based on the self-preservation theory of daytime fluxes, which states that the ratio between the latent heat flux and the available energy (R_n-G) remains fairly constant during the day (Bastiaanssen et al., 1998). This ratio between LE and R_n-G is termed as the evaporative

fraction (EF). For this application, daily ET (ET_{24}) was estimated by assuming that the instantaneous crop coefficient (K_c), computed at image time, is the same as the average K_c over the 24hr period. Therefore, the value of ET_{24} for each pixel is calculated as

$$K_c = \frac{ET}{ET_o} = \frac{ET_{24}}{ET_{o24}} \Rightarrow ET_{24} = K_c \times ET_{o24} \quad (3)$$

Where K_c, ET, and ET_o: instantaneous values of crop coefficient, actual and reference evapotranspiration, for the time when the satellite image was taken; and ET_{24} and ET_{o24}: corresponding daily values (24hr) of actual and reference ET. The hypothesis here is that the relationship between actual and reference ET remains relatively constant during the daytime as demonstrated in various experiments (Trezza, 2002; Allen et al., 2005). In other words, this approach assumes that the crop coefficient (K_c) remains constant during the day, which is reasonable if one takes into account that both actual and reference ET might have similar response to the variation of the weather parameters.

2.7 Crop and Irrigation Water Requirement

The term water requirements of a crop means the total quantity of all water and the way in which a crop requires water, from the time it is sown to the time it is harvested. Although the values for crop water requirement (CWR) and crop evapotranspiration (ET_c) are identical, CWR refers to the amount of water that needs to be supplied, while ET_c refers to the amount of water that is lost through evapotranspiration. The irrigation water requirement (IR) basically represents the difference between the CWR and effective precipitation. For better understanding of CWR, it is prudent to have knowledge of functions of irrigation water and it is important to make a distinction between CWR and IR. CWR refers to the water used by crops for cell construction and transpiration whereas the IR is the water that must be supplied through the irrigation system to ensure that the crop receives its full CWR. IR can also be defined as the quantity, or depth, of irrigation water in addition to precipitation required to produce the desired crop yield and quality and to maintain an acceptable salt balance in the root zone.

Crop water requirements (CWR) encompass the total amount of water used in evapotranspiration. FAO (1984) defined crop water requirements as ‘the depth of water needed

to meet the water loss through evapotranspiration of a crop, being disease-free, growing in large fields under non restricting soil conditions, including soil water and fertility, and achieving full production potential under the given growing environment'. The CWR is also called crop evapotranspiration and is usually represented as ET_c. Crop water use, also known as evapotranspiration (ET), is the water used by a crop for growth and cooling purposes. This water is extracted from the soil root zone by the root system, which represents transpiration and is no longer available as stored water in the soil. Consequently, the term "ET" is used interchangeably with crop water use. All these terms refer to the same process, ET, in which the plant extracts water from the soil for tissue building and cooling purposes, as well as soil evaporation.

Once the three parameters (daily water requirements, available soil moisture and effective root zone depth) are known, an irrigation schedule can be established. While estimated values of ETc, based on climatic data, are sufficient for planning and designing purposes, for more accurate scheduling more accurate field data are necessary. Irrigation scheduling means how much water should be applied and when to irrigate. To make this decision, there is some steps should be followed to make right decision. First of all crop pattern and information of each crop such as growing season, growing and harvesting date, root depth, and allowable depletion, soil physical properties, climate, availability of water resources, and field water losses also should be known. Good irrigation management insures that an adequate supply of soil moisture is maintained throughout the season and this helps farmers and irrigators to use the available water resources efficiently. Informed irrigation decision making requires knowledge of the water use requirements of the crops and irrigation system performance, including the uniformity of application and delivery rates. Information on how productivity is affected by suboptimal irrigation practices also can be used to guide irrigation decision making. I believe that this study on sugarcane crop water use provide growers with the agronomic information necessary to successfully manage irrigation, both in normal water years and in drought periods.

The soil in the root zone has an upper as well as a lower limit of storing water that can be used by crops. The upper limit is called the field capacity (FC), which is the amount of water that can be held by the soil against gravity after being saturated and drained; typically attained after 1 day of rain or irrigation for sandy soils and from two to three days for heavier-textured soils that contain more silt and clay. A practical lower limit of soil water content below which crop growth

is severely reduced by water stress has been defined as the permanent wilting point (PWP).The difference between FC and PWP is termed the available water content (AWC) and is the maximum amount of soil water that can be used by the plants. Crop growth decreases before the entire root zone reaches the PWP. For this reason, you should usually irrigate before the root zone water content reaches a level that restricts growth below its maximum potential. Unfortunately, no single soil water level can be recommended for all situations. The safe amount of depletion [called allowable depletion (AD) or yield threshold depletion (YTD) and usually referred to as a percentage of the total available water in the root zone] depends on numerous factors, including rooting density, soil texture, and the weather. The AD concept is important only for surface irrigation and sprinklers; it is irrelevant for drip and microsprinklers. The objective of irrigation is to keep adequate moisture in the soil. Estimates of allowable depletion allow use of the maximum amount of soil water (consistent with optimal crop performance) between irrigations. This approach means growers can irrigate the fewest times possible and, because there are fixed costs associated with each irrigation, this is usually the most economical practice.

3. MATERIALS AND METHODS

3.1 Description of the Study Area

3.1.1 Location

The Wonji-Shoa Sugar Estate lies downstream of the Koka Dam in the Central Rift Valley of Ethiopia in the upper Awash River basin. The study site Wonji-Shoa Sugar estate is located in the upper Awash River valley around 114 km from Addis Ababa in East Shewa Zone of the Oromia National Regional State within the geographical boundaries of 8^0 21' to 8^0 29' N latitudes and 39^0 12' to 39^0 18' E longitudes at an altitude of about 1,540 m above sea level (Melaku, 2009). Currently the estate is cultivating more than 9352 hectare of irrigated land using furrow irrigation system. The first large public irrigation scheme Wonji-Shoa Sugar Plantation was constructed in 1956 as a private farm by HVA (Handels Vereniging Amsterdam) and now it is subordinated under the authority of Ethiopian Sugar Corporation Company.

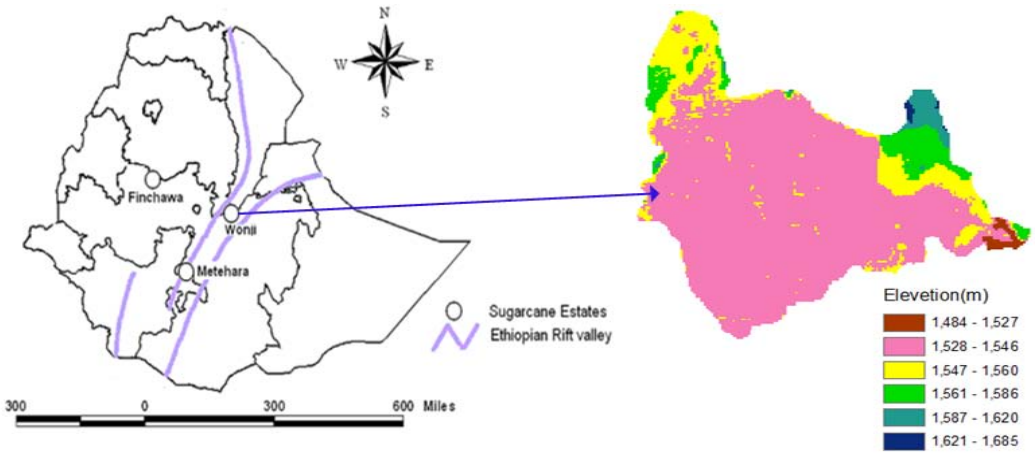

Figure 2. Location and topographic map of the study area

Table 1. Land holding of the study area

Description	Gross area(ha)	Net area(ha)
Estate proper	5930.10	5689.4
Existing out growers	1717.45	1660.13
North Dodota expansion project	2110.59	2002.4
Total	9758.14	9351.93

Table 2. Summary of total cane and fallow crop growing area (ha) in each plantation section

Plantation section	Gross area (ha)	Net area (ha)
R1	631.28	607.78
R2	679.43	646.94
R3	680.24	652.12
L1	668.82	633.85
L2	620.42	589.56
L3	658.65	626.91
E1	685.82	649.50
E2	659.32	630.14
E3	635.51	606.90
Total	5,919.49	5,643.70

Net area: comprises area used for cane and fallow crop growing, feeder ditch and infield drain.

Gross area: comprises net area, area used to establish supervision path and area of those special feeder ditches and infield drains stretched over a long distance.

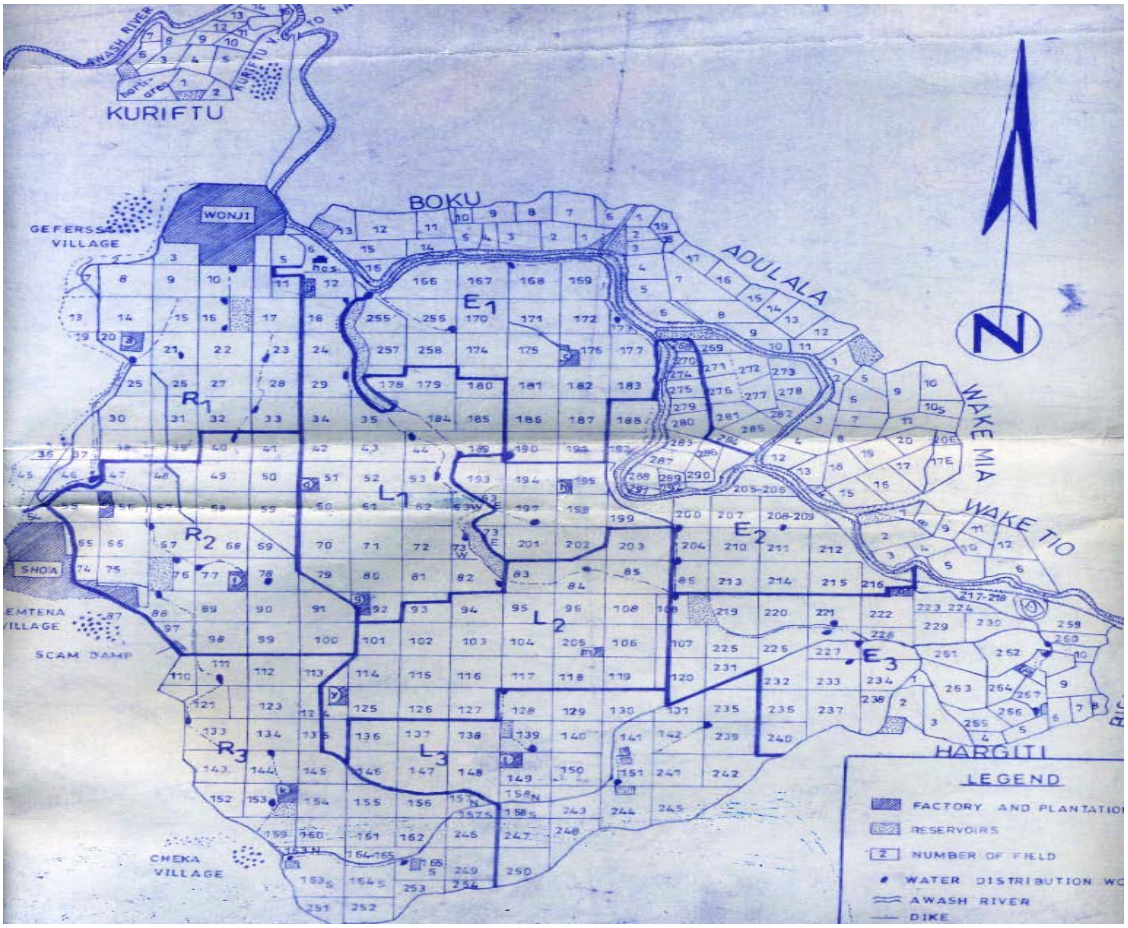

Figure 3. Layout of Wonji Shoa sugarcane estate

3.1.2 Soil types and vegetation

In the estate, generally, the topography of the farm is very gentle slopes with flood prone plains of Awash River. The surrounding topography is steep on all sides. North and East being bounded by river Awash and the west and south by the border drain which protects the estate from the runoff and sedimentation from these steep slopes. The soils of Wonji-Shoa have been described predominantly as a complex of gray, cracking clays in the topographic depressions and semiarid, brown soils. More than 50 percent of the farm is heavy clay soil and the rest is light soil and slight to moderate soil infiltration and water logging problems are expected if groundwater occurs at shallow depths. Hence as stated by Girma and Awulachew (2007), Wonji-Shoa, sugarcane fields are prone to water logging and physical degradation of topsoil. Land use/cover affects water circulation and is an important factor for analyzing evapotranspiration in a certain area. Due to population growth and urbanization, land cover type continually changes. Since land use/cover is sensitive to interference, it is difficult to obtain accurate land use/cover grid. The main crops cultivated are sugarcane, haricot bean and crotalaria. Sugarcane is planted at a rate of 16-18 t/ha in the estate and it is cultivated as perennial monocrop.

Among the many varieties of sugarcane in the world, ten major cane varieties are grown in Wonji sugarcane plantation. These are: B52-298, CO-421, M165/38, NCO-334, N-14, DB414/66, Mex 54/245, B58-230, B59-212, and B41-227. Of these B52-298 is widely grown and forms the dominant variety in the area. The cane plant flourishes in a wide variety of soils, ranging from very heavy clay soils to light brown sandy loam soils. These soils in the area are locally classified in to five classes for management practices. A1, A2, and BA2 are clubbed as heavy black soils and B14, and C1 as light brown soils. The way to establish a cane field is by planting sets. Seeds are used only for breeding new varieties. But growth of the cane also commences with tillering followed by crop growth, crop maturity and harvest. When crop yield becomes too low, new sets are planted. The crop cycle of the cane can be looked at two stages: the first from the original set planting new set planting and the second from set planting or the previous harvest to the following harvest. The first or complete crop cycle lasts from three to ten years or longer if the crop is well managed. The second is called the harvest or annual cycle and usually lasts from ten to twenty four months (Wonji-Shoa Sugar Factory Working Manual, 2004).

3.1.3 Climate

Rainfall at Wonji is scanty. Since air humidity is very low in the hot, dry season; the need of water is very great. Short rains, March to May merge into the main rainy season from mid- June to mid-September. The highest rainfall was registered in July and August and minimum in October and November. The mean annual relative humidity ranges from 43.2 to 68.4%. It is described as tropical wet climate with uniform warmth throughout the year and receives an average annual rainfall of 831.2 mm, average daily evapotranspiration of 4.5 mm/day, mean annual maximum and minimum temperatures of 27.6 ^{0}C and 15.2 ^{0}C, respectively and the average sunshine hour is 9 hours in dry summer and 6.5 hours in August as cited in (Girma and Awulachew, 2007). At Wonji, in the Upper Valley, the mean annual PET is 1810 mm, over twice the mean annual rainfall, with average monthly rainfall exceeding average monthly evapotranspiration only in July and August (Behailu, 2004). The mean annual discharge for upper Wonji basin is 4.3 m^3/sec (Dechasa, 1999).

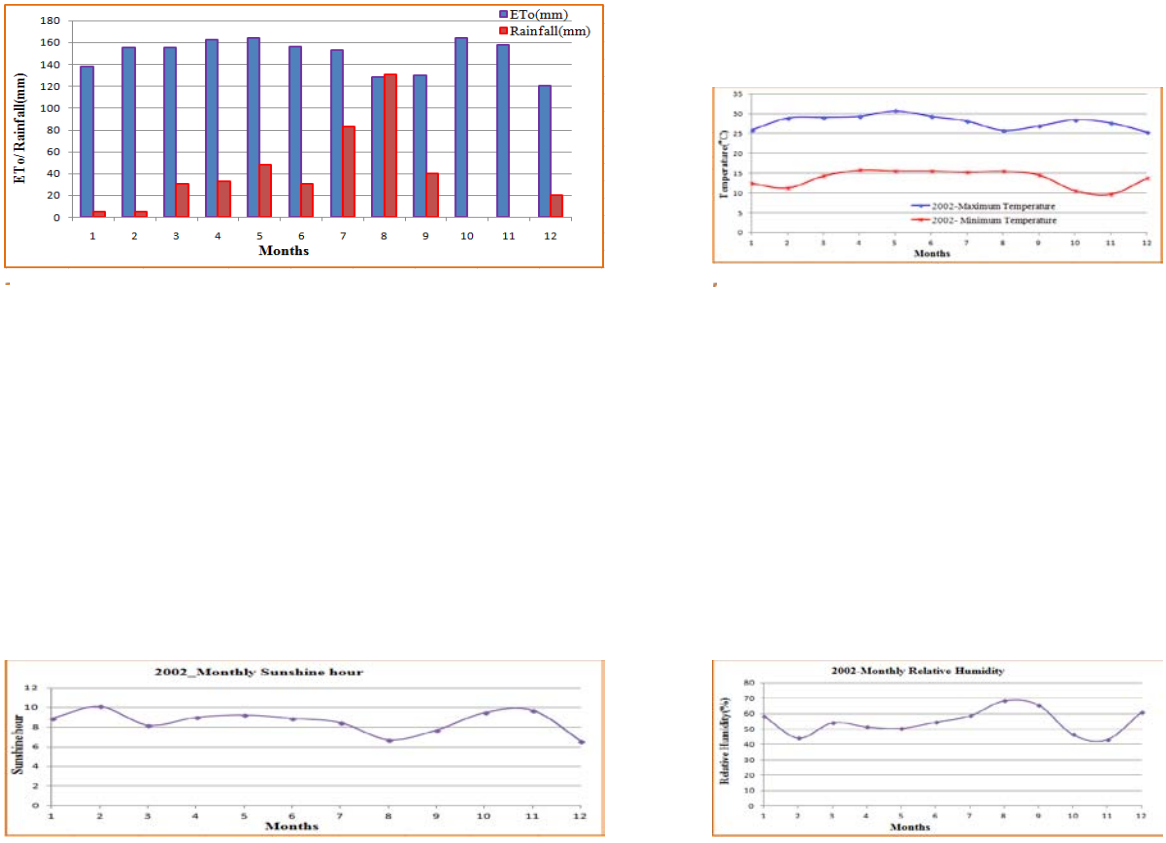

Figure 4. Meteorological parameters at Wonji in 2002.

The water delivery infrastructures are all open canals in which water is pumped from Awash River through a pumping station at Wonji and almost the entire estate is fed from this pumping station through an extensive earthen canal system and storage facilities. Pumps run continuously to store water in reservoirs, which are spread at various locations in the estate, and the estate is irrigated partly from the water supplied directly by the pumps and the rest from the reservoirs. There are seven main, and twelve, tertiary night storage reservoirs in the estate and irrigation development in the area impacts rising of water table and seepage of reservoirs.

The kind of irrigation practiced at Wonji can be termed as "blocked end furrow irrigation system." Water applied to each furrow is cut off as it reaches the end of the furrow, which is blocked, and ponds up with in the furrow. The furrow length for a part of a field depends on the gradient available and three lengths 32m, 48m, and 64m are being currently used. The advantage of this system is that there is no runoff and the entire water applied to the field is incorporated in to the soil. As such, in addition to the infiltration characteristics of the soil, the size of the inflow stream and the gradient of the furrow become important variables to control the rate of advance of water front to the end of the furrow, which determines the cut off time for the inflow.

3.2 Data Collection and Analysis

3.2.1 Data collection

3.2.1.1 Remote sensing data

The main remote sensing input used for this study is Landsat7 ETM+ data having spatial resolution of 30m for visible and near infrared bands (b1 to b5 and b7) and 60m resolution for thermal band (b61 and b62) at satellite nadir provided by the United States Geological Survey (USGS) Earth Observation System (EOS) Data Gateway and MODIS (the MOD16 global ET) datasets with 1000m by 1000m resolution. Four relatively cloud free Landsat7 ETM+ images covering the entire study site (Path 168, Row 54) bounded by 8°24'20"N and 39°16'2"E in the period between January and October, 2002 were acquired and downloaded from the USGS website (http://edcsns17.cr.usgs.gov/EarthExplorer/) freely. The MODIS-MOD16 global evapotranspiration (ET)/latent heat flux (LE)/potential ET (PET)/potential LE (PLE) datasets

with Wonji Shoa sugarcane estate bounding coordinates for MODIS sinusoidal grid projections were downloadable freely from the website (http://edcimswww.cr.usgs.gov/pub/imswelcome).

3.2.1.2 Header file information

Landsat Thematic Maper (TM) images are generally created with an associated "header" file which is a relatively small file that contains important information for satellite image processing of ET algorithms like SEBAL, SSEB, $SSEB_{op}$ and others. The basic information obtained from the header file includes: the satellite overpass date and time which is expressed as Greenwich Mean Time (GMT) and must be converted to local time, the latitude and longitude of the center of the image, the sun elevation angle (β) at the overpass time and the gain and bias for bands 1-5 and 7 for entry into ET algorithms such as SEBAL. These parameters are used to convert digital numbers (DN's) in the original files into energy units. For band 6, the thermal band, both high and low gain images are supplied and for SEBAL, it is recommended to use the Low gain image, even though it has slightly less resolution, since it is less likely to suffer from saturation.

3.2.1.3 Meteorological data

Meteorological factors such as air temperature, relative humidity, wind speed, solar radiation and precipitation has a considerable effect on the rate of evapotranspiration and hence the water resource is largely dependent on the source, latitudinal setting, physiographic and vegetation cover of the area. The wind speed (u) at the time of the satellite overpass is required for the computation of sensible heat flux (H) and for the reference evapotranspiration (ET_o) calculation. Precipitation data is used to evaluate the general "wetness" of areas that have received rain within four or five days before the image date. Humidity data are necessary for the ET_o calculation. Solar radiation data are useful for the estimation of the cloudiness of the image and for adjusting the atmospheric transmissivity (τ_{sw}). ET_o is the estimated ET for a well-watered reference crop, usually alfalfa. It is used to compute H at the "cold" anchor pixel and to compute the reference ET fraction (ET_rF) that is used to predict 24-hour and seasonal ET. These important meteorological observations are required by ET algorithms for accurate ET estimation. The meteorological data sources of this study are hourly and daily climatic data which were collected from the representative ground stations of the National Meteorological Service Agency (NMSA) of Ethiopia (wind speed, relative humidity, solar radiation, air temperature and

reference ET) and also filling of missing data and checking for consistency had been done. Meteorological data in daily time steps from one representative weather station located in the Wonji Shoa sugarcane estate were collected and used in SSEB, $SSEB_{op}$ and SEBAL processing. The weather conditions prevailing on the four satellite overpass date at Wonji meteorological station are shown below.

Table 3. Average/ daily weather conditions at the satellite overpass time

Dates	Temperature (^{o}C)	Humidity (%)	Wind speed at 2m (m/sec)	Actual sunshine hour (hour)	Precipitation (mm)	ETo Penman (mm)
Jan 25,2002	17.4	43	3.1	10.5	0.0	5.49
Feb 26,2002	20.5	36	2.8	11	0.0	6.31
Sept 6,2002	21.8	58	1.7	0.0	0.0	3.11
Oct 8,2002	19.4	46	2.4	11	0.0	5.39

3.2.1.4 Software packages used

The main software packages used were Earth Resource Data Analysis System (ERDAS) IMAGINE 10, CROPWAT8, and ArcGIS 9.3. All remote sensing image processing: image rectification, sub-setting image, band combinations and layering, classification and modeling were done with ERDAS IMAGINE spatial modular tool which enable to create and run models for image processing and GIS analysis. It is a highly flexible tool which uses Model Maker and the Spatial Modeler Language. The Spatial Modeler Language is a modeling language that is used internally by Model Maker to execute the operations specified in the graphical models that were created. GIS (ArcGIS 9.3: ArcMap with spatial extension, Map Algebra, ArcCatalog, ArcMap and ArcToolbox), Saga software and satellite based GPS were used for mapping contours, soils and ground data to display and provide accurate geo-referenced data (in terms of latitude & longitude) positional locations, boundaries for accurate assessment of evapotranspiration.

3.2.2 Data analysis

3.2.2.1 Remote sensing based data analysis

The original satellite images must be properly prepared for use in SEBAL as described below. The Penman Monteith method was used to calculate reference evapotranspiration (ET_o) and also

the SEBAL, SSEB and $SSEB_{op}$ algorithms were applied to Landsat-7 ETM+ data for assessing the actual ET by calculating the ET flux for each pixel of the satellite image and weather data as a "residual" of the surface energy budget equation. During the image analysis, the selected algorithms used the following spectrum of Landsat ETM+ seven bands (Band1 to Band7).

Band 1.....visible (blue)
Band 2.....visible (green)
Band 3.....visible (red)
Band 4.....near infrared
Band 5.....near infrared
Band 6.....thermal infrared
Band 7.....near infrared

These bands were layered inside ERDAS IMAGINE, in order from band 1 to band 7 to create an image file for use in the image analysis process. After that, a smaller subset image was created for Wonji Shoa sugarcane plantation farm. The steps used for layering a Landsat 7 ETM+ images are depicted as follows:

1. The GeoTIF format image was browsed
2. The details viewed
   - The six large files with a "t" in the name are the bands 1 - 5 and 7, in order.
   - The two large files with a "k" in the name are for band 6, low gain and high gain in that order (the low gain is used).
   - The large file with a "p" in the name is for band 8 (Panchromatic) and is not used.
3. In ERDAS modeler maker, the Layer stack process was made as follows

a. The input file was taken from the file in a geo-TIFF format.
b. A unique output file name created. The name include the date, path, and row of the image.
c. The seven layers in order beginning with band 1 (the first large "t" file) up to band 5, band 6 (the first large "k" file for low gain) and then band 7 (the last large "t" file) were added.

The area of interest can now be viewed with the ERDAS Viewer tool and a subset image for the study area was created.

The images were first radiometrically calibrated and georeferenced to local projections to obtain land surface parameters such as NDVI, reflectance, emissivity and temperature. The original

Landsat images were checked for geo-rectified for use in the algorithms with appropriate coordinates. The rectified images were saved in the GeoTIF format and the nearest neighborhood resembling was used during rectification to preserve spectral information. The satellite images were preprocessed and further processed to derive the land surface parameters as required by the energy balance models to derive ET. Having estimated the land surface parameters, the selected algorithms were employed to estimate daily actual ET.

The procedures involved by ET models and the associated techniques are indicated in the following section.

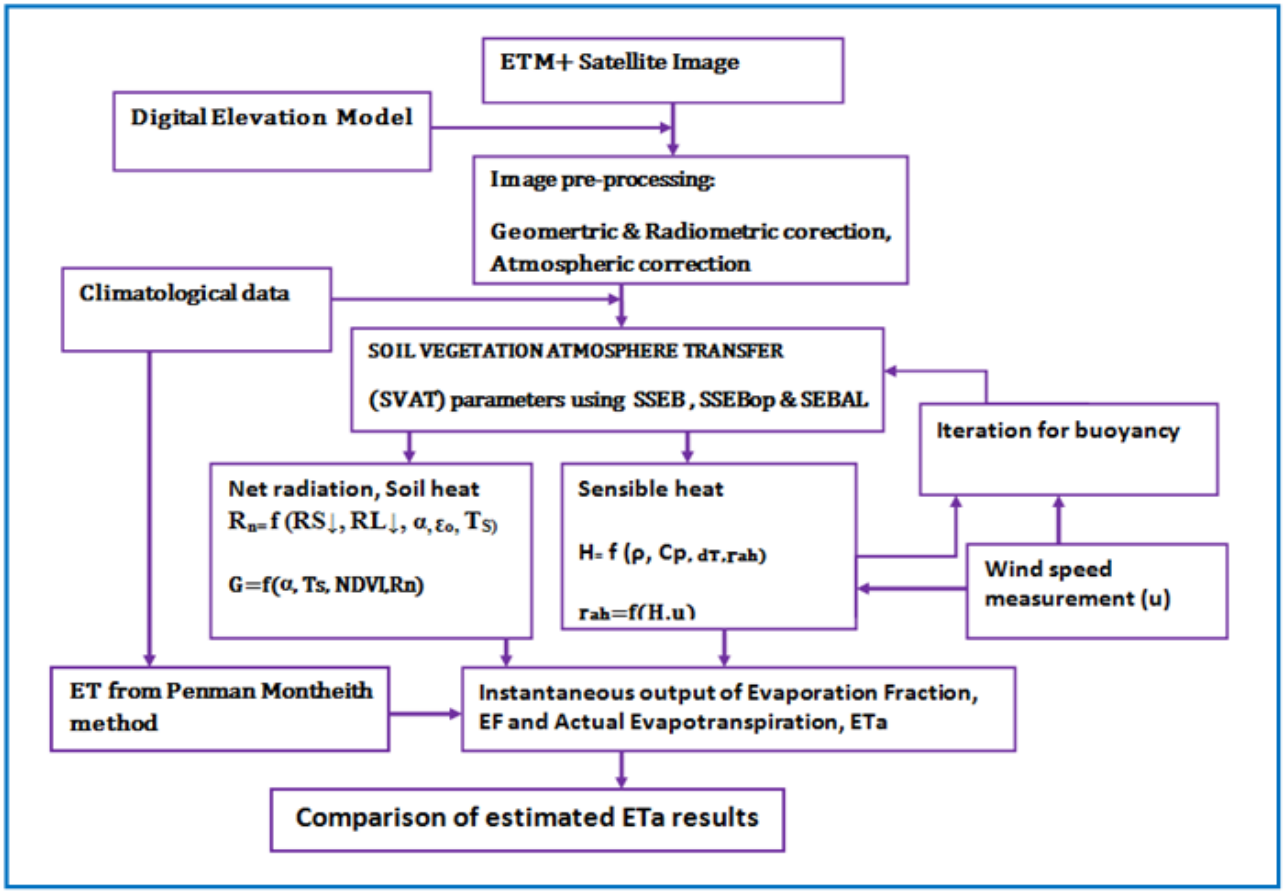

Figure 5. Flow chart of the research approach

3.2.2.2 Image analysis for SEBAL parameter extraction

Satellite based measurements provide information on atmosphere and land surface condition useful for evapotranspiration rate estimation. The method involves image rectification processes and multi-spectral image analysis to derive surface variables and energy balance components.

The net radiation flux at the surface (R_n) represents the actual radiant energy available at the surface. It is computed by subtracting all outgoing radiant fluxes from all incoming radiant fluxes. The first step used in the SEBAL procedure was to compute the net surface radiation flux (R_n) using the surface radiation balance equation.

$$R_n = (1-\alpha)R_{S\downarrow} + R_{L\downarrow} - R_{L\uparrow} - (1-\varepsilon)R_{L\downarrow} \quad (4)$$

$R_{S\downarrow}$ is incoming shortwave radiation (W/m^2), α is broadband surface albedo (dimensionless), $R_{L\downarrow}$ is incoming long wave radiation (W/m^2), $R_{L\uparrow}$ is outgoing long wave radiation (W/m^2), ε is surface thermal emissivity (dimensionless), R_n represents the actual radiant energy available at the surface (100-700 W/m^2).

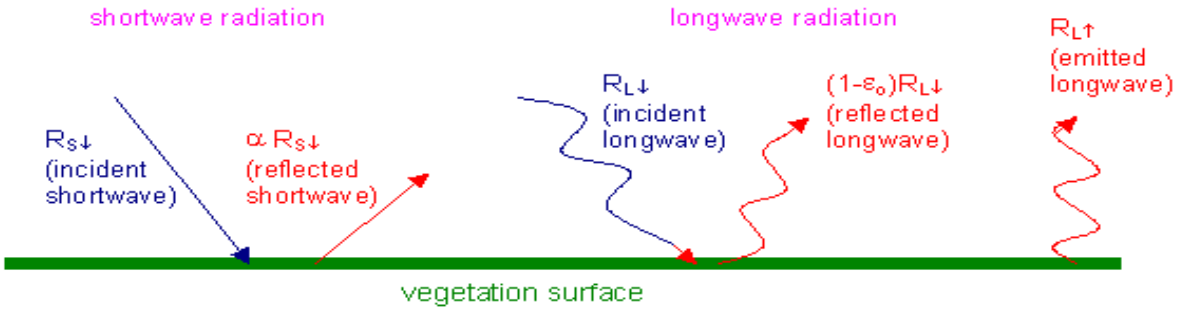

Figure 6. Surface radiation balances

This was accomplished in a series of steps using the ERDAS Model Maker tool to compute the terms in the following equation. A flow chart of the process is shown in the Figure below.

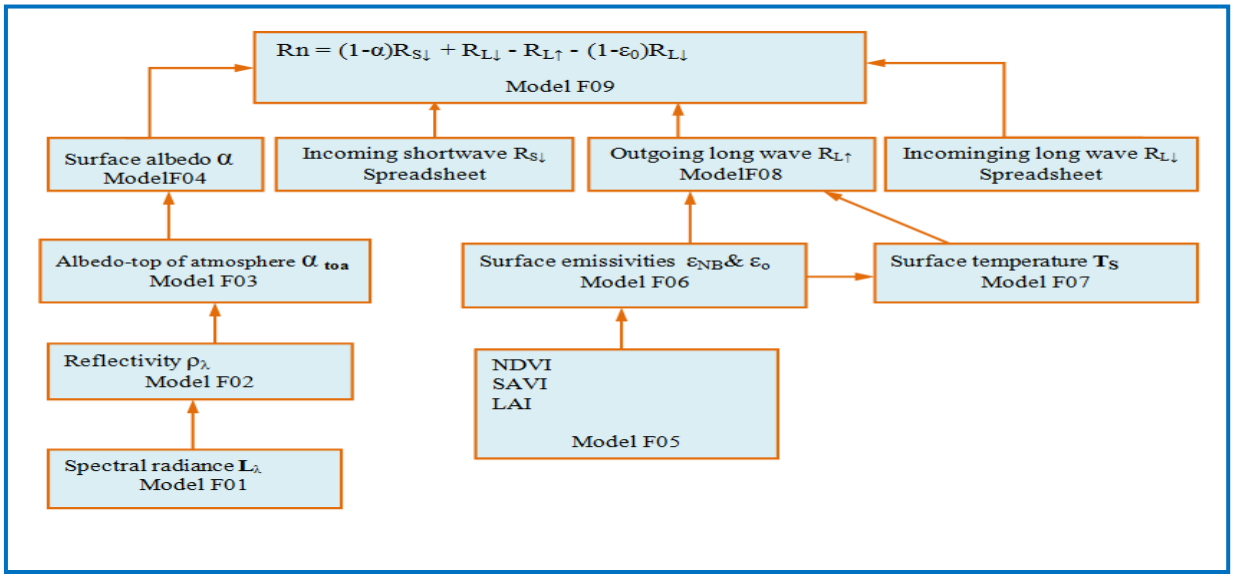

Figure 7. Flow Chart of the Net Surface Radiation Computation (Bastiaanssen, 2002)

The model number used for each computation is given along with the variable name. The computation steps begin at the bottom of the figure with model F01 and continue upward to model F09 for the computation of R_n. The two terms $R_{S\downarrow}$ and $R_{L\downarrow}$ are computed with a spreadsheet or a calculator rather than the Model Maker tool.

Surface Albedo: Surface albedo is defined as the ratio of the reflected radiation to the incident shortwave radiation. A considerable amount of solar radiation reaching the earth's surface is reflected. The fraction α, of the solar radiation reflected by the surface is termed as the albedo. The albedo is highly variable for different surfaces and for the angle of incidence or slope of the ground surface.

Table 4. Typical albedo values

Fresh snow	0.80 – 0.85	Water	0.025 – 0.348
Old snow and ice	0.30 – 0.70	Deciduous forest	0.15 – 0.20
Black soil	0.08 – 0.14	Coniferous forest	0.10 – 0.15
Clay	0.16 – 0.23	Rice field	0.17 – 0.22
White-yellow sand	0.34 – 0.40	Corn field	0.14 – 0.22
Gray-white sand	0.18 – 0.23	Grass or pasture	0.15 – 0.25

(Depending on solar elevation angle)
(FAO, 2006 Guidelines for computing crop water requirements)

It was computed in SEBAL through the following steps given for Landsat images:

A. **The spectral radiance for each band (L_λ)** is computed (model F01). This is the outgoing radiation energy of the band observed at the top of the atmosphere by the satellite. Sensors on board satellite record radiance from earth surface as electrical signals in the form of Digital Numbers (DN) by the process of analog to digital converter to be readily usable for interpretation purposes. However, for temperature estimation the absolute radiance is used. Thermal band 6 of Landsat ETM+ band (B61) are used for the estimation of temperature in the study area. Especially for the second sensor, the low gain state is chosen because of the fact that it automatically calibrates the solar brightness situation of the Wonji Shoa sugarcane plantation area. It was calculated using the following equation:

$$L_\lambda = \left(\frac{L_{max} - L_{min}}{Q_{calmax} - Q_{calmin}}\right) \times (DN - Q_{calmin}) + L_{min} \quad (5)$$

Where; DN is the digital number of each pixel, LMAX and LMIN are calibration constants, QCALMAX (255) and QCALMIN (1) are the highest and lowest range of values for rescaled radiance in DN that are used in this research. The units for L_λ are $W/m^2/sr/\mu m$.

B. The reflectivity for each band (ρ_λ) is computed (model F02). The reflectivity of a surface is defined as the ratio of the reflected radiation flux to the incident radiation flux. It was computed using the following equation

$$\rho_\lambda = \left(\frac{\pi \times L_\lambda \times {d_r}^2}{ESUN_\lambda \times \cos\theta} \right) \quad (6)$$

where; L_λ is the spectral radiance for each band computed in model F01, $ESUN_\lambda$ is the mean solar exo-atmospheric irradiance for each band ($W/m^2/\mu m$), $\cos\theta$ is the cosine of the solar incidence angle (from nadir), and d_r is the inverse squared relative earth-sun distance.

Values for $ESUN_\lambda$ are known for each band of Landsat 7 (table 3). Cosine θ is computed using the header file data on sun elevation angle (β) during the satellite overpass time, where $\theta = (90^o - \beta)$. The term d_r is defined as $1/{d_{e\text{-}s}}^2$ where $d_{e\text{-}s}$ is the relative distance between the earth and the sun in astronomical units. d_r is computed using the following equation given in FAO 56 paper: Crop Evapotranspiration (Allen et al., 1998):

$$d_r = 1 + 0.033 cos\left(DOY \frac{2\pi}{365} \right) \quad (7)$$

Where; DOY is the sequential day of the year and the angle ($DOY \times 2\pi/365$) in radians for the image used in this research. Value of dr is 1.03 with no dimension.

Table 5. $ESUN_\lambda$ for Landsat 7 ETM+ (Landsat 7 Science User Data Handbook Chap.11, 2002); both are in $W/m^2/\mu m$

	Band1	Band2	Band3	Band4	Band5	Band6	Band7
Landsat 7	1969	1840	1551	1044	225.7	-	82.07

Note: a dummy value of 1 was entered for band 6.

C. The albedo at the top of the atmosphere (α_{toa}) is computed (model F03). This is the albedo unadjusted for atmospheric transmissivity and is computed as follows:

$$\alpha_{toa} = \Sigma (\omega_\lambda \times \rho_\lambda) \quad (8)$$

Where; ρ_λ is the reflectivity computed in step 2 and ω_λ is a weighting coefficient for each band computed as follows:

$$\omega_\lambda = \frac{ESUN_\lambda}{\Sigma ESUN_\lambda} \quad (9)$$

Values for the weighting coefficient, ω_λ, are known for Landsat images.

Values for ω_λ are entered into the table of the model with a dummy value of zero for band 6. The file for reflectivity (ρ_λ) computed in model F02 is also input.

Table 6. Weighting coefficients, ω_λ

	Band1	Band2	Band3	Band4	Band5	Band6	Band7
Landsat 7	0.293	0.274	0.231	0.156	0.034	-	0.012

Note: a dummy value of 0 is entered for band 6.

D. The final step is to compute the **surface albedo** (model F04). Surface albedo is computed by:

$$\alpha = \frac{\alpha_{toa} - \alpha_{path\ \_radiance}}{\tau_{sw}^2} \quad (10)$$

Where; $\alpha_{path\text{-}radiance}$ is the average portion of the incoming solar radiation across all bands that are back-scattered to the satellite before it reaches the earth's surface, values for $\alpha_{path\text{-}radiance}$ range between 0.025 and 0.04 and for SEBAL 0.03 is a recommended value based on Bastiaanssen (2000) and τ_{sw} is the atmospheric transmissivity defined as the fraction of incident radiation that is transmitted by the atmosphere and it represents the effects of absorption and reflection occurring within the atmosphere. This effect occurs to incoming radiation and to outgoing radiation and is thus squared in the above equation. τ_{sw} is calculated by assuming clear sky and relatively dry conditions using an elevation-based relationship from FAO-56:

$$\tau_{sw} = 0.75 + 2 \times 10^{-5} \times Z \quad (11)$$

Where; Z is the elevation above sea level (1540m) which represents the area of interest that is the elevation of Wonji weather station. In the location or image date there was no atmospheric dusts or clouds that affect the atmospheric transmissivity in each band. So the result for τ_{sw} is 0.781.

For conditions having high levels of atmospheric aerosols or dust, the user may wish to predict α separately for each individual band using an atmospheric radiation transfer model such as Modtran along with radiosonde data for the location and image date. In most situations, however, because of the design of SEBAL, where the energy balance and ET are specified for the two extreme conditions (maximum ET and minimum ET), some error in estimated albedo caused by uncertainty in values for transmissivity and αpath_radiance, cause little error in the final ET computation. Therefore, for general application, Equation (10) is adequate. The surface albedo for all pixels has now been computed and these values can be checked with the land use map of the area to see if they are realistic based on the standard (table 4). For example, trees generally have smaller albedo than agricultural crops. Generally, albedo values for clear water are very small. Shortwave radiation penetrates into a water body according to the transparency of the water and is absorbed at a range of depths below the surface where it is converted into heat.

Incoming Shortwave Radiation ($R_{S\downarrow}$): Incoming shortwave radiation is the direct and diffuse solar radiation flux that actually reaches the earth's surface (W/m^2). It is calculated, assuming clear sky conditions, as a constant for the image time using:

$$R_{s\downarrow} = G_{sc} \times \cos\theta \times d_r \times \tau_{SW} \qquad (12)$$

where; G_{sc} is the solar constant (1367 W/m^2), cosθ is the cosine of the solar incidence angle as in step 2 above, d_r is the inverse squared relative earth-sun distance, and τ_{sw} is the atmospheric transmissivity.

Outgoing Longwave Radiation (RL↑): The outgoing longwave radiation is the thermal radiation flux emitted from the earth's surface to the atmosphere (W/m2). It is computed in SEBAL through the following steps (see the flow chart, Figure 6):

A. **Three commonly used vegetation indices** are computed (model F05). Normalized Difference Vegetation Index (NDVI), Soil Adjusted Vegetation Index (SAVI), and Leaf Area

Index (LAI) are computed using the reflectivity values found in model F02. Any one of these indices can be used to predict various characteristics of vegetation, according to preferences of the user.

The NDVI is the ratio of the differences in reflectivities for the near-infrared band (ρ4) and the red band (ρ3) to their sum:

$$\text{NDVI} = (\rho_4 - \rho_3) / (\rho_4 + \rho_3) \quad (13)$$

Where; ρ4 and ρ3 are reflectivities for bands 4 and 3 and are found in the output file of model F02. The NDVI is a sensitive indicator of the amount and condition of green vegetation. Values for NDVI range between -1 and +1. Green surfaces have a NDVI between 0 and 1 and water and cloud are usually less than zero.

The SAVI is an index that attempts to "subtract" the effects of background soil from NDVI so that impacts of soil wetness are reduced in the index. It is computed as:

$$\text{SAVI} = (1 + \text{L})(\rho_4 - \rho_3) / (\text{L} + \rho_4 + \rho_3) \quad (14)$$

Where; L is a constant for SAVI. If L is zero, SAVI becomes equal to NDVI. A value of 0.5 frequently appears in different literatures for L as cited by Bandara (2006). So, this value is used to better represent soils of the study area.

The LAI is the ratio of the total area of all leaves on a plant to the ground area represented by the plant. It is an indicator of biomass and canopy resistance. LAI is computed for Wonji Shoa sugarcane estate using the following empirical equation:

$$LAI = -\frac{ln\left(\frac{0.69 - SAVI}{0.59}\right)}{0.91} \quad (15)$$

The maximum value for LAI is 6.0, which corresponds to a maximum SAVI of 0.687. Beyond SAVI = 0.687, the value for SAVI "saturates" with increasing LAI and does not change significantly. The relationship between SAVI and LAI vary with location and crop type (Bastiaanssen et al., 2002).

B. Surface emissivity (ε): is the ratio of the thermal energy radiated by the surface to the thermal energy radiated by a blackbody at the same temperature. The satellite thermal sensor measures the absolute temperature of a black body, which could be an ideal/perfect absorber and re-emitter of all the irradiance falling on it. However, in real sense, due to atmospheric effects, surface roughness, moisture content, field of view and viewing angle of sensors, earth surface features have different gray levels other than being black. In SEBAL, emissivity is computed as a function of a vegetation index. The final term in Equation (4), $(1- \varepsilon) R_{L\downarrow}$, represents the fraction of incoming long wave radiation that is lost from the surface due to reflection. The emissivity of the study area is estimated based on NDVI images, through setting conditions for emissivity of crystal water to be 0.98 based on negative NDVI values with the assumption that they belong to water bodies which is regarded as near perfect emitter.

An alternative, operative (easy to apply) procedure is to obtain the land surface emissivity (LSE) image from the NDVI. Of the different approaches given in the literature (Sobrino & Raissouni, 2000; Valor & Caselles, 1996; Van de Griend & Owe, 1993), a modification of the last one has been used, the NDVI Thresholds Method—$NDVI^{THM}$, which shows a good working in comparison to a reference method as the one based on the Temperature independent spectral indices (TISI) indices (Becker & Li, 1990), as is pointed by Sobrino et al. (2001). The method proposed obtains the emissivity values from the NDVI considering different cases:

(a) NDVI < 0.2

In this case, the pixel is considered as bare soil and the emissivity is obtained from reflectivity values in the red region.

(b) NDVI >0.5

Pixels with NDVI values higher than 0.5 are considered as fully vegetated, and then a constant value for the emissivity is assumed, typically of 0.99

(c) $0.2 \leq NDVI \leq 0.5$

In this case, the pixel is composed by a mixture of bare soil and vegetation, and the emissivity is calculated according to the following equation:

$$\varepsilon = \varepsilon_v + P_v + \varepsilon_s(1 - P_v) + d_\varepsilon \quad (16)$$

Where ε_v is the vegetation emissivity and ε_s is the soil emissivity, P_v is the vegetation proportion obtained according to (Carlson & Ripley, 1997):

$$P_v = \left[\frac{NDVI - NDVI_{min}}{NDVI_{max} - NDVI_{min}}\right]^2 \quad (17)$$

where $NDVI_{max} = 0.5$ and $NDVI_{min} = 0.2$.

The term d_ε in Eq. (16) includes the effect of the geometrical distribution of the natural surfaces and also the internal reflections. For plain surfaces, this term is negligible, but for heterogeneous and rough surfaces, as forest, this term can reach a value of 2% (Sobrino, 1989). A good approximation for this term can be given by

$$d_\varepsilon = (1 - \varepsilon_s)(1 - P_v)F\ \varepsilon_v \quad (18)$$

where F is a shape factor (Sobrino et al., 1990) whose mean value, assuming different geometrical distributions, is 0.55.

Taking into account Equations (16) and (18), the LSE can be obtained as:

$$\varepsilon = m\ P_v + n \quad (19)$$

with

$$m = \varepsilon_v - \varepsilon_s - (1 - \varepsilon_s)F\ \varepsilon_v \quad (20a)$$

$$n = \varepsilon_s + (1 - \varepsilon_s)F\ \varepsilon_v \quad (20b)$$

In order to apply this methodology, values of soil and vegetation emissivities are needed. To this end, a typical emissivity value of 0.99 for vegetation has been chosen. The choice of a typical value for soil is a more critical question, due to the higher emissivity values variation for soils in comparison with vegetation ones. A possible solution is to use the mean value for the emissivities of soils included in the ASTER spectral library (http://asterweb.jpl.nasa.gov) and

filtered according to band TM6 filter function. In this way considering a total of 49 soils spectra, a mean value of 0.973 (with a standard deviation of 0.004) is obtained. Using these data (TM6 soil and vegetation emissivities of 0.97 and 0.99, respectively), the LSE are computed in model F06 using the following final empirical equations given by

$$\varepsilon_{TM6} = 0.004\, P_v + 0.986 \tag{21}$$

C. **The corrected thermal radiance from the surface** (R_c) is calculated following Coll *et al* 2010 as:

$$R_c = \frac{L_{6-}R_P}{\tau_{NB}} - (1-\varepsilon)R_{sky} \tag{22}$$

where; L_6 is the spectral radiance of band 6 from model F01 ($W/m^2/sr/\mu m$), R_p is the path radiance in the 10.4 – 12.5 μm band ($W/m^2/sr/\mu m$), R_{sky} is the narrow band downward thermal radiation for a clear sky ($W/m^2/sr/\mu m$), and τ_{NB} is the narrow band transmissivity of air (10.4 – 12.5 μm). Units for R_c are $W/m^2/sr/\mu m$.

The corrected thermal radiance (R_c) is the actual radiance emitted from the surface whereas L6 is the radiance that the satellite "sees". In between the surface and the satellite two things occur. First, some of the emitted radiation is intercepted by the atmosphere (transmissivity). Second, some thermal radiation is emitted by the atmosphere in the direction of the satellite (path radiance) and the satellite "thinks" that this is from the surface is confused as being emitted from the surface. Values for R_p and τ_{NB} require the use of an atmospheric radiation transfer simulation model such as Modtran and radiosonde profiles representing the image and date. In the absence of values for these terms, they can be ignored by setting $R_p = 0$ and $\tau_{NB} = 1$ and the R_{sky} term can also be ignored by setting $R_{sky} = 0$. This converts R_c into an uncorrected radiance (L_6). Fortunately, the effects of the three parameters on R_c are largely self-canceling. However, the result of no correction to L6 will be a general underestimation of surface temperature (Ts) by up to about 5 ^oC for warmer portions of an image.

Applying Atmospheric Correction: An atmospheric correction can be applied to Landsat data if you have local values for several meteorological parameters. NASA has a web page (http://atmcorr.gsfc.nasa.gov) that provides local values for transmittance, upwelling radiance, and downwelling radiance. Data are currently available from 2000 to the present.

Table 7. Atmospheric transmittance and path radiance during satellite overpasses time.

Parameters	Jan, 25	Feb, 26	Sept,06	Oct,08
τ_{NB}	0.92	0.88	0.87	0.83
R_p	0.53	0.91	0.91	1.16
R_{sky}	0.91	1.53	1.32	1.93

D. Land Surface temperature (T_s): The electromagnetic radiation exiting an object is termed radiant flux. The radiant temperature is highly correlated to the kinetic temperature. Thermal infrared system records radiant temperature. For a black body, the radiant temperature is the same as the kinetic temperature. The estimation of surface temperature depends on mineral composition of rocks, the condition of vegetation, roughness properties of land surfaces, thermal properties and moisture content of soils. The surface temperature (T_s) is computed in model F07 using the following modified Plank equation:

$$T_s = \frac{K_2}{\ln\left(\frac{\varepsilon \times K_1}{R_c} + 1\right)} \qquad (23)$$

Where; R_c is the corrected thermal radiance from the surface using L_6 from model F01. K1 and K2 are constants for Landsat images (table 6). Units for R_c must be the same as those for K1.

Table 8. Constants for Equation23 for Landsat7 ETM+ in $W/m^2/sr/\mu m$ (Landsat 7 Science User Data Handbook Chap.11, 2002).

	K1	K2
Landsat7 ETM+ Band6	666.09	1282.71

E. The outgoing longwave radiation ($R_{L\uparrow}$**)** is computed (model F08). This is computed using the Stefan-Boltzmann equation:

$$R_{L\uparrow} = \varepsilon \times \sigma \times T_s^4 \quad (24)$$

Where; ε is the "broad-band" surface emissivity (dimensionless), σ is the Stefan-Boltzmann constant (5.67×10^{-8} W/m^2/K^4), and T_s is the surface temperature (K).

Choosing the "Hot" and "Cold" Pixels: the SEBAL process utilizes two "anchor" pixels to fix boundary conditions for the energy balance. These are the "hot" and "cold" pixels and are located in the area of interest. The "cold" pixel is selected as a wet, well-irrigated crop surface having full ground cover by vegetation. The surface temperature and near-surface air temperature are assumed to be similar at this pixel. The "hot" pixel is selected as a dry, bare agricultural field where ET is assumed to be zero. Both of these "anchor" pixels should be located in large and homogeneous areas that contain more than one band 6 pixels (i.e. 60m×60m for Landsat 7). The selection of these "anchor" pixels requires skill and practice. The quality of the ET computations in SEBAL depends on a careful selection of these two pixels.

Incoming Longwave Radiation ($R_{L\downarrow}$**)**: The incoming longwave radiation is the downward thermal radiation flux from the atmosphere (W/m^2). It is computed using the Stefan-Boltzmann equation:

$$R_{L\downarrow} = \varepsilon \times \sigma \times T_a^4 \quad (25)$$

Where; ε is the atmospheric emissivity (dimensionless), σ is the Stefan-Boltzmann constant (5.67×10^{-8} W/m^2/K^4), and T_a is the near surface air temperature (K). The following empirical equation for ε by Bastiaanssen (1995) is applied using data from alfalfa fields in Idaho:

$$\varepsilon = 0.85 \times (-\ln \tau_{sw})^{0.09} \quad (26)$$

Where; τ_{sw} is the atmospheric transmissivity.

Substituting Equation (25) into Equation (26) and using T_{cold} from our "cold" pixel for Ta yields the following equation:

$$R_{L\downarrow} = 0.85 \times (-\ln \tau_{sw})^{0.09} \times \sigma \times T_{cold}^4 \quad (27)$$

Estimation of the Fluxes in the Surface Energy Balance Equation:

The second step of the SEBAL procedure is to compute the terms G and H of the surface energy budget equation. The net radiation flux (R_n) is the net amount of radiant energy that is available at the surface for warming the soil, warming the air, or evaporating soil moisture. This is written as the surface energy budget equation:

$$R_n = G + H + \lambda ET \quad (28)$$

Where; R_n is the net radiation at the surface (W/m^2), G is the soil heat flux (W/m^2), H is the sensible heat flux to the air (W/m^2), and λET is the latent heat flux (W/m^2). SEBAL computes λET as a "residual" of net radiant energy after soil heat flux and sensible heat flux are subtracted. This equation is solved through the following steps using the ERDAS Model Maker tool.

A. Soil Heat Flux (G)

Soil heat flux is the rate of heat storage into the soil and vegetation due to conduction. It depends on temperature gradient between the surface and soil and on thermal conductivity of the soil. SEBAL first computes the ratio G/R_n using the following empirical equation developed by Bastiaanssen (2000) representing values near midday:

$$\frac{G}{R_n} = \frac{(T_s - 273)}{\alpha}(0.0038\alpha + 0.0074\alpha^2)(1 - 0.98\,NDVI^4) \quad (29)$$

Where; Ts is the surface temperature (^oC), α is the surface albedo, and NDVI is the Normalized Difference Vegetation Index. G is then readily calculated by multiplying G/R_n by the value for R_n computed in model F09.

Soil heat flux is a difficult term to evaluate and care should be used in its computation. One must understand the area of interest in order to evaluate the accuracy of Equation (29). Values of G should be checked against actual measurements on the ground. Land classification and soil type will affect the value of G and a land-use map is valuable for identifying the various surface types.

B. Sensible Heat Flux (H)

Sensible heat flux is the rate of heat loss to the air by convection and conduction, due to a temperature difference. The sensible heat flux (H) is a function of the temperature gradient, surface roughness, and wind speed. It is computed using the following equation for heat transport:

$$H = \frac{\rho \times c_p \times dT}{r_{ah}} \tag{30}$$

Where; ρ is air density (kg/m^3), c_p is air specific heat (1004 J/kg/K), dT (K) is the temperature difference ($T_1 - T_2$) between two heights (z1 and z2), and r_{ah} is the aerodynamic resistance to heat transport (m/s).

Equation (30) is difficult to solve because there are two unknowns, r_{ah} and dT. To facilitate this computation, the two "anchor" pixels (where reliable values for H can be predicted and a dT estimated) and the wind speed at a given height were utilized.

The aerodynamic resistance to heat transport (r_{ah}) is computed for neutral stability as:

$$r_{ah} = \frac{ln\left(\frac{Z_2}{Z_1}\right)}{u_* \times K} \tag{31}$$

where; z_1 and z_2 are heights in meters above the zero plane displacement (d) of the vegetation, u_* is the friction velocity (m/s) which quantifies the turbulent velocity fluctuations in the air, and k is von Karman's constant (0.41). The friction velocity (u_*) is computed using the logarithmic wind law for neutral atmospheric conditions:

$$u_* = \frac{K u_x}{ln\left(\frac{Z_x}{Z_{om}}\right)} \tag{32}$$

where; k is von Karman's constant, u_x is the wind speed (m/s) at height z_x, and z_{om} is the momentum roughness length (m). Z_{om} is a measure of the form drag and skin friction for the layer of air that interacts with the surface.

The following steps are used to compute sensible heat flux (H):

1. The friction velocity (u_*) at the weather station is calculated for neutral atmospheric conditions using Equation (32).The assumption of neutral conditions for the weather station is reasonable if the weather station is surrounded by well-watered vegetation. The calculation of u_* requires a wind speed measurement (u_x) at a known height (z_x) at the time of the satellite image. This measurement is taken from the weather data that was set up earlier in the SEBAL process. The momentum roughness length (z_{om}) is empirically estimated from the average vegetation height around the weather station using the following equation (Brutsaert, 1982):

$$z_{om} = 0.12 \times h \quad (33)$$

Where; h is the vegetation height (m). (h=0.3m was chosen to represent the weather station).

2. The wind speed at a height above the weather station where one can assume no effect from the surface roughness is calculated. This height is referred to as the "blending height" and 200 meters is used. u_{200} is calculated using a rearranged Equation (32):

$$u_{200} = u_* \frac{\ln\left(\frac{200}{Z_{om}}\right)}{K} \quad (34)$$

The friction velocity (u_*) for each pixel is computed using the ERDAS Model Maker tool. u_{200} is assumed to be constant for all pixels of the image since it is defined as occurring at a "blending height" unaffected by surface features. From Equation (32):

$$u_* = \frac{Ku_{200}}{\ln\left(\frac{200}{Z_{om}}\right)} \quad (35)$$

Where; Z_{om} is the particular momentum roughness length for each pixel.

Momentum Roughness: The momentum roughness length (Z_{om}) is an important parameter in energy balance models, which influence the turbulent characteristics near the surface where the heat fluxes originate. There are different methods for determining Z_{om}: wind profile method, vegetation height, look-up table etc. In this study, its value was retrieved from the following empirical relation that involves computation of soil adjusted vegetation index developed by Moran and Jackson (1991).

$$Z_{om} = \exp(-5.809 + 5.62\ SAVI) \quad (36)$$

Where, Z_{om} is momentum roughness length and SAVI is soil adjusted vegetation index.

The aerodynamic resistance to heat transport (rah) is computed above and as is u_* in step 3. A series of iterations is required to determine the value for rah for each period that considers the impacts of instability (i.e., buoyancy) on rah and H. Assuming neutral atmospheric conditions, an initial rah is computed using Equation (31). z_1 is the height just above the zero plane displacement (d = 0.67 × height of vegetation) for the surface or crop canopy and z_2 is some distance above the zero plane displacement, but below the height of the surface boundary layer. Based on experienced analysis, values of 0.1 meter for z_1 and 2.0 meters for z_2 are assigned.

To compute the sensible heat flux (H) from Equation (30), the near surface temperature difference (dT) for each pixel needs to be defined. This is given as $dT = T_{z1} - T_{z2}$. The air temperature at each pixel is unknown, along with explicit values for T_{z1} and T_{z2}. Therefore, only the difference dT is utilized. SEBAL computes dT for each pixel by assuming a linear relationship between dT and T_s:

$$dT = b + a \times T_s \quad (37)$$

where; b and a are the correlation coefficients. To define these coefficients, SEBAL uses the two "anchor" pixels where a value for H can be reliably estimated. Values for H and dT at these "anchor" pixels are computed in a spreadsheet format and in the following steps. The linearity of the dT vs T_s function is a major presumption of SEBAL. However, research by Bastiaanssen and others and by the University of Idaho at Kimberly, indicate that this assumption appears to fit a large range of conditions.

Therefore, the dT coefficients were calculated as

$$a = \frac{dT_{hot} - dT_{cold}}{T_{shot} - T_{scold}} \quad (38)$$

$$b = dT_{cold} - a \times T_{scold} \quad (39)$$

Where dT_{hot} and dT_{cold}: dT values for the hot and cold pixels, respectively; T_{shot} and T_{scold}: corresponding values of surface temperature.

a) The cold pixel is located in the image as a pixel having one of the lowest surface temperatures, which is taken in SEBAL as indication of wetness. At the "cold" pixel, the sensible heat flux is defined as $H_{cold} = R_n - G - \lambda ET_{cold}$. Experience in Idaho shows that the most "cold" (wet) agricultural fields have an ET rate about 5% larger than the reference ET (ET_o). Hence, ET_{cold} is assumed to be $1.05 \times ET_o$ (which was calculated earlier in the SEBAL process).

H_{cold} is now calculated in the spreadsheet as: $H_{cold} = R_n - G - 1.05 \times \lambda ETr$. dT_{cold} is computed in the spreadsheet using the inverse of Equation (40):

$$dT_{cold} = \frac{H_{cold} \times r_{ah_{cold}}}{\rho_{cold} \times c_p} \quad (40)$$

Note: An alternative method used by Bastiaanssen is to choose the "cold" pixel at a body of water where one assumes $H_{cold} = 0$; and therefore, $\lambda ET_{cold} = R_n - G$ and $dT_{cold} = 0$ (in the "cold" pixel evaporation, most of the available energy (R_n-G) is assumed to be consumed by evapotranspiration, so that sensible heat flux (H), and consequently near surface air-temperature difference, dT, are both assumed to be near zero.) The use of Equation (40) and ET_o helps to consider the impact of regional advection and wind speed on ET. It also helps account for any error in image estimates for albedo and R_n by SEBAL.

b) The "dry" pixel is represented by a pixel with high temperature, which is taken in SEBAL as indicator of lack of surface moisture, where evaporation is near zero so that all the available energy is converted essentially into sensible heat. At the "hot" pixel, $H_{hot} = R_n - G - \lambda ET_{hot}$; where ET_{hot} is assumed to be zero for a "hot" (dry) agricultural field having no green vegetation and with dry soil surface layer. The weather data should be checked to see if this assumption is correct. If there was some precipitation 1-4 days before the image date, then ET_{hot} should be

estimated using a water balance model and tracking the soil moisture of the "hot" pixel. H_{hot} is now calculated in the spreadsheet and dT_{hot} computed from Equation (40). The correlation coefficients, b and a, are now computed for the linear relationship: $dT = b + aT_s$. The temperature differential (dT) for each pixel can now be computed using the coefficients b and a and the surface temperature (T_s). The determination of dT at the anchor pixels and b and a are done in the spreadsheet.

3. In order to account for the buoyancy effects generated by surface heating, SEBAL applies the Monin-Obukhov theory in an iterative process (Figure 8). Atmospheric conditions of stability have a large effect on the aerodynamic resistance (r_{ah}) and must be considered in the computation of sensible heat flux (H), especially for dry conditions. SEBAL repeats the computation of H through a number of iterations, each one correcting for buoyancy effects, until the value for rah stabilizes.

The Monin-Obukhov length (Q) is used to define the stability conditions of the atmosphere in the iterative process. It is a function of the heat and momentum fluxes and is computed as follows:

$$Q = \frac{\rho\, C_P\, u_*^3\, T_s}{K\, g\, H} \tag{41}$$

where; ρ is the density of air (kg/m^3), cp is the air specific heat (1004 J/kg/K), u_* is the friction velocity (m/s), Ts is the surface temperature (K), g is the gravitational constant (9.81 m/s^2), and H is the sensible heat flux (W/m^2). Values of Q define the stability conditions of the atmosphere. If Q<0, the atmosphere is considered unstable; if Q>0, the atmosphere is considered stable; if Q=0, the atmosphere is considered neutral. Depending on the atmospheric conditions, the values of the stability corrections for momentum and heat transport (ψ_m and ψ_h) are computed using the formulations by Paulson (1970) and Webb (1970):

$$\psi_m = 2\ln\left(\frac{1+x}{2}\right) + \ln\left(\frac{1+x^2}{2}\right) - 2\tan^{-1}x + \frac{\pi}{2} \tag{42}$$

$$\psi_h = 2\ln\left(\frac{1+x^2}{2}\right) \tag{43}$$

where, x is given by:

$$x = \left(1 - 16\,\frac{Z_{ref}}{Q}\right)^{0.25} \tag{44}$$

4. A corrected value for the friction velocity (u_*) is now computed for each successive iteration as:

$$u_* = \frac{u_{200} \times K}{\ln\left(\frac{200}{Z_{om}}\right) - \psi_{m(200m)}} \tag{45}$$

where; u_{200} is the wind speed at 200 meters (m/s), k is von Karman's constant (0.41), Z_{om} is the roughness length for each pixel (m), and ψ_m(200m) is the stability correction for momentum transport at 200 meters.

5. A corrected value for the aerodynamic resistance to heat transport (r_{ah}) is now computed during each iteration as:

$$r_{ah} = \frac{\ln\left(\frac{Z_2}{Z_1}\right) - \psi_{h(Z_2)} + \psi_{h(Z_1)}}{u_* \times k} \tag{46}$$

where; z_2 = 2.0 meters, z_1 =0.1 meters, and $\psi_{h(z2)}$ and $\psi_{h(z1)}$ are the stability corrections for heat transport at 2 meters and 0.1 meters.

This iterative process is repeated until the successive values for dT_{hot} and r_{ah} at the "hot" pixel has stabilized and next the final corrected value for the sensible heat flux (H) at each pixel is computed, which will be used in the computation of the instantaneous ET at each pixel.

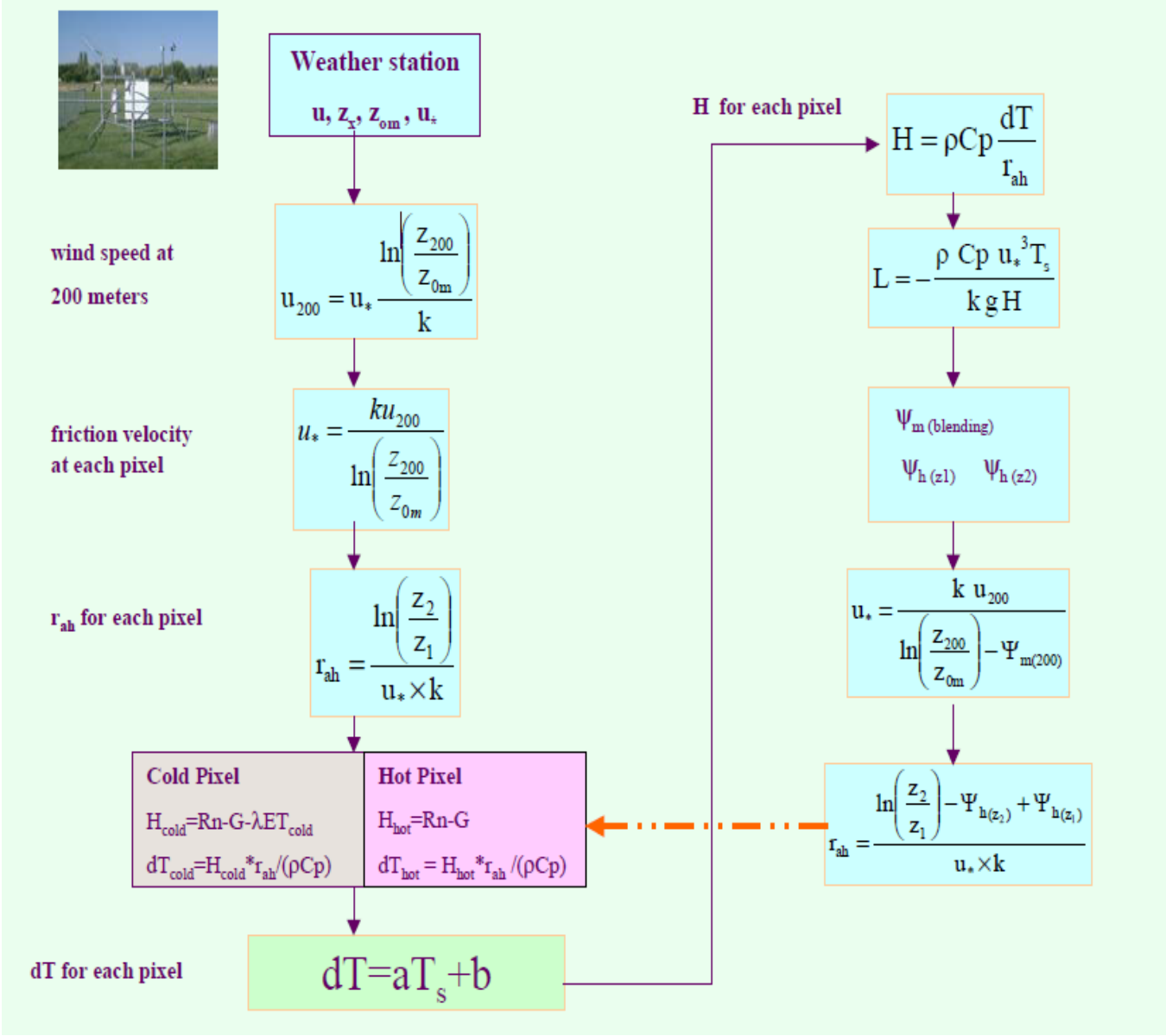

Figure 8. Flow Chart of the Iterative Process for the Calculation of Sensible Heat (H)

C. Latent Heat Flux (λET), Instantaneous ET (ET_{inst}), and Reference ET Fraction (ET_rF)

Evaporation process needs conversion of water into water vapor. This requires energy input known as latent heat of vaporization which is the rate of latent heat loss from the surface due to evapotranspiration. In SEBAL mode latent heat flux is computed as residual variables of the energy balance equation. It can be computed for each pixel using Equation (1):

$$\lambda ET = R_n - G - H \quad (1)$$

Where; λET is an instantaneous value for the time of the satellite overpass (W/m^2).

An instantaneous value of ET in equivalent evaporation depth is computed as:

$$\mathrm{ETinst} = 3600\ \frac{\lambda \mathrm{ET}}{\lambda} \tag{47}$$

where; ET_{inst} is the instantaneous ET (mm/hr), 3600 is the time conversion from seconds to hours, and λ is the latent heat of vaporization or the heat absorbed when a kilogram of water evaporates (J/kg).

The reference ET Fraction (ET_rF) is defined as the ratio of the computed instantaneous ET (ET_{inst}) for each pixel to the reference ET (ET_o) computed from weather data:

$$\mathrm{ETrF} = \frac{\mathrm{ETinst}}{\mathrm{ET_o}} \tag{48}$$

Where; ET_{inst} is from Equation 28 (mm/hr) and ET_o is the reference ET at the time of the image from the CROPWAT software (mm/hr). ET_rF is similar to the well-known crop coefficient, K_c. ET_rF is used to extrapolate ET from the image time to 24-hour or longer periods.

One should generally expect ET_rF values to range from 0 to 1. At a totally dry pixel, ET = 0 and ET_rF = 0. A pixel in a well-established field of alfalfa or corn can occasionally have an ET slightly greater than ET_o and therefore ET_rF > 1, perhaps up to 1.1. However, ET_o generally represents an upper bound on ET for large expanses of well-watered vegetation. Negative values for ET_rF can occur in SEBAL due to systematic errors caused by various assumptions made earlier in the energy balance process.

Daily (24-Hour) Evapotranspiration (ET_{24}): Daily values of ET (ET_{24}) are often more useful than instantaneous ET. SEBAL computes the ET_{24} by assuming that the instantaneous ET_rF computed above is the same as the 24-hour average and ET varies throughout the day while ET_rF is relatively constant. Finally, the ET_{24} (mm/day) can be computed as:

$$\mathrm{ET_{24}} = \mathrm{ETrF} \times \mathrm{ET_{o-24}} \tag{49}$$

Where; $ET_{o\text{-}24}$ is the cumulative 24-hour ET_o for the day of the image. This is calculated by adding the hourly ET_o values over the day of the image.

MODIS ETa Estimation: The MOD16 global ET datasets were estimated using Mu et al.'s improved ET algorithm (2011) over previous Mu et al.'s paper (2007a). The ET algorithm is based on the Penman-Monteith equation (Monteith, 1965) and finally the processed MODIS-MOD16 global ET values were multiplied by 0.1 and then divided by 8 to get the real ET values in mm/day for all image dates considered in this study (Mu et al., 2011).

3.2.2.3 SSEB model overview and parameter estimation

Land surface Energy Balance (EB) approaches are based on the rationale that ET is a function of change of the state of water using available energy in the environment for vaporization (Su et al., 2005). Remote sensing based EB models convert satellite sensed radiances into land surface characteristics such as albedo, leaf area index, vegetation indices, surface emissivity, and surface temperature to estimate ET as a "residual" of the land surface energy balance equation.

Although solving the full EB-based approach has been shown to give good results, the data and skill requirements to solve various terms in the equation are prohibitive for operational applications. The SSEB approach estimates actual ET while maintaining and extending the major assumption in SEBAL (Bastiaanssen et al., 1998) and METRIC (Allen et al., 2007a), whereby the aerodynamic temperature gradient between the land surface and air (near-surface temperature gradient) varies linearly with land surface temperature. This relationship is based on two anchor pixels known as the hot and cold pixels, representing bare dry agricultural fields and well-vegetated wet fields, respectively. In SEBAL, at the cold (satellite) pixel, H is assumed negligible (i.e. H_{cold}=0) and at the hot pixel, LE is set to zero which results in $H_{hot} = (R_n – G)$ hot. In METRIC, at the cold pixel, H is based on a reference ET (Allen et al., 2007a) using ground weather data using the Penman-Monteith equation for tall (~0.5 m) alfalfa and at the hot pixel, LE is set to zero which results in $H_{hot} = (R_n – G)$hot similar to SEBAL. In SSEB, this assumption is extended where LE also varies linearly between the hot and cold pixels in proportion to the land surface temperature. This assumption is based on the logic that the temperature difference between soil surface and air is linearly related to soil water (Sadler et al., 2000). Furthermore, crop water balance models estimate actual ET using a linear reduction from the potential ET depending on the soil water (Allen et al., 1998; Senay and Verdin, 2003). Furthermore, this approach can be compared with the Crop Water Stress Index (CWSI) (Jackson, 1982) derived

from the temperature difference between the crop canopy and the air. Dividing the canopy-air temperature difference by the known upper and lower canopy-air temperature difference creates a ratio index varying between 0 and 1. The upper limit is reached when plant transpiration is zero, because no plant available water in the soil profile (Qiu et al., 1999) and the lower limit is reached when the crop transpires at full rate. In SSEB, surface temperature values of cold and hot pixels are equivalent to the lower and upper limiting canopy temperatures of the CWSI method.

The SSEB model, driven by the ET fraction calculated from the thermal data provide reasonable ET estimation for irrigated fields with uniform topography. The main concept of the SSEB approach in Senay et al. (2007) is the joint use of reference ET and land surface temperature data. The surface energy balance is first solved for a reference crop condition (assuming full vegetation cover and unlimited water supply) using the standardized Penman–Monteith equation (Allen et al., 1998). ET fractions (ETf) account for differences in water availability in the landscape; and are used to adjust the reference ET (ET_o) based on the LST of the pixel (Eq. (2) for ETf).

In the SSEB model formulation, ET fractions are calculated from the LST data sets based on the assumptions that hot pixels experience little or no ET (Bastiaanssen et al., 1998; Allen et al., 2005), cold pixels represent “maximum” ET, and, with the simplified assumption, that ET can be scaled between these values in proportion to LST. Allen et al. (2005, 2007a) have outlined a procedure for using a water balance approach to determine the ET of a moist bare soil in case satellite images are acquired after rainfall events. This ET estimate is used to define the ET fraction for the hot pixel.

In principle, instantaneous LST at satellite overpass time can be used to identify hot and cold pixels which in turn can be used to calculate proportional fractions of ET on a per pixel basis. The hot and cold pixels are selected using an NDVI image as a guide to identify dry and bare areas for the hot pixels. Similarly, the cold pixels are selected from well-watered, well-vegetated areas or nearby water bodies.

In this study, irrigated areas were used to select the cold pixels, following similar procedures used in METRIC (Allen et al., 2007a). Cool (lower LST) irrigation fields with higher NDVI

values were used for guidance. The hot pixels were selected from bare (dry) areas found close to irrigated fields based on the guidance and justification provided by Allen et al. (2007a) to avoid desert soil pixels that may develop crusts and delamination with mulches which in turn tend to reduce the thermal conductivity of the surface that again reduces soil heat flux density. Choosing desert pixels for the "hot" would result in unrealistically higher ET values for the generally cooler (which maybe be wrongly attributed to ET) but dry bare agricultural soils due to their relatively higher ground heat conductivity.

The approach of most energy balance models requires solving the energy balance (Eqs. (1)) at the land surface, where the latent heat flux, comparable to ETa, is calculated as the residual of the difference between the net radiation to the surface and losses due to the sensible heat flux (energy used to heat the air) and ground heat flux (energy stored in the surface).

The ET fraction (ETf) is calculated for each pixel "x" by applying Eq. (50) to each of the 4-date Landsat LST grids.

$$\mathrm{ETf} = \frac{\mathrm{TH} - \mathrm{Tx}}{\mathrm{TH} - \mathrm{TC}} \tag{50}$$

where TH and TC are the average radiometric surface temperature at hot and cold pixels, respectively; and Tx is the radiometric surface temperature for any given pixel in that image.

The basic approach of calculating ETa involves only two steps: ETa is simply a product of the ET fraction (ETf) and ET_o via Eqs. (51) and (52).

$$\mathrm{ETa} = \mathrm{ETf} \times \mathrm{ETm} \tag{51}$$

where ETa is actual ET, ETf is ET fraction, and ETm is maximum ET for the region. When grass reference ETo is calculated from weather data, ETm is estimated as:

$$\mathrm{ETm} = \alpha \times \mathrm{ET_o} \tag{52}$$

where the multiplier α is recommended to be 1.2 to estimate ET for tall, full cover crops such as alfalfa, corn, sugarcane and wheat.

Crops such as alfalfa, corn, sugarcane and wheat are aerodynamically rougher than the clipped grass reference and have greater leaf area and thus greater canopy conductance (Allen et al.,

1998). Thus, the 1.2 multiplier is not needed if ETr (based on alfalfa crop) is used instead of ET_o. Alternatively, α can be determined using localized calibration such as one with Gowda et al. (2009) who determined α to be 1.1 using Lysimeter data in the Texas Panhandle.

3.2.2.4 New parameterization approach ($SSEB_{op}$)

The method is developed by Senay et al. (2013) and it is based on the Simplified Surface Energy Balance (SSEB) approach which is now parameterized for operational applications, renamed as $SSEB_{op}$. The innovative aspect of the $SSEB_{op}$ parameterization is that it uses pre-defined, boundary conditions that are unique to each pixel for the "hot" and "cold" reference conditions. This approach pre-defines unique sets of "hot" and "cold" reference values for each pixel unlike the original SSEB formulation or similar models (e.g., SEBAL or METRIC) that uses a set of reference hot and cold pixels pairs applicable for a limited, uniform hydro-climatic region. To estimate ET routinely, the only data needed for this method are T_s, climatology air temperature (T_a) and ET_o. This is a bold proposition, but grounded in the scientific knowledge that most of the surface energy balance process is driven by the available net solar radiation. Since thermal remote sensing is conducted under-clear sky conditions, it is assumed that the boundary conditions for the hot and cold reference points should not change from year-to-year or the changes are little in relation to the accuracy level obtained through varying boundary conditions. With this basic assumption the hot and cold boundary conditions for a given pixels and periods are fixed as a function of largely the net solar radiation.

With this simplification, actual ET (ET_a) is estimated using equation 53 as a fraction of the ET_o and the ET fraction (ETf) is calculated using equation 54.

$$ETa = ETf \times \alpha ET_o \quad (53)$$

Where ET_o is the grass reference ET for the location; α is a coefficient that scales up grass reference ET into the level of a maximum ET experienced by an aerodynamically rougher crop. A recommended value for α is 1.2. However, the actual magnitude of α should be determined using a validation/calibration process using field data such as Lysimeter or Flux Towers since the calculation of the pre-defined parameters may already incorporate a compensating bias.

$$ETf = \frac{T_h - T_s}{T_h - T_c} \quad (54)$$

Where T_s is the satellite observed land surface temperature of the pixel whose ETf is being evaluated on a given time-period. T_h is the estimated Ts at the idealized reference "hot" condition of the pixel for the same time periods, the cold reference value Tc, is the estimated *Ts* at the idealized reference "cold" condition of the pixel of the same time period. The difference between T_h and T_c is simply the dT that will be discussed later.

T_c determination: With the new parameterization in SSEBop, T_c for any given period and pixel is approximated as being close (with a correction factor to be discussed later) to the corresponding climatological T_a. This is based on the established fact that for a given clear-sky day, the land surface will experience an ET rate equal to the potential rate (healthy, well-watered vegetation, or well-watered bare soil) when its T_s is close to the near-surface air temperature (i.e., little or no sensible heat). The operational processing can be simplified by using a climatological maximum T_a instead of the hourly T_a temperature that corresponds with the satellite overpass.

Exploratory work showed that the year-to-year variability of air temperature over well watered vegetation (NDVI > 0.8) is relatively small, with a much lower variability compared to the T_s over the same surface. Although comparable results can be obtained using either the daily average or maximum Ta, the use of the daily maximum T_a is easier to understand in relation to the instantaneous T_s. However, a correction is necessary for using the T_a as surrogate for T_c for two reasons: a) T_s and T_a are not expected to correspond in magnitude (even at the cold pixel) since the methods and principles of data acquisition are different, but they are expected to correlate well in temporal variability for a given location b) the two temperatures will be acquired at different times; the maximum Ta generally occur in the afternoon while the day time satellite overpass (Landsat) for the T_s occurs before noon.

The use of T_a for the cold boundary condition is a very important assumption and holds one of two keys for the simplification process. Thus, careful attention should be given to make sure the two datasets correspond well. This can be checked using the corresponding T_s and T_a from well

watered vegetation in different parts of the study region. When there is a systematic bias in this relationship, a simple correction for bias is performed to solve the problem.

The T_c boundary condition was determined using the following correction coefficient.

$$T_c = c \times T_a \quad (55)$$

Where T_a is the climatology near-surface maximum T_a for the period; c is a correction factor that relates T_a to T_s on a well-watered, fully transpiring vegetation surface. The correction coefficient c is determined as a seasonal average between T_s and T_a on all pixels where NDVI is greater or equal to 0.8. Preliminary results showed that this coefficient vary little from place to place; therefore, a single spatially averaged c factor were used for the entire study area for simplicity and with this assumption the spatial differences were too small for operational application. However, for localized applications, one is advised to develop local-specific 'c' values.

$$c = \frac{T_{scold}}{T_a} \quad (56)$$

Where T_{scold} is the satellite-based T_s at the cold pixel where NDVI > 0.8 and T_a is the corresponding air temperature at same location and season. The correction is calculated as the spatially averaged values of available locations. These areas are usually obtained in peak-season irrigated areas and forested regions. The value of this correction factor was determined to be 0.989 when both T_s and T_a were processed in Kelvin units.

Pre-defined dT and hot boundary condition: Once the T_c is defined as the fraction of the climatological T_a, the hot boundary condition (T_h) can also be defined by a constant difference (dT) that will be added to the T_c of each pixel on a given time period. The observed dT (difference between hot and cold image T_s value) during the peak crop growing season has been observed to be in the order of 20 K (roughly varying between 15 and 25 degrees based on location, in most locations (evaluated using T_s data in US, Africa and Afghanistan by Senay et al., 2007 and Senay, 2011a). Similar dT ranges have been reported by Qiu et al., 1998. In this new parameterization, the innovative approach is to use a pre- determined seasonally dynamic

dT that is unique to each location anywhere in the world. Thus, the second key component of the simplification is in the estimation of dT from energy balance principles for a clear sky condition. Clear sky is specified because that is an important condition for the usefulness of the thermal-based remote sensing ET estimation.

The pre-defined dT is solved from the R_n equation solved for a bare, dry soil where ET is assumed to be zero and sensible heat is assumed maximum (Bastiaanssen, 1998; Allen et al., 2007a). The radiation balance for a bare, dry soil can be written as follows:

$$R_n = LE + H + G \quad (57)$$

where LE is the latent heat flux (equivalent to ET with the use of the heat of vaporization multiplier), H is the sensible heat flux and G is the ground heat flux in energy units. Since *LE* and *G* are considered 0.0, the magnitude of the R_n can be equated with the sensible heat equation as:

$$R_n = H = p \times c_p \times dT/r_a \quad (58)$$

Since all R_n is now assumed to be used for sensible heat flux at the hot boundary condition, H will be approximated by the clear-sky net radiation received at an idealized bare and dry surface for a given pixel on a given period. The next step is to estimate the available clear-sky net radiation that is available for a given period so that dT can be solved by rearranging Equation 58 as shown in Equation 68.

Clear-sky net radiation is estimated using a series of equations as presented with the Food and Agricultural Organization (FAO) publication number 56 (Allen et al., 1998). R_n is estimated as the difference between net shortwave (R_{ns}) and the outgoing net long-wave radiation (R_{nl}).

$$R_n = R_{ns} - R_{nl} \quad (59)$$

$$R_{ns} = (1 - \alpha)R_s \quad (60)$$

Where R_{ns} [MJ $m^{-2}day^{-1}$] is net solar or shortwave radiation; α is the albedo or canopy reflection coefficient. A value of 0.23 is recommended for grass reference crop and this value is assumed the same for the general landscape; Rs [MJ $m^{-2}day^{-1}$] is incoming solar radiation.

$$R_s = 0.75 \times R_a \quad (61)$$

Where R_a is extraterrestrial radiation [$MJm^{-2}day^{-1}$]; 0.75 is a suggested correction coefficient in the absence of measured data to represent a fraction of R_a reaching the surface of the earth on clear days (Allen et al., 1998).

R_a for each day of the year and a given modeling pixel (latitude) can be estimated from a solar constant, the solar declination and time of the year (Allen et al, 1998).

$$R_a = \frac{24 \times 60}{\pi} G_{sc} d_r [\omega_s \sin(\varphi)\sin(\delta) + \cos(\varphi)\cos(\delta)\sin(\omega_s)] \quad (62)$$

Where, G_{sc} [$MJm^{-2}day^{-1}$] is solar constant (0.0820); d_r [-] is inverse relative earth-sun distance (Equation 11), δ [rad] is solar declination, (Equation 12). The latitude φ [rad] is positive for northern hemisphere and negative for southern hemisphere. ω_s [rad] is sunset hour angle (Equation 13); the inverse relative earth-sun distance, d_r is given by:

$$d_r = 1 + 0.033 \times \cos\left(\frac{2\pi}{365} J\right) \quad (63)$$

The solar declination angle δ is given by:

$$\delta = 0.409 \sin\left(\frac{2\pi}{365} J - 1.39\right) \quad (64)$$

Where J is the day number in a year, between January 1 and December 31st.

The sunset hour angle ω_s is given by:

$$\omega s = \arccos[-\tan(\phi)\tan(\delta)] \quad (65)$$

To solve Equation 7, we also need the estimation of R_{nl}. There are several equations to estimate R_{nl}; due to its simplicity and availability of limited data, the one proposed by FAO 56 in Allen et al. (1998) were used. Because the boundary conditions are established under the assumption of clear-sky, Rnl is estimated as

$$R_{nl} = \sigma\left(\frac{T_{max}{}^4 + T_{min}{}^4}{2}\right)\left(0.34 - 0.14\sqrt{e_a}\right)\left(1.35\left(\frac{R_s}{R_{so}}\right) - 0.35\right) \quad (66)$$

Where R_{nl} is net long-wave radiation [$MJm^{-2}day^{-1}$]; σ is Stefan-Boltzmann constant ($4.903*10^{-9}$) ($MJK^{-4}m^{-2}day^{-1}$]; T_{max} and T_{min} are maximum and minimum absolute temperature [K], i.e., $K={}^{o}C$ + 273.16; $\frac{R_s}{R_{so}}$ is the relative shortwave radiation (<= 1.0) where R_s is the calculated solar radiation (Equation 9) based on the cloudiness factor; R_{so} is the calculated clear-sky radiation. In this case, the ratio is 1.0 due to the assumption of clear-sky boundary condition; e_a is the actual vapor pressure [kPa] estimated with the following equation (67);

$$e_a = e^o(T_{min}) = e^{\left(\frac{17.27\times T_{min}}{T_{min}+237.3}\right)} \quad (67)$$

Where $e^o(T_{min})$ is the saturated vapor pressure that is occurring at daily minimum temperature (T_{min} in ^{o}c). Allen et al. (1998) recommends the use of dew point temperature (approximated by T_{min}) for the estimation of e_a when humidity data are not available or of questionable quality.

Although the assumption of equating the minimum temperature to the dew point is only valid in well-watered covers, it is assumed that this will serve the purpose of establishing generalized boundary conditions, considering the many simplifications in the approach. Furthermore, both T_{max} and T_{min} in Equation 15 are based on climatology data. After R_n is estimated for each pixel, the pre-defined dT was solved using Equation 68 below, a rearranged form of Equation 58.

dT was solved using R_n, c_p and ρ and r_a as follows:

$$dT = \frac{R_n \times r_a}{\rho \times c_p} \quad (68)$$

Where c_p is the specific heat of air at constant pressure (1.013 kJ kg^{-1} $^oC^{-1}$); ρ is the density of air which is calculated using Equation 17 (Allen et al., 1998); r_a is the aerodynamic resistance to heat flow from a hypothetical bare and dry surface; it was determined through a quasi-calibration process as explained later.

$$\rho = \frac{1000P}{T_{kv} R} = \frac{3.486P}{T_{kv}} \quad (69)$$

Where ρ is the atmospheric density [kg m^{-3}]; R is the specific gas constant of 287 [J $kg^{-1}K^{-1}$]; T_{kv} is the virtual temperature, a temperature at which dry air must be heated to equal the density of moist air at the same pressure. For the average condition (e_a in the range of 1 to 5 kPa and P between 80 and 100 kPa), Allen et al. (1998) recommends the use of T_{kv} = 1.01 (T + 273) where T is the mean daily temperature [^o_C].

$$P = 101.3\left(\frac{293 - 0.0065 \times Z}{293}\right)^{5.26} \quad (70)$$

Assuming atmospheric pressure at sea level is 101.3 [kPa]; 293 is reference temperature [K] at sea level; Z is elevation [m].

Obviously, given a set of field dT values (obtained from Ts imagery as the difference between the hot and cold pixel values), the r_a magnitude will depend on the R_n calculation since the other parameters are relatively stable or change in small magnitude. A trial-and-error approach was used to determine the r_a value for SSEBop. This was done by inspecting the r_a value that matches the dT differences observed between the observed hot (bare areas) and cold (vegetated) Ts values in several well irrigated fields of Wonji Shoa sugarcane plantation during the peak growing season.

Qiu et al. (1998) showed that r_a of a dry soil is the same everywhere. Earlier, Calder (1977) stated that the improvements obtained by varying r_a with wind speed maybe small. Qui et al. (1998) showed that the r_a values for a drying soil surfaces (bare area with different levels of soil moisture) to be in the range between 60 and 120 ms^{-1}, indicating the dry part of the r_a value being close to the higher end. This suggests that r_a value of 110 ms^{-1} for the dry boundary condition can be used for a useful operational estimation of ET, in this method where the interest is the use of

remotely sensed thermal data for a quick and consistent estimation of ET using one single variable alone, i.e., as a result of changes in land surface temperature. Furthermore, comparison with 45 US flux tower ET in 2005 shows that 110 ms^{-1} gives a reasonable agreement and decided to fix the r_a value at 110 ms^{-1}.

Note that a different R_n calculation will require a different estimation of r_a. However, the most important point is once the r_a is fixed, the dT equation can be applied to any location and season to obtain a location-specific and seasonally varying dT that is expected to occur under clear sky conditions. The minimum dT occurs in the winter and since the accuracy of the method reduces at lower dT and does not make physical sense to have a negative dT for a relevant ET estimation, dT minimum have limited to 1K.

Therefore, once the expected dT is determined, the hot boundary condition can be defined simply by adding the dT to the Tc as shown in Equation 71.

$$Th = Tc + dT \tag{71}$$

Table 9. dT values of each image for use in SSEBop

Serial Number	Acquisition Date	DOY	dT(K)
1	January 25,2002	25	17.57
2	February 26,2002	57	20.01
3	September 06,2002	249	21.25
4	October 08,2002	281	19.46

3.2.2.5 Estimating potential evapotranspiration (ET_o)

It is evapotranspiration if adequate water supply is available to a vegetated surface. As water is abundantly available at the reference evapotranspiring surface, soil factors do not affect ET. Relating ET to a specific surface provides a reference to which ET from other surfaces can be related. It obviates the need to define a separate ET level for each crop and stage of growth. To obviate the need to define unique evaporation parameters for each crop and stage of growth, the

concept of a reference surface was useful in cropped area. Evapotranspiration rates of the various crops were related to the evapotranspiration rate from the reference surface (ET_o) by means of crop coefficients (k_c).

The FAO Expert Consultation on Revision of FAO Methodologies for Crop Water Requirements accepted the following unambiguous definition for the reference surface:

"A hypothetical reference crop is with an assumed crop height of 0.12 m, a fixed surface resistance of 70 m s^{-1} and an albedo of 0.23."

The only factors affecting ET_o in the study area are climatic parameters. Consequently, ET_o is a climatic parameter and is computed from weather data. ET_o expresses the evaporating power of the atmosphere at a specific location and time of the year and does not consider the crop characteristics and soil factors. The FAO Penman-Monteith method is used as the sole method for determining ET_o and explicitly incorporates both physiological and aerodynamic parameters.

$$ET_o = \frac{0.408\,\Delta(R_n - G) + \gamma \frac{900}{T + 273} u_2 (e_s - e_a)}{\Delta + \gamma(1 + 0.34\,u_2)} \qquad (72)$$

Where ET_o reference evapotranspiration [mm/month],

R_n net radiation at the grass surface [MJ m^{-2} $month^{-1}$],

G soil heat flux density [MJ m-2 month-1],

T mean hourly air temperature [°C],

Δ saturation slope vapour pressure curve at T [kPa °C-1],

γ psychrometric constant [kPa °C-1],

e_s-e_a saturation vapour pressure deficit [kPa],

e_s saturation vapour pressure [kPa],

e_a average hourly actual vapour pressure [kPa],

u_2 average hourly wind speed [m s-1].

R_n and G is energy available per unit area and expressed in MJ m^{-2} day^{-1}. To convert the energy units for radiation to equivalent water depths (mm) the latent heat of vaporization, λ is used as a conversion factor.

$$\gamma = \frac{C_p P}{\varepsilon \lambda} = 0.665 \times 10^{-3} P \quad (73)$$

where γ psychrometric constant [kPa °C^{-1}],

P atmospheric pressure [kPa],

λ latent heat of vaporization, 2.45 [MJ kg^{-1}],

c_p specific heat at constant pressure, 1.013×10^{-3} [MJ kg^{-1} °C^{-1}],

ε ratio molecular weight of water vapour/dry air = 0.622.

$$P = 101.3 \left(\frac{293 - 0.0065\, z}{293}\right)^{5.26} \quad (74)$$

Where P atmospheric pressure [kPa],

z elevation above sea level [m],

As saturation vapour pressure is related to air temperature, it is calculated from the air temperature. The relationship is expressed by:

$$e^0(T) = 0.6108\, exp\left(\frac{17.27\, T}{T + 237.3}\right) \quad (75)$$

Where e°(T) saturation vapour pressure at the air temperature T [kPa],

T air temperature [°C],

exp(...) 2.7183 (base of natural logarithm) raised to the power [..].

Due to the non-linearity of the above equation, the mean saturation vapour pressure for a day, week, decade or month should be computed as the mean between the saturation vapour pressure at the mean daily maximum and minimum air temperatures for that period:

$$e_s = \left(\frac{e^0(T_{max}) - e^0(T_{min})}{2}\right) \quad (76)$$

For the calculation of evapotranspiration, the slope of the relationship between saturation vapour pressure and temperature, Δ, is required. The slope of the curve at a given temperature is given by:

$$\Delta = \frac{4098\left[0.6108\ exp\left(\frac{17.27\ T}{T + 237.3}\right)\right]}{(T + 237.3)^2} \quad (77)$$

The actual vapour pressure can also be calculated from the relative humidity. Depending on the availability of the humidity data, different equations should be used.

$$e_a = \frac{e^0(T_{min})\frac{RH_{max}}{100} + e^0(T_{max})\frac{RH_{min}}{100}}{2} \quad (78)$$

where e_a actual vapour pressure [kPa],

e^0 (Tmin) saturation vapour pressure at daily minimum temperature [kPa],

e^0 (Tmax) saturation vapour pressure at daily maximum temperature [kPa],

RH_{max} maximum relative humidity [%],

RH_{min} minimum relative humidity [%].

The extraterrestrial radiation, Ra, for each day of the year and for different latitudes can be estimated from the solar constant, the solar declination and the time of the year by:

$$R_a = \frac{24(60)}{\pi}\ G_{sc} d_r [\omega_s sin(\varphi) sin(\delta) + cos(\varphi) cos(\delta) sin(\omega_s)] \quad (79)$$

Where R_a extraterrestrial radiation (MJ m^{-2} day^{-1}),

G_{sc} solar constant = 0.0820 (MJ m^{-2} min^{-1}),

d_r inverse relative Earth-Sun distance,

ω_s sunset hour angle (rad),

φ latitude (rad)

δ solar declination [rad].

Table 10. ETo computed by CROPWAT

MONTHLY REFERENCE EVAPOTRANSPIRATION PENMAN MONTEITH							
Country: Ethiopia Station: Wonji Altitude: 1540 m			Latitude: 8.25° N Longitude: 39.15° E				
Month	Min Temp	Max Temp	Humidity	Wind	Sunshine	Radiation	ETo
	°C	°C	%	km/day	hours	MJ/m²/day	mm/month
January	12.4	25.9	58	193	8.9	20.8	137.95
February	11.3	29	44	199	10.1	23.8	155.68
March	14.3	29.2	54	157	8.2	22	155.31
April	15.8	29.4	51	169	9	23.4	162.9
May	15.6	30.8	51	139	9.3	23.2	164.61
June	15.6	29.4	55	176	8.9	22.1	156.3
July	15.3	28.2	59	180	8.4	21.5	153.45
August	15.5	25.8	68	150	6.7	19.5	128.34
September	14.6	27	66	115	7.7	21.1	129.9
October	10.6	28.6	47	177	9.5	23.1	164.3
November	9.7	27.7	43	210	9.7	22.1	157.8
December	13.7	25.4	61	189	6.5	17	120.59
Average	13.7	28	55	171	8.6	21.6	1787.13
Cropwat 8.0							

As it is shown in Table 10, annual potential evapotranspiration rate of Wonji Shoa sugarcane plantation was estimated to be 1787.13 mm. Lower monthly PET was observed in the months of August (128.34 mm) and December (120.59 mm) because of low rain fall and the available moisture in the study area. A lower PET value during August is due to higher relative humidity and lower sunshine hours in the summer season. Most of the actual evapotranspiration during the dry season comes from sub-surface water via transpiration through the plant tissues.

3.2.2.6 Methods of crop evapotranspiration (ET_c) estimation

Evaporation and transpiration occur simultaneously and there is no easy way of distinguishing between the two processes. Apart from the water availability in the topsoil, the evaporation from a cropped soil is mainly determined by the fraction of the solar radiation reaching the soil surface. This fraction decreases over the growing period as the crop develops and the crop canopy shades more and more of the ground area. When the crop is small, water is predominately lost by soil evaporation, but once the crop is well developed and completely covers the soil, transpiration becomes the main process.

The Penman-Monteith method as modified by Allen (1986) was the most accurate for either environment to estimate evapotranspiration. Because of its accuracy and the availability of all required meteorological data, the Penman-Monteith method was adjusted to the physical features of the Wonji weather station and used for crop ET estimation. The amount of water that is lost through the evapotranspiration process from the disease free and well-fertilized crops fields is known as potential crop evapotranspiration (ET_c). Value of ET_c is different for different crops as the groundcover; canopy properties and aerodynamic resistance of crops are different from each other. Before estimating ET_c for every crop, reference crop evapotranspiration (ET_o) has to be computed in monthly time step by using Penman- Monteith method (recommended by the FAO).

Crop evapotranspiration is calculated by multiplying ET_o by K_c, a coefficient expressing the difference in evapotranspiration between the cropped and reference grass surface. In this study the difference were combined into one single coefficient that means the effect of crop transpiration and soil evaporation are combined into a single K_c coefficient. The coefficient integrates differences in the soil evaporation and crop transpiration rate between the crop and the grass reference surface. As soil evaporation may fluctuate daily as a result of rainfall or irrigation, the single crop coefficient expresses only the time-averaged (multi-day) effects of crop evapotranspiration.

The time-averaged single K_c is used in the case for furrow irrigation systems where the time interval between successive irrigation is of several days, often ten to thirty days depending on the soil type.

For typical irrigation management, the time-averaged single K_c is valid.

$$ET_c = K_c \times ET_o \quad (80)$$

Where ET_c crop evapotranspiration (mm d^{-1}),

K_c crop coefficient (dimensionless),

ET_o reference crop evapotranspiration (mm d^{-1})

Figure 9 Furrow irrigation for Sugarcane crop in the Wonji Shoa sugarcane estate

Most of the effects of the various weather conditions are incorporated into the ET_o estimate. Therefore, as ET_o represents an index of climatic demand, K_c varies predominately with the specific crop characteristics and only to a limited extent with climate. This enables the transfer of standard values for K_c between locations and between climates.

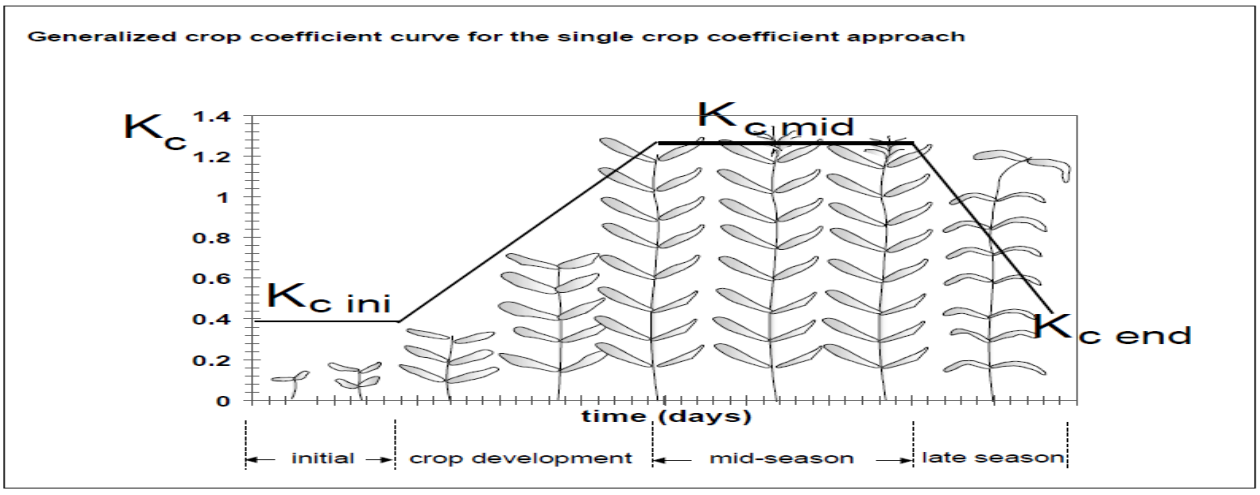

Figure 10 Crop coefficient curve for the single crop in the study area

The CWR module includes calculations, producing the irrigation water requirement of the crop on a decadal basis and over the total growing season, as the difference between the crop evapotranspiration under standard conditions (ET_c) and the Effective rainfall. The water requirement of a crop must be satisfied to achieve potential yields. Crop water requirements (CWR) were calculated on the basis of monthly effective rainfall (P_{eff}) and reference evapotranspiration (ET_o), the first being calculated from average rainfall following the Penman-Monteith approach (FAO-56, 2006). The Penman Monteith method was used to calculate reference evapotranspiration (ET_o). Crop water requirement (ET_c) was calculated by the formula ($ET_c = ET_o \times K_c$). Net irrigation (In) was also calculated as $In = ET_c - P_{eff}$ and approximate net irrigation depth per irrigation application could be taken by assuming the root depth of each sugarcane crop and soil type of the study area. Number of irrigation application was calculated as the ratio of irrigation water need over growing season and net depth of each irrigation application (FAO, 1995).

The CROPWAT model (CROPWAT windows version 8.0) - a computer program for crop and irrigation water requirement calculations developed by FAO (FAO, 1995a) – was used to compute net irrigation water requirements. Inputs for the model are climatic parameters – rainfall, ET_o and crop coefficients, and output from CROPWAT includes monthly net irrigation water requirements by crop. The programme is interactive in nature and allows the development of irrigation schedules for different management conditions and the estimation of scheme water supply for varying cropping patterns. It also helps in the development of recommendations for improved irrigation practices and planning of irrigation schedules under varying water supply conditions. Computerized irrigation scheduling allows for the storage and easy transfer of data, easy access to data and calculations using the most advanced and complex methods for predicting crop evapotranspiration using the FAO CROPWAT model and It can easily access databases for climate and crop characteristics to allow for quick calculations of irrigation water requirements. It has enabled the use of real-time weather data from on-site weather stations to improve efficiency.

The CROPWAT model is based on a water balance model where the soil moisture status is determined on a daily basis from calculated evapotranspiration and inputs of rainfall and irrigation, accounting for incoming and outgoing water in the root zone. Methodologies for crop water requirements and yield response to water are used, while the actual evapotranspiration is determined from the satellite images. Based on the cropping programme adopted and the crop data, the CROPWAT programme were used to calculate the crop water requirements for the sugarcane crops. The crop data required are the crop planting dates, the crop coefficient (K_c) values at the different growth stages, the length of growth stages, the crop rooting depth at the different growth stages, the allowable soil moisture depletion levels and the yield response factors (K_y). After the input of the crop data, CROPWAT proceeds to calculate the crop water and irrigation requirements of the sugarcane cropping pattern, using the entered crop data and the ET_o and effective rainfall values calculated earlier. The calculation of crop water requirements is done on a decade (10-day period) basis.

4. RESULTS AND DISCUSSION

4.1 Relationship of Land Surface Temperature and NDVI in 2002

In this section, the subset images generated using ERDAS IMAGINE tool are presented and discussed. Also the estimated actual evapotranspiration results using different algorithms are presented and compared. Finally in an effort to compare those ET_a derived from the algorithms considered with global MODIS product, results obtained from MODIS16 are presented.

Figure 11 shows the subset images of the study area created using the ERDAS IMAGINE tool with natural (true) color combination of Band 5, Band 4, and Band 3 correspondingly. This shows the different land cover and land features of the study area during the satellite overpass times. At the same time this helps to distinguish the distribution of NDVI, LST and ET between different land covers. The figures show Awash River and water storage reservoirs marked with blue color, the sugarcane estate covers by sugarcane crop is marked by dark green color, irrigated wet fields are seen as black color and bare agricultural areas are marked by light pink color.

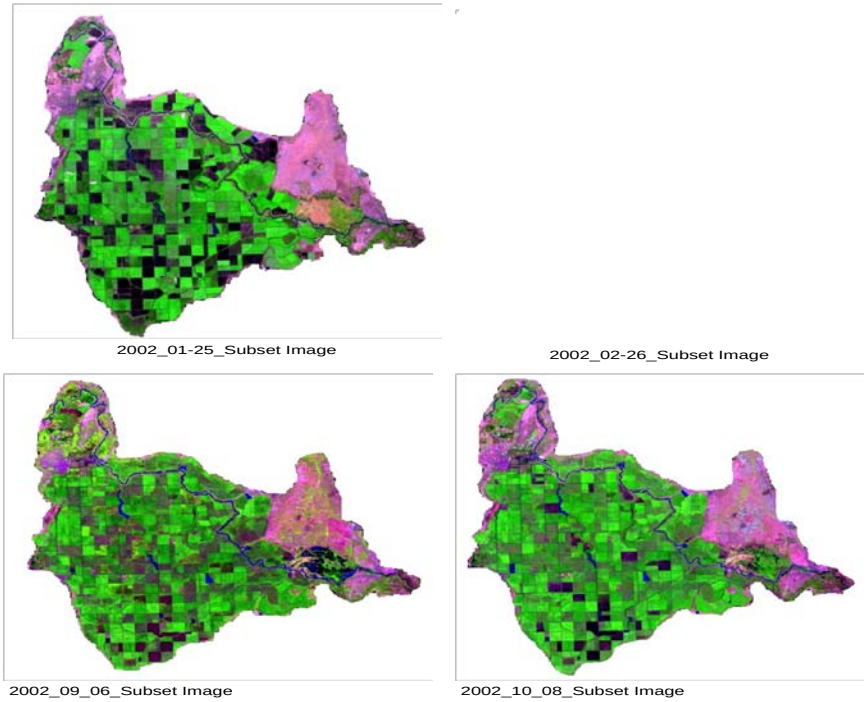

Figure 11. Land cover and features subset images of Wonji Shewa sugarcane estate

The main purpose of this comparison was to show how surface temperature varied with the available moisture on the sugarcane farms, water bodies and vegetation surfaces. The spatiotemporal variability of land surface temperature was found to be strongly dependent on the season. The statistical values (mean and standard deviation) derived from the images are given in Table12. Most of the agricultural fields covered by sugarcane plantation and the water storage reservoirs exhibit lower land surface temperature than bare agricultural fields in all images generated. The influence of moisture status was also clearly noted. The images from the predominantly hotter and drier pixels contrast well with the generally cooler and wetter surface covers. There is good linear relationship between NDVI and LST with an r^2 value of Jan, Feb, Sept, and Oct images of 0.72, 0.704, 0.38, and 0.60, respectively (Figure 12).

Table 11. Mean daily temperature and NDVI values of selected days in 2002.

Parameters	Statistics	Image dates			
		Jan	Feb	Sept	Oct
LST(K)	Minimum	291	297	297	296
	Maximum	313	325	319	324
	Mean	300	310	304	306
	Standard deviation	4.49	5.89	3.73	4.97
NDVI	Minimum	-0.33	-0.37	-0.23	-0.25
	Maximum	0.77	0.765	0.86	0.81
	Mean	0.314	0.305	0.42	0.37
	Standard deviation	0.16	0.15	0.21	0.20

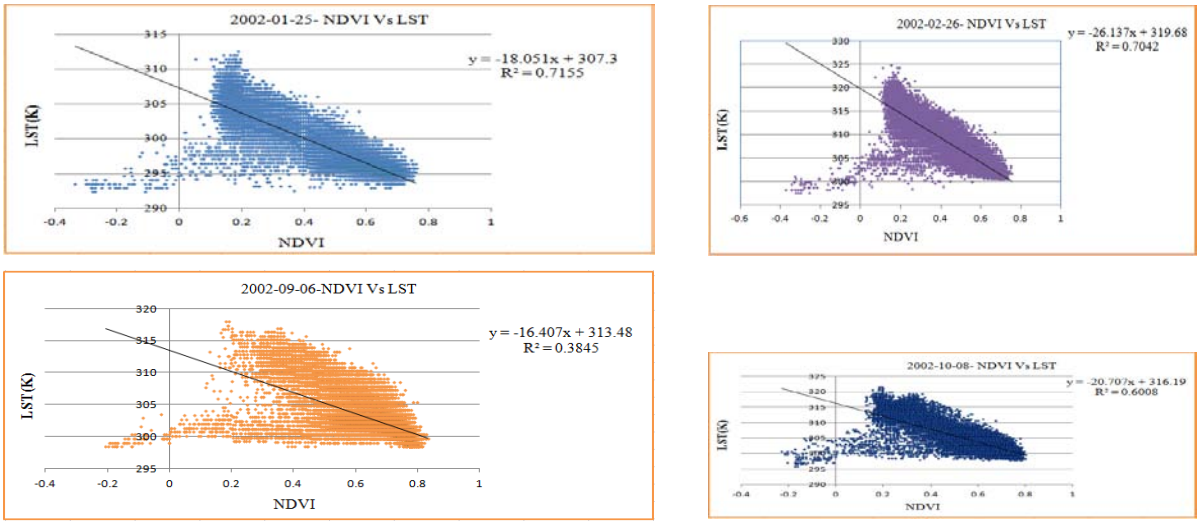

Figure 12. Relationship between land surface temperature and NDVI in the study area.

4.2 Spatial and Temporal Distribution of Evapotranspiration

The spatial and temporal variability in the actual evapotranspiration estimated using the SEBAL, SSEB, and $SSEB_{op}$ algorithms are presented and discussed in the following subsections.

4.2.1 Spatial distribution of ET_a during January, 2002

The estimated daily minimum and maximum ET_a values in January using SEBAL, SSEB and $SSEB_{op}$ algorithms were 0.0 and 6.85, 0.0 and 6.78, and 0.05 and 8.25 mm/day respectively with mean and standard deviation values of 2.88 and 1.41, 3.45 and 1.66, and 4.88 and 1.68 respectively. The SEBAL algorithm ET_a estimation on well grown and irrigated moist sugarcane fields, water storage reservoirs and on the Awash River was higher than the other cultivated sugarcane plantation fields. It also showed that no moisture was lost by ET in most of bare agricultural fields. SSEB and $SSEB_{op}$ ET_a estimation over moist and cultivated sugarcane fields looked consistent and good. The ET over some bare agricultural fields especially $SSEB_{op}$ contradicted SEBAL results. All the three algorithm results showed that moist surfaces have higher ET_a values. Moreover, dry agricultural fields exhibits generally lower ET_a values. This shows that the remote sensing technique can capture the spatial variability. This is unlike the results we obtained using the MOD16 Product which will be explained latter.

The evaporation fraction (ET_rF) of each algorithm also follows the same pattern as daily evapotranspiration. One should generally expect ET_rF values to range from 0 to 1. On a totally dry pixel, ET = 0 and ET_rF = 0 and a pixel in a well-watered vegetation can occasionally have an ET slightly greater than ET_r (ET_rF> 1), perhaps up to 1.1 (Mohamed et al, 2004). But in some wet fields and water bodies (reservoirs, river and swamp areas), SEBAL and $SSEB_{op}$ ET_rF greater than 1.1 was observed. This may be attributed due to the effect of tall aerodynamically rough sugarcane crop had higher evaporation rate compared with standard clipped grass considered in the definition of ET_o. It should be noted that the FAO generic K_c values for sugarcane in the middle growing season is 1.25 (Allen et al., 1998). Hence the value obtained on these fields was in good agreement with tall well established sugarcane crop fields and with the abundant water provided to the schemes (Figure 10). On the other hand, sometimes this could occur due to systematic errors caused by various assumptions made earlier in the energy balance process (Mohamed et al, 2004). The highest mean ET_a values in the well watered sugarcane

fields resulted due to mid-season stage crop developed through irrigation and in swamp of the plain and night water storage reservoirs.

According to $SSEB_{op}$, SSEB and SEBAL ET_a results more than 65 % of the area exhibit nearly 3.6 - 8.2, 3.0 - 6.8, and 2.4 - 4.8 mm/day respectively. Well watered sugarcane fields in the mid-season growing stage of the crop and water storage areas reveals higher ET_a values compared to the other dry agricultural fields which indicated that they are more water user fields. ET_a estimated over dry agricultural (uncultivated) fields using $SSEB_{op}$, SSEB and SEBAL ranges from 0.0 – 2.6, 0.0 - 2.2, and 0.0 – 2.2 mm/day respectively. Comparative assessment of standard deviation of ET_a over the sugarcane plantation indicated moderate spatial variability of ET_a due to soil moisture variability which itself is dependent on irrigation application and rainfall availability. The standard deviations are linked with soil moisture condition in certain period of time. Dry periods exhibit greater variability than wetter periods. The evaporation loss in this month is higher than the monthly precipitation in the sugarcane plantation farm and irrigation water is the source for an optimum climatic condition to satisfy the evaporative demand of the area. This clearly demonstrated that the seasonal distribution of ET is related to the moisture availability and the surface types. Therefore it can be concluded that, during the dry season, ET were limited to the well watered sugarcane fields and water storage areas only, which were fed continuously from the irrigation. During the peak of the rainy season, ET was high throughout the entire sugarcane plantation due to soil moisture availability.

The residual difference of ET_a estimated between $SSEB_{op}$ and SSEB looked consistent and good throughout the sugarcane estate with values in the range of 0.9 – 1.47 and 0.05 – 0.89 mm/day over moist sugarcane fields and dry agricultural lands, respectively. The residual difference of ETa estimation between $SSEB_{op}$ and SEBAL ranged from -1.18 – 5.53 mm/day, while between SSEB and SEBAL ranged nearly from -2.59 – 4.08 mm/day. Generally higher residual values were observed over well grown sugarcane fields and water storage areas and lower values were observed over dry agricultural fields. The Root Mean Square Error (RMSE) values between SSEB and SEBAL, $SSEB_{op}$ and SEBAL, and SSEB and $SSEB_{op}$ ET_a estimates were 0.548, 0.548, and 0.99 respectively (Fig 13) .

Figure 13. Comparison among SSEB, $SSEB_{op}$, and SEBAL ET_a estimates for January 25, 2002.

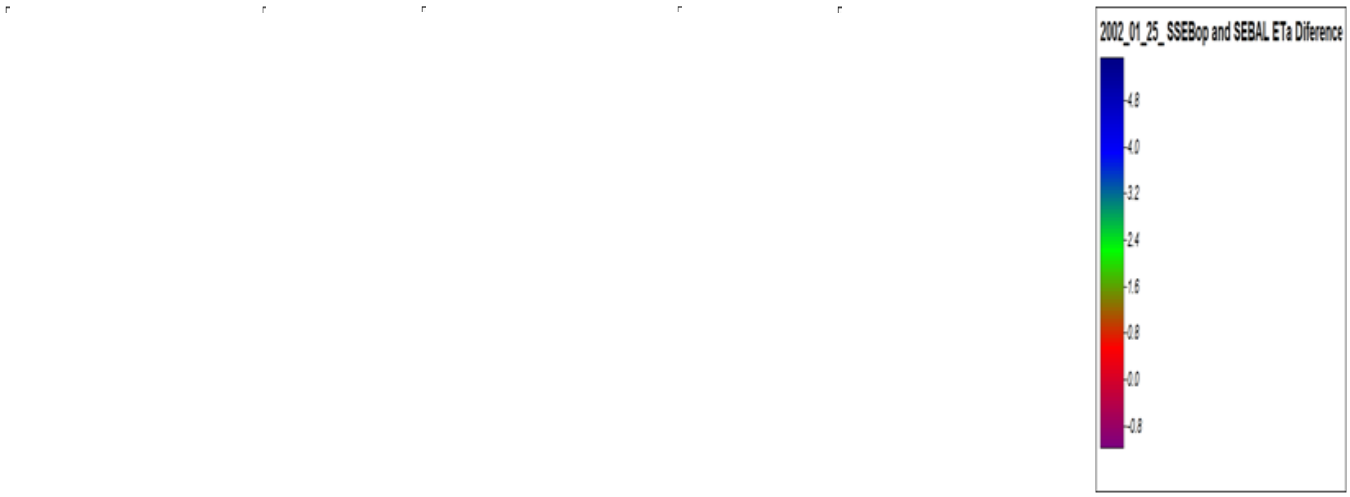

Figure 14. January 25, 2002 actual evapotranspiration (mm/day) at Wonji sugarcane estate

4.2.2 Spatial distribution of ET_a during February 26, 2002

The daily minimum and maximum ET_a values of February 26, 2002 using SEBAL, SSEB and $SSEB_{op}$ algorithms were found to be between 0.0 and 9.36, 0.0 and 7.81, and 0.0 and 8.82 mm/day, respectively. The corresponding mean values (mm/day) were 2.82 and 1.68, 3.01 and standard deviation values were 2.13, and 3.95 and 2.23 mm/day, respectively. The SEBAL algorithm ET_a estimates over water storage areas (night storage reservoirs and Awash River) were higher than $SSEB_{op}$ and SSEB ET_a estimates. On the other hand, SEBAL ET_a estimates over well grown sugarcane fields were lower than $SSEB_{op}$ and SSEB ET_a estimates. All the three algorithms ET_a estimates on well irrigated and moist sugarcane fields, water storage reservoirs and on the Awash River were higher than the uncultivated sugarcane plantation fields and bare agricultural fields. SEBAL algorithm showed no moisture loss by ET in most bare agricultural (uncultivated) fields while $SSEB_{op}$ results showed the presence of ET over bare agricultural fields contradicting SEBAL estimates. SSEB and $SSEB_{op}$ ET_a estimates over the entire sugarcane estate looked consistently close to each other. All the three algorithm results showed that well grown and well irrigated moist sugarcane fields in the mid-season growing stage and water storage areas exhibited higher ET_a values compared to other dry agricultural fields.

On February 26, 2002, 65% of the area in the estate resulted in ET_a values between 2.4 - 8.8mm/day for $SSEB_{op}$, 2.2- 7.8mm/day for SSEB, and 2.4 - 5.8 mm/day for SEBAL. On the other hand ET_a estimated over dry agricultural (uncultivated) fields were between 0.0 – 2.3mm/day for $SSEB_{op}$, 0.0 - 2.1mm/day, for SSEB, and 0.0 – 2.3 mm/day for SEBAL. During February, the atmospheric evaporative demands in the area were higher than that of January. The standard deviations of ET_a over the sugarcane plantation were also higher indicating higher spatial variability of ET_a due to soil moisture variability. The evaporation fraction (ET_rF) of each algorithm also followed the same pattern as daily actual evapotranspiration. SEBAL ETrF values greater than 1.25 were observed only in few water bodies such as night storage reservoirs and Awash River. This might also be occurred due to systematic errors caused by various assumptions made earlier in the energy balance process. The highest mean ET_a values were obtained again on fields where the crop is at the mid-season growing stage, swamps and night storage reservoirs.

The residual difference of ET_a estimation between $SSEB_{op}$ and SSEB looked consistent and good throughout the sugarcane estate with a value of 0.7 – 1.0 and 0.0 – 0.6 mm/day over moist sugarcane fields and dry agricultural lands, respectively. On the other hand the $SSEB_{op}$ and SEBAL residual ranged from -2.23 – 4.65 mm/day, while between SSEB and SEBAL residual varied between -3.25 – 3.64 mm/day. Generally, higher residual values were observed over well grown sugarcane fields and water storage areas, but lower values were observed over dry agricultural fields. In summary, it was noted that $SSEB_{op}$ and SSEB ET_a estimates were closer and consistent over fully covered and well grown sugarcane field, and also were consistently higher than SEBAL ET_a estimates. On the contrary, SEBAL ET_a estimates over well prepared uncultivated sugarcane fields were observed to be higher than $SSEB_{op}$ and SSEB ET_a estimates. Over dry agricultural fields, the ET_a estimates of all the three algorithms were close to each other. The Root Mean Square Error (RMSE) values of 0.739between SSEB and SEBAL, 0.753 between $SSEB_{op}$ and SEBAL, and 0.994 between SSEB and $SSEB_{op}$ ET_a were observed (Figure 15).

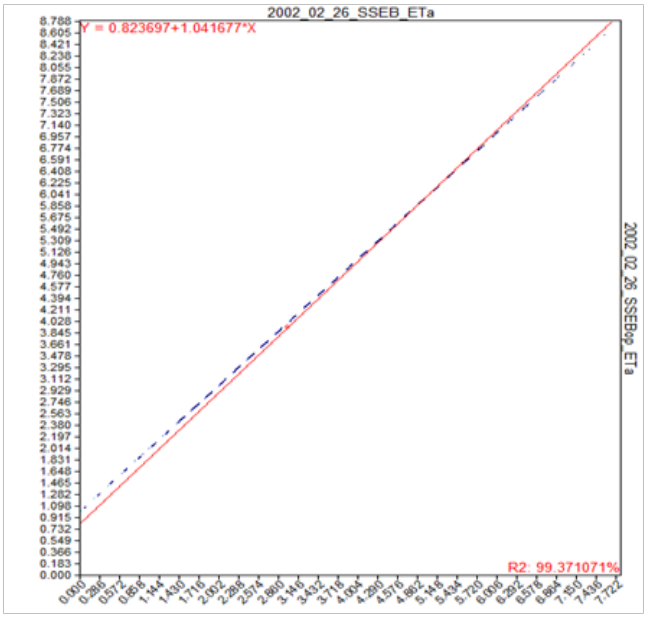

Figure 15. Comparison among SSEB, $SSEB_{op}$, and SEBAL ET_a estimates for February 26, 2002.

Figure 16. February 26, 2002 actual evapotranspiration (mm/day) at Wonji sugar estate

4.2.3 Spatial distribution of ET_a during September 06, 2002

The September 06, 2002 minimum and maximum daily ET_a values were 0.0 and 3.61 mm/day for SEBAL, 0.0 and 3.65 mm/day for SSEB and 0.2 and 4.0 mm/day for $SSEB_{op}$ algorithms. The overall field average SEBAL, SSEB, and $SSEB_{op}$ mean (mm/day) values were 2.31, 2.46. 2.92, while the corresponding standard deviations were 0.43, 0.7, and 0.64, respectively. All the three algorithms ET_a estimates on well grown and moist sugarcane fields, night storage reservoirs and on the Awash River were higher than other dry agricultural (uncultivated) fields. The comparisons with earlier months showed that more water was lost by ET_a on bare agricultural (uncultivated) fields. This is expected as September is end of the rainy month and the soil should contain more moisture for subsequent evaporation. In the month of September, generally all of the three algorithms ET_a estimates were lower. This was due to higher humidity and a decreased solar radiation associated with the effect cloud cover at the satellite overpass time.

According to $SSEB_{op}$, SSEB and SEBAL ET_a results, more than 80% of the area exhibit nearly 2.4 – 4.0, 2.2- 3.65, and 2.0 – 3.61 mm/day, respectively. The ranges of ET_a estimated over dry agricultural (uncultivated) fields using $SSEB_{op}$, SSEB and SEBAL were respectively 0.2 – 2.3, 0.0 - 2.1, and 0.0 – 1.9 mm/day. During September, the optimum climatic condition to satisfy the evaporative demand of the area were higher than the other months except the cloud cover which resulted in lower ET_a values throughout the sugarcane estate. The standard deviation of ET_a over the sugarcane plantation were also lower indicating lower spatial variability of ET_a due to less soil moisture variability. Even though the soil was saturated due to excess summer rainfall providing the opportunity for ample evapotranspiration in the area, lower atmospheric demand (low radiant energy of the sun) due to cloud cover causes the entire sugarcane estate to have lower ET_a values.

The residual difference of ET_a estimates between $SSEB_{op}$ and SSEB looks consistent and good throughout the sugarcane estate with values 0.50 – 0.69 for moist sugarcane fields and 0.2 – 0.49 mm/day for dry agricultural lands of the estate. The residual difference of ETa estimates between $SSEB_{op}$ and SEBAL ranged from -0.81 – 1.85 mm/day, while that of SSEB and SEBAL ranged from -1.49 – 1.35 mm/day. In general, higher residual values were observed over well grown sugarcane fields and water storage areas, and lower values were observed over dry agricultural fields. ET_a estimate for $SSEB_{op}$, SSEB and SEBAL during September were close to each other

and looked consistent and higher over the entire sugarcane estate. Even bare agricultural fields had excess rainfall to evapo-transpire into the atmosphere. The Root Mean Square Error (RMSE) values were 0.847 for SSEB and SEBAL, 0.846 for $SSEB_{op}$, and SEBAL, and 0.999 for SSEB and $SSEB_{op}$ ETa estimates (Figure 17).

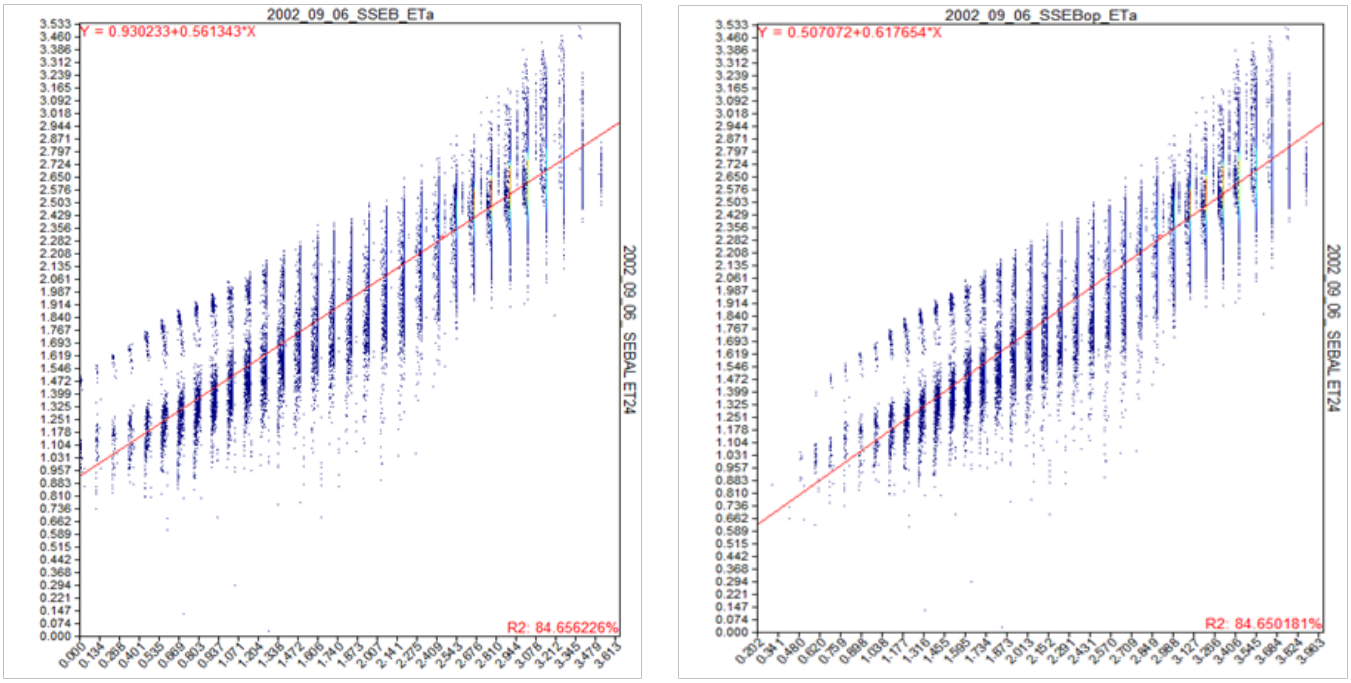

Figure 17. Comparison among SSEB, $SSEB_{op}$, and SEBAL ET_a estimates for September 6, 2002.

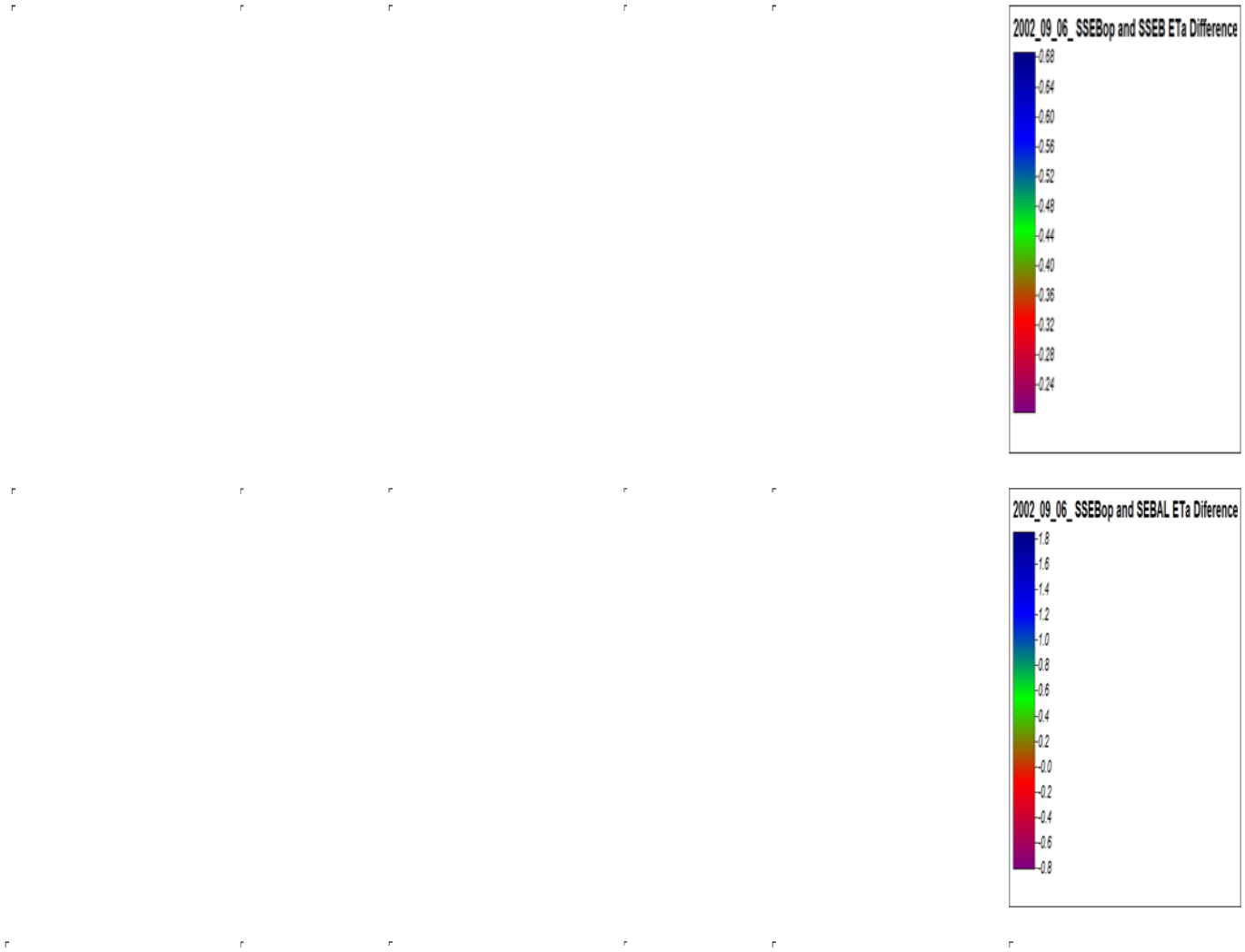

Figure 18. September 6, 2002 actual evapotranspiration (mm/day) at Wonji sugar estate

4.2.4 Spatial distribution of ET_a during October 8, 2002

The estimated daily minimum and maximum ET_a values on October 8,2002 using SEBAL, SSEB and $SSEB_{op}$ algorithms were 0.0 and 6.83, 0.0 and 6.46, and 0.0and 7.4 mm/day, respectively. The corresponding mean and standard deviation values respectively were 1.57 and 1.08 for SEBAL, 3.62 and 1.46 for SSEB, and 4.18 and 1.65 for $SSEB_{op}$. The SEBAL algorithm ET_a estimates on well grown and moist sugarcane fields, night storage reservoirs and on the Awash River were higher than the other cultivated sugarcane plantation fields. It also showed that there were no moisture losses by ET in most of bare agricultural (uncultivated) fields due to soil moisture stress. SSEB and $SSEB_{op}$ ET_a estimation over water bodies, moist and cultivated sugarcane fields looked closer and consistent. The ET_a values obtained on bare agricultural fields suggested that there were still adequate residual moisture from the preceding rainy months contributing to the overall evaporation. All the three algorithm results consistently exhibited that moist surfaces have higher ET_a values. Dry agricultural fields (uncultivated) exhibited generally lower ET_a values as would be expected. This is taken as good indicator of how the algorithms and spatial resolutions are fairly capturing ET_a variability in the estate.

The results on October 8, 2002 showed that 65% of the area in the estate had ET_a values in the ranges of 3.2 – 7.4, 3.6- 6.46, and 1.2 – 4.5 mm/day according to $SSEB_{op}$, SSEB and SEBAL estimates, respectively. The ranges of ET_a values estimated over dry agricultural (uncultivated) fields using $SSEB_{op}$, SSEB and SEBAL algorithms were between 0.0 – 3.1, 0.0 – 3.5, and 0.0 – 1.1 mm/day, respectively. During October 2002, the optimum climatic condition to satisfy the evaporative demand of the area were higher and the standard deviation of ET_a over the sugarcane plantation were lower indicating lower spatial variability of ET_a in relation to the soil moisture variability. Even during this month, much of the evapotranspiration occurs on these well watered sugarcane fields. The evaporation fraction of each algorithm in this month also showed the same pattern as ET_a distribution of the month.

The residual difference of ET_a estimates between $SSEB_{op}$ and SSEB varied from 0.4 – 0.94 on moist sugarcane fields, and 0.0 – 0.39 mm/day over dry agricultural lands. The ranges of the residual difference of ET_a estimates between $SSEB_{op}$ and SEBAL were -1.29 – 5.98 mm/day, between SSEB and SEBAL were from -1.7 – 5.2 mm/day. Generally higher residual values are observed over well grown sugarcane fields and night storage areas. Lower values were observed

over dry agricultural fields. The Root Mean Square Error (RMSE) value between SSEB and SEBAL, $SSEB_{op}$ and SEBAL, and SSEB and $SSEB_{op}$ ETa estimation were 0.573, 0.573, and 1.00, respectively (Figure 19).

Figure 19. Comparison among SSEB, $SSEB_{op}$, and SEBAL ET_a estimates for October 8, 2002.

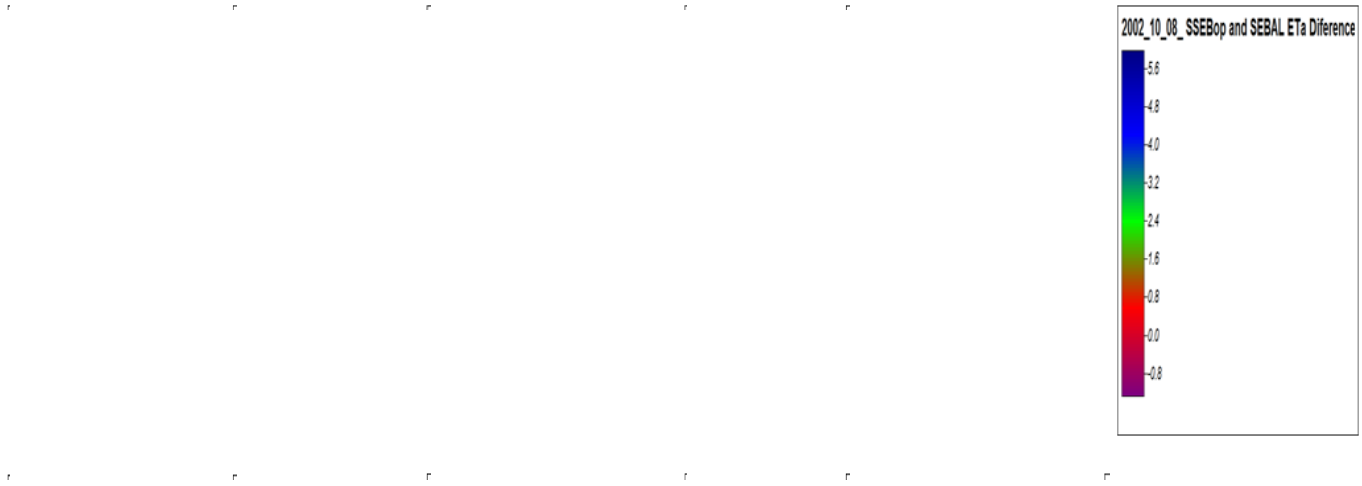

Figure 20. October 8, 2002 daily evapotranspiration (mm/day) at Wonji sugar estate

Table 12. Statistics of daily actual evapotranspiration of the study area in 2002.

Algorithms	Statistical parameters	Dates			
		JAN,2002	FEB,2002	SEPT,2002	OCT,2002
SEBAL ET_a (mm/day)	N	66915	66915	66915	66915
	Minimum	0.0	0.0	0.0	0.0
	Maximum	6.85	9.36	3.61	6.83
	Mean	2.88	2.82	2.31	1.57
	Standard deviation	1.41	1.68	0.43	1.08
	Variance	1.98	2.84	0.19	1.18
	Median	3.23	3.23	2.46	1.7
	Mode	0.0	0.0	2.51	0.0
SSEB ET_a (mm/day)	N	66915	66915	66915	66915
	Minimum	0.0	0.0	0.0	0.0
	Maximum	6.78	7.81	3.65	6.46
	Mean	3.45	3.01	2.46	3.62
	Standard deviation	1.66	2.13	0.70	1.46
	Variance	2.75	4.54	0.5	2.12
	Median	3.78	3.08	2.67	4.33
	Mode	4.87	0.0	2.91	4.68
$SSEB_{op}$ ET_a (mm/day)	N	66915	66915	66915	66915
	Minimum	0.053	0.0	0.20	0.0
	Maximum	8.25	8.82	4.00	7.40
	Mean	4.88	3.95	2.92	4.18
	Standard deviation	1.68	2.23	0.64	1.65
	Variance	2.83	4.96	0.41	2.74
	Median	5.21	4.09	3.11	4.99
	Mode	6.32	6.42	3.33	5.38
MODIS(MOD16) global ET_a (mm/day)	N	65939	65939	65939	65939
	Minimum	0.25	0.0	0.68	0.0
	Maximum	4.19	3.94	7.39	5.01
	Mean	1.23	1.26	2.66	1.99
	Standard deviation	1.1	2.23	1.18	1.47
	Variance	1.21	0.81	1.39	2.17
	Median	0.44	0.57	2.25	2.13
	Mode	0.44	0.63	2.25	0

4.3. Comparison of MODIS ET_a Estimations with SEBAL, SSEB, and $SSEB_{op}$ in 2002

The estimated daily minimum and maximum MOD16 ET_a values in January 25, 2002 were 0.25 and 4.19 mm/day respectively with mean and standard deviation values of 1.23 and 1.1 mm/day respectively. Only few water bodies, well watered and well grown sugarcane fields in the midseason growing stage of the crop exhibited higher ET_a values. Most of other agricultural and sugarcane fields had low ET_a values as shown in Figure 21.The Root Mean Square Error (RMSE) value among MOD16, SEBAL, $SSEB_{op}$, and SSEB ET_a estimation were 0.05 (Figure 22).

The daily minimum and maximum MOD16 ET_a values on February 26, 2002 were 0.0 and 3.94 mm/day, respectively. The mean and standard deviation values were 1.26 and 0.9 mm/day respectively. Most of the sugarcane estate exhibited an ET_a value less than 2 mm/day. Only few moist sugarcane fields and water bodies exhibited relatively higher ET_a values (Figure 21).The Root Mean Square Error (RMSE) value among MOD16, SEBAL, $SSEB_{op}$, and SSEB ET_a estimation were 0.14 (Figure 23).

The MOD16 ET_a estimated daily minimum and maximum values in September 6, 2002were 0.68 and 7.39 mm/day respectively, and with mean and standard deviation values of 2.66 and 1.18 mm/day respectively. The distribution of ET_a on wet sugarcane fields and dry agricultural areas looked consistent and good over the entire sugarcane estate. Higher values were obtained because of the soil was saturated due to excess summer rainfall. This also created an opportunity for the entire sugarcane estate to have had a higher evapotranspiration rate (Figure 21).The Root Mean Square Error (RMSE) value (0.03) among MOD16, SEBAL, $SSEB_{op}$, and SSEB ET_a during this month was also low (Figure 24).

The October 8, 2002 estimated daily minimum and maximum MOD16 ET_a values varied from 0.0 and 5.01 mm/day respectively with mean and standard deviation values of 1.1 and 1.47 mm/day respectively. The MOD16 ET_a estimates distribution were fair and consistent being indicative of moisture status of the entire sugarcane estate. Generally wet areas such as well grown sugarcane fields, night storage reservoirs, Awash River got higher ET_a values compared to the other dry agricultural fields as seen in Figure 21. However, generally lower Root Mean

Square Error (RMSE) value of 0.23 among MOD16, SEBAL, $SSEB_{op}$, and SSEB ET_a estimates were observed (Figure 25).

Figure 21.Global MOD16 ET_a estimates on January 25, February 26, September 06, and October 08, 2002 for Wonji Shoa sugarcane estate.

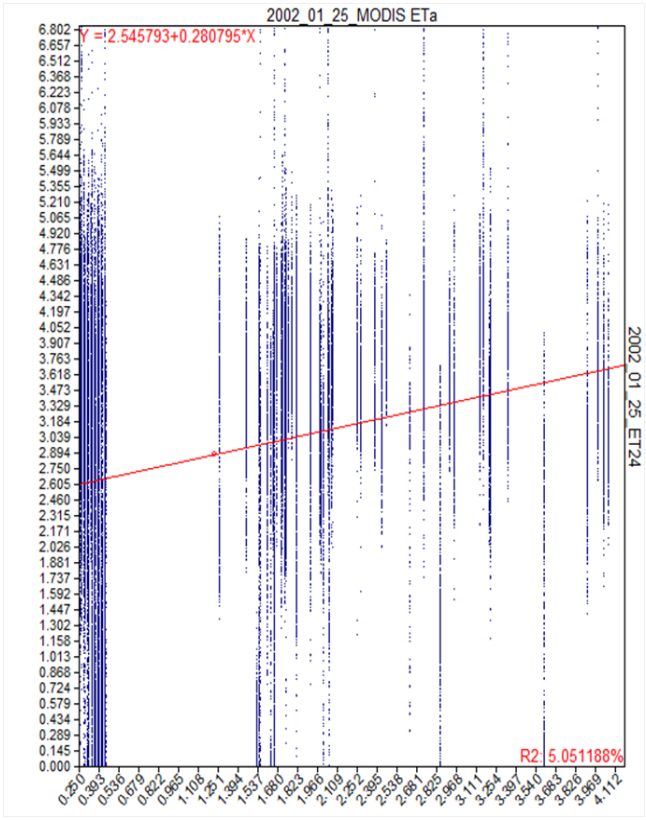

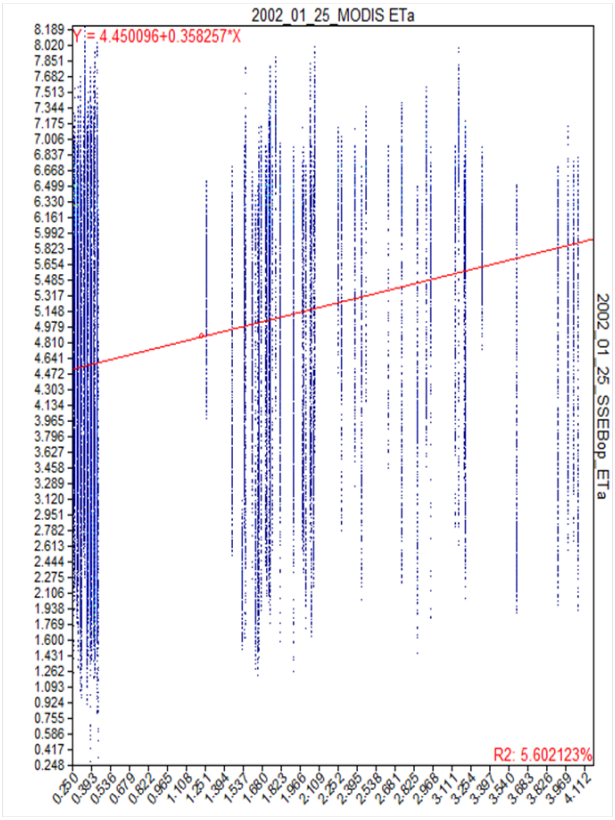

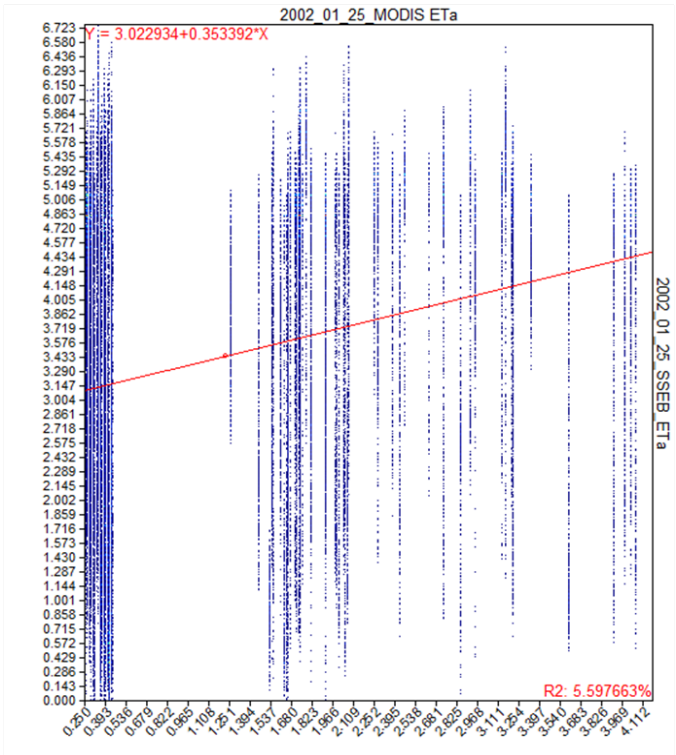

Figure 22Comparison of MODIS with SSEB, SSEBop, and SEBAL ET_a estimates for 25 January 2002.

Figure 23. Comparison of MODIS with SSEB, SSEBop, and SEBAL ET_a estimates for 26 February 2002.

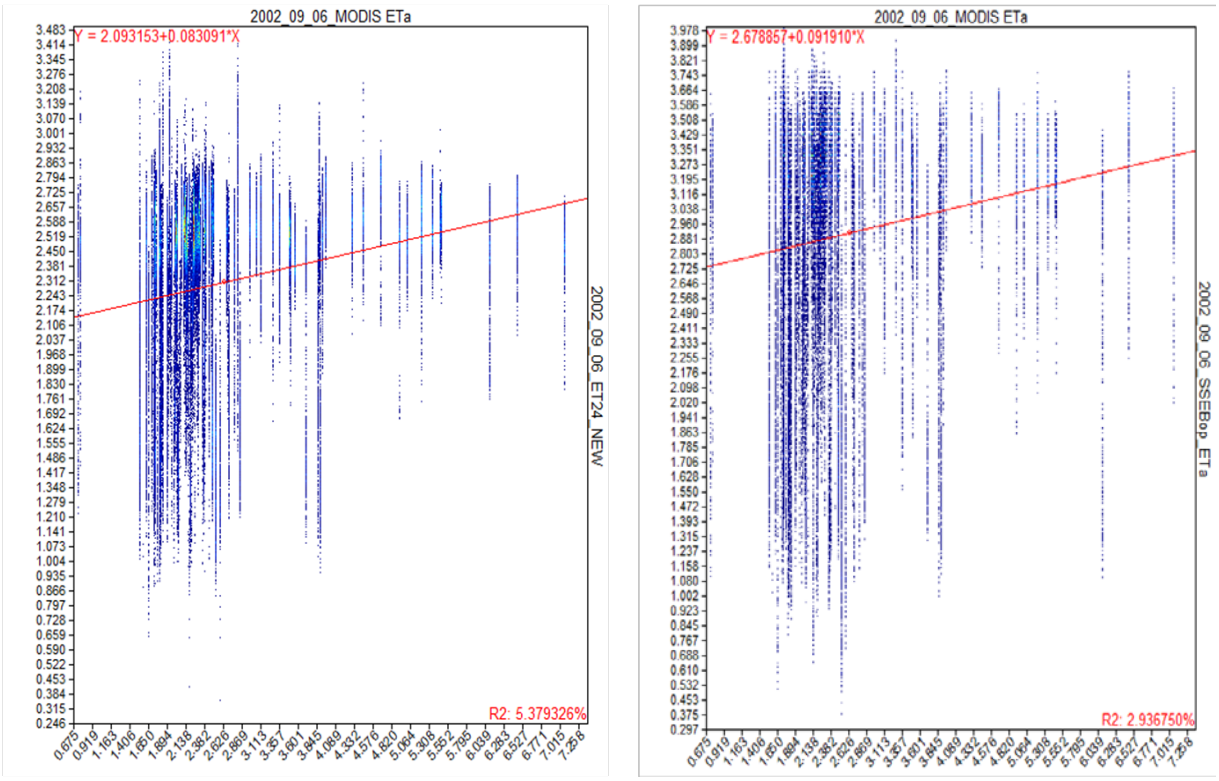

Figure 24. Comparison of MODIS with SSEB, SSEBop, and SEBAL ET_a estimates for 06 September 2002.

Figure 25. Comparison of MODIS with SSEB, SSEBop, and SEBAL ET_a estimates for 08 October 2002.

4.4 Crop and Irrigation Water Requirement

As shown in Table 13, estimates of the average annual water consumption by $SSEB_{op}$ were 40 % higher than SEBAL, 21% higher than SSEB and 55 % higher than MOD16. The mean annual ET_a estimated for the whole estate were 107 Mm^3, 140 Mm^3, 178 Mm^3 and 80 Mm^3 using SEBAL, SSEB, $SSEB_{op}$ and MOD16, respectively and the mean annual PET was 219Mm^3.

Table 13. Monthly and annual average actual evapotranspiration for Wonji Shoa sugar cane Estate using different algorithms

	Monthly Average Estates Consumptive Water Use (Mm3)							
	SSEBAL		SSEB		$SSEB_{op}$		MOD16	
	mm/day	mm/month	mm/day	mm/month	mm/day	mm/month	mm/day	mm/month
Jan	2.88	11	3.45	13	4.88	18	1.23	5
Feb	2.82	10	3.01	11	3.95	15	1.26	5
Sept	2.31	8	2.46	9	2.92	11	2.66	10
Oct	1.57	6	3.62	13	4.18	15	1.99	7
	Annual Estates Consumptive Use Estimates (Mm3)							
Average	2.39	107	3.14	140	3.98	178	1.79	80

The level of maximum soil water depletion allowed varies with the crop. The depth of water readily available to crop is defined as $p \times S_a$. Where S_a is the total available soil water and p is the fraction of the Total Available soil Water (TAW) that can be used by the crop without affecting its evapotranspiration and growth.Net depth of irrigation, d (mm) = $(p \times S_a)$ D. Where D is the rooting depth which was observed to have an average value of 100cm. Taking the value of p as 0.65 (FAO, paper 24) for sugarcane, however limiting it to 0.5 for lighter soil categories, the application rates are given in Table 13.

The Estates water application plan is shown in Table 14 and this irrigation application is known to be dependent on Soil Management Group (SMG) of the sugarcane estate.

Table 14 water application rates in the study area

Soil cycle	Available water (mm/m)	Allowable depletion fraction (p)	pDS_a (mm)	Application Efficiency (Ea)	Gross depth of application(mm)	Application volume (m^3/ha)
A1	190-250	0.65	143	0.7	205	2050
A2	180-220	0.65	130	0.7	185	1850
BA2	140-190	0.65	107	0.7	153	1530
B14	120-150	0.5	67.5	0.6	113	1130
C1	110-150	0.5	65	0.6	108	1080

The soil category A1 and A2 comprises primary of vertisols with a local slopes of less than 0.25%. The soils have more than 40% clay in the surface horizon and more than 75 % in the middle part of the soil profiles. Average water range is reported as 110mm to 250 mm for top one meters of the soil profile.

The interval of irrigation application, I, is given as the ratio of $p \times S_a \times D$ and the crop reference evapotranspiration. RAW = p×TAW, where RAW is Readily Available soil Water in the root zone (mm). Prior to harvesting of a crop, a drying period, depending on the SMG, of 60 to 74 days application of first irrigation is allowed. For heavier soils, when soil moisture drops below 65% of the TAW, irrigation should start.

Table 15 Irrigation interval for different Soil Management Group (SMG) of Wonji sugarcane plantation estate

Soil cycle	Irrigation Interval (days)
A1	30-34
A2	28-30
BA2	22-25
B14	15-17
C1	14-16

The required timing and amount of applied water for the sugarcane were calculated based upon the prevailing climatic conditions, growing season, growing and harvesting date, root depth, and allowable depletion, soil physical properties (such as water holding capacity), availability of water resources, field water losses and useful rainfall and therefore the CWR and IR of sugarcane crop were computed by considering the field water balance in the crop root zone as show in Figure 26. It is important to realize that the estimation of crop water requirements is the first stage in the estimation of irrigation requirements of a given cropping programme. Hence the

calculation of crop water requirements and irrigation requirements must not be viewed as two unrelated procedures.

The CWR and IR of sugarcane in the study area were highest from the second decade of the first month to the first decade of the second month and from the third decade of the ninth month to the first decade of the eleventh month and minimum from the third decades of the third month to the first decades of the fifth month and from the third decade of the seventh month to the second decade of the eighth months of the year. The total CWR, IR and effective rain for January and March planted sugarcane were estimated to be 2468.8, 2061.6 and 423.8 mm/yr and 2281.9, 1851.0 and 437.8 mm/yr respectively.

Figure 26. Plot of ET_c and IR for sugarcane crop planted in 2001

5. CONCLUSIONS AND RECOMMENDATIONS

Evapotranspiration from irrigated agriculture is an important component of water management for arid and semi-arid regions. Accurate determination of crop ET is essential to optimize irrigation water management at scheme level. However, the application of direct method of evapotranspiration has been difficult. Recently, remote sensing data has been used to provide a direct method of monitoring the actual evapotranspiration. This has been achieved by solving the energy balance of thermodynamics fluxes at the surface of the earth. A number of algorithms have been developed to estimate actual evapotranspiration and tested widely. Among these methods are SEBAL, SSEB, and $SSEB_{op}$. In this research, evapotranspiration estimates were made using these three algorithms for the Wonji Shoa Sugarcane Estate. Landsat ETM+ and MODIS images of four days in 2002, (i.e. January 25, February, 26, September 6 and October, 8 2002), were used. The actual evapotranspiration was computed using the three algorithms. The major findings of the study clearly showed that remote sensing can have a tremendous potential for estimating evapotranspiration and water management at farm and basin level. The simple averaged annual actual evapotranspiration by SEBAL, SSEB, $SSEB_{op}$ and MOD16 showed that the estate losses respectively 107, 140, 178, and 80 Mm^3 of water due to evaporation per year and these values are closer to actual evaporation need to be substantiated through field measurement.

Based on the results obtained the following specific conclusions have been made:-

- The remote sensing technology can be applied for the measurement, monitoring and reporting of water use and management in irrigated agriculture like large sugarcane estates. It also helps an irrigator to know the ET rate and to apply the right amount of water at the right time to ensure that the crop is not stressed, particularly during critical stages of growth which results in improved sugarcane yield production provided that real time image is available.
- The remote sensing techniques enable us to get vital information on evaporative loss and moisture condition of the sugarcane estate and water used by different land uses at different time steps to support planning for resource allocation and management.

- The analysis of actual evapotranspiration in the sugarcane estate estimated by remote sensing method revealed large spatial and temporal variability which closely followed the variability in soil moisture (wetness and dryness) and land use characteristics which otherwise would have been difficult to get it using the indirect methods.
- The evaporative fraction (parameter determines energy partitioning) in the sugarcane estate, exhibits similar regional distribution patterns as evaporation rate in the sugarcane estate. For dry agricultural fields, the average evaporative fractions were lower, highlighting the dominance of sensible heat flux across the sugarcane estate, and the corresponding rise in observed surface temperatures.

- Comparison of ET_a obtained from the MODIS Product (MOD16) with those obtained from the Landsat based algorithms resulted in a very poor correlation and it under estimates ET_a over the entire sugarcane estate.

The result of this study generally demonstrates that $SSEB_{op}$, SSEB, and SEBAL could be used to provide vital information on evaporative loss and moisture condition of the sugarcane estate. It can be considered as operational and feasible methods to predict actual ET and improve water management and modeling processes in the sugarcane estate. But should be tested and validated with results of field measurements in different environments. The integration of remote sensing techniques and distributed hydrological modeling can produce better results. Evaporation loss and moisture condition derived from $SSEB_{op}$, SSEB, and SEBAL models can be an important data input for distributed hydrological modeling and to improve their performance.

As a recommendation, since field measurements were not done in this research, it is not possible to say one method is better than the other. We now have adapted the algorithms, comparing the results obtained using field measurement must be done before recommending any of the methods for actual use. Moreover, the MODIS product used to generate the ET_a was found poor. This is expected to be a problem associated with the spatial resolution or scale problem. Hence, rerunning the model using fine spatial resolution product is recommended.

6. REFERENCES

Ahmed, M.D., and Bastiaanssen, W.G.M., 2003. Retrieving soil moisture storage in the unsaturated zone from satellite imagery and bi-annual phreatic surface fluctuations. Irrig. Drain. Syst. 17(2), 3–18.

Allen, R.G., 1986. A Penman for all seasons. Irrigation and Drainage Engineering 112(4):348-368.

Allen, R.G., Bastiaanssen, W.G.M., Tasumi, M., Morse, A., 2001. Evapotranspiration on the watershed scale using the SEBAL model and Landsat images, ASAE Meeting Presentation, Paper Number 01-2224, Sacramento, California, USA, July 30– August 1, 2001.

Allen, R.G., L.S. Pereira, D. Raes, M. Smith, 1998. Crop evapotranspiration: guidelines for computing crop water requirements. In: United Nations FAO, Irrigation and Drainage Paper 56, FAO, Rome, Italy.

Allen, R.G., Morse, A., Tasumi, M., Trezza, R., Bastiaanssen, W.G.M., Wright, J.L., Kramber, W., 2002. Evapotranspiration from a satellite based surface energy balance for the Snake Plain Aquifer in Idaho, Proceedings of the National USCID Conference, San Luis Obispo, California, July 8–10, 2002, 10 pp.

Allen, R.G., Tasurmi, M., Morse, A., Trezza, R., 2005. A Landsat-based Energy Balance and Evapotranspiration Model in Western US Water Rights Regulation and Planning. Journal of Irrigation and Drainage Systems, 19 (3-4): 251-268(18).

Allen, R.G., Tasumi, M., Morse, A.T., Trezza, R., Kramber, W., Lorite, I., Robison, C.W., 2007a. Satellite-based energy balance for mapping evapotranspiration with internalized calibration (METRIC) – applications. ASCE J. Irrig. Drain. Eng. 133, 395–406.

Allen, R.G., Tasumi, M., Trezza, R., 2007b. Satellite-based energy balance for mapping evapotranspiration with internalized calibration (METRIC) – model. ASCE J. Irrig. Drain. Eng. 133, 380–394.

Almhab, A., and Busu,I., 2008. Estimation of Evapotranspiration Using Fused Remote Sensing Image Data and M-Sebal Model for Improving Water Management in Arid Mountainous Area. The 3rd International conference on Water Resources and Arid Environments (2008) and the 1st Arab Water Forum, (pp. 1-24). Malaysia.

Anderson, M.C., Norman, J.M., Diak, G.R., Kustas, W.P., Mecikalski, J.R., 1997. A two-source time-integrated model for estimating surface fluxes using thermal infrared remote sensing. Remote Sens. Environ. 60, 195–216.

Anderson, M.C., Norman, J.M., Mecikalski, J.R., Otkin, J.A., Kustas, W.P., 2007. A climatological study of evapotranspiration and moisture stress across the continental United States based on thermal remote sensing: 1. Model formulation. J. Geophys. Res. 112, doi: 10.1029/2006JD007506.

Awulachew, S., Merrey J., Kamara, A., Van Koopen, B., De Vries, F. and Boelle E., 2005. Experiences and Opportunities for Promoting Small-Scale/Micro Irrigation and Rainwater Harvesting for Food Security in Ethiopia. IWMI Working Paper 98, 2005.

Awulachew, S. B., Yilma, A. D., Loulseged, M., Loiskandl, W., Ayana, M., Alamirew, T., 2007.

Water Resources and Irrigation Development in Ethiopia. Colombo, Sri Lanka: International Water Management Institute. 78p. (Working Paper 123).

Bandara, K.M.P.S., 2006. Assessing irrigation performance by using remote sensing. Doctoral thesis, Wageningen University, Wageningen, The Netherlands.

Bastiaanssen W.G.M., 1995. Regionalization of surface flux densities and moisture indicators in composite terrain, Doctoral thesis, Agricultural University, Wageningen, The Netherlands, pp 273.

Bastiaanssen, W.G.M., Menenti, M., Feddes, R.A., Holtslag, A.A.M., 1998a. The Surface energy balance algorithm for land (SEBAL). Part 1. Formulation. J. Hydrol. 212/213, 198–212.

Bastiaanssen, W.G.M., Menenti, M., Feddes, R.A., Holtslag, A.A.M., 1998. A remote sensing surface energy balance algorithm for land (SEBAL): 1) Formulation. Journal of Hydrology, 212

(213):213-229.

Bastiaanssen, W.G.M., 2000. SEBAL-based sensible and latent heat fluxes in the irrigated Gediz Basin, Turkey. J. Hydrol. 229, 87–100.

Bastiaanssen, W.G.M., Ud-din-Ahmed, M., Chemin, Y., 2002. Satellite surveillance of evaporative depletion across the Indus Basin. Water Resour. Res. 38 (12), 1273–1282.

Bastiaanssen, W.G.M., and Ali, S., 2003. A new crop yield forecasting model based on satellite measurements applied across the Indus Basin, Pakistan. Agriculture, Ecosystems and Environment, 94:321-340.

Bastiaanssen,W.G.M, and Chandrapala,L., 2003. Water balance variability across Sri Lanka for assessing agricultural and environmental water use. Agricultural water management , 171-192.

Bastiaanssen, W.G.M., Noordman, E.J.M., Pelgrum, H., Davids, G., Thoreson, B.P., Allen, R.G., 2005. SEBAL model with remotely sensed data to improve waterresources management under actual field conditions. J. Irrig. Drain. Eng. 131, 85–93.

Becker, F., and Li, Z. -L., 1990. Temperature independent spectral indices in thermal infrared bands. Remote Sensing of Environment, 32, 17– 33.

Brutsaert, W.H. 1982. Evaporation into the atmosphere. D.Riedel Publishing Co., Dordretch, pp 299.

Chow V.T., Maidment, D.R., and Mays, L. W., 1988. Applied Hydrology, McGraw-Hill, USA.

C. Coll, J. M. Galve, J. M. Sánchez, and V. Caselles, "Validation of Landsat-7/ETM+ Thermal-Band Calibration and Atmospheric Correction with Ground-Based Measurements", IEEE Trans. Geosci. Remote Sens., vol. 48, no. 1, pp. 547–555, Jan. 2010.

Comprehensive Assessment of Water Management in Agriculture. 2007. Water for food, water for life: A comprehensive assessment of water management in agriculture. 645 p. London, UK: Earthscan, and Colombo, Sri Lanka: International Water Management Institute.

De Oliveira,A,S., Trezza,R., Holzapfel,E,A, Lorite,I., and Paz,V,S., 2009. Irrigation water management in Latin America.

Dingman, S.L., 1994. Physical hydrology. Prentice-Hall, NewJersy, 557pp.

FAO, 1995. CROPWAT, a computer program for irrigation planning and management. FAO Irrigation and Drainage Paper 46. Rome. 126 p.

FAO, 2006. Crop Evapotranspiration (guidelines for computing crop water requirements): Irrigation and Drainage Paper No. 56

Farah, H.O., 2001. Estimation of regional evaporation under different weather conditions from satellite and meteorological data. PhD Thesis. Department of Water Resources, Wageningen University, 170 pp.

Farah, H.O., and Bastiaanssen, W.G.M., 2001. Impact of spatial variations of land surface parameters on regional evaporation: a case study with remote sensing data. Hydrol. Process. 15 (9), 1585–1607.

Fetter, C.W., 1994. Applied hydrogeology. Third edition, Prentice-Hall, New Jersy, 695PP.

Freeze, R. A. and Cherry J. A., (1979). Ground water. Prentice-Hall, New Jersy, 616pp.

Girma, M.M., and Awulachew,B.S., 2007. Irrigation Practices in Ethiopia:Characteristics of Selected Irrigation Schemes. Working Paper *124* , 1-84.

Gowda, P.H., Chavez, J.L., Colaizzi, P.D., Evett, S.R., Howell, T.A., Tolk, J.A., 2008. ET mapping for agricultural water management: present status and challenges. Irrig. Sci. 26, 223–237.

Gowda, P, H., Senay, G, B., Colazzi, P, D., and Howell, T, A., 2008. Simplified Surface Energy Balance (SSEB) approach for estimating actual ET: an evaluation with lysimeter data.

Gowda, P.H., Senay, G.B., Howell, T.A., Marek, T.H., 2009. Lysimetric evaluation of Simplified Surface Energy Balance approach in the Texas high plains. Appl. Eng. Agric. 25, 665–669.

Hafeez, M. and Khan, S., 2002. Remote sensing application for estimation of irrigation water consumption in Liuyuankou irrigation system in China.

Hamdy, A., Ragab, R., Scarascia-Mugnozza, E., 2003. Coping with water scarcity: water saving and increasing water productivity. Irrigation and Drainage 52(1), 3-20.

Hemakumara, H.M., Chandrapala, L., Moene, F.A. 2003. Evapotranspiration fluxes over mixed vegetation areas measured from large aperture scintillometer. Agricultural Water Management 58:109-122.

Hoffman, G.J., and Evans, R.E., 2007. Introduction.p. 1-32. *In* Hoffman, G.J., *et al.* (eds.) Design and operation of farm irrigation systems. 2nd ed. American Society of Agricultural and Biological Engineers, St. Joseph, Michigan, USA.

Howell, T.A., 2001. Enhancing water use efficiency in irrigated agriculture. Agron. J. 93:281-289.

Jackson, R. D. 1982. Canopy temperature and crop water stress. Volume 1. Advances in Irrigation, 43-85. New York: Academic Press.

Jagadeesha, C. J., 1999. Water Resources Development and Management. Asia's firs on water and the environment: Development issues for the 21st century, Dublin, Ireland.

Jensen, M.E. 2007. Sustainable and productive irrigated agriculture. p. 34-56. *In* Hoffman, G.J., *et al.* (eds.) Design and operation of farm irrigation systems. 2nd ed. American Society of Agricultural and Biological Engineers, St. Joseph, Michigan, USA.

Jin, X. Z., 2008. Evapotranspiration of Hailiutu River Basin in Erdos Plateau Using Remote Sensing Data. waterresources , 1-4.

Kalma, J.D., McVicar, T.R., McCabe, M.F., 2008. Estimating land surface evaporation: a review of methods using remotely sensed surface temperature data. Surv. Geophys. 29, 421–469.

Kustas, W.P., Norman, J.M., 2000.Atwo-source energy balance approach using directional radiometric temperature observations for sparse canopy covered surfaces. Agron. J. 92, 847–854.

Lillesand, T. M., and Kiefer, R. W., 1987. Remote sensing and image interpretation. New York: John Wiley and Son.

Maidment, D. R., 1993. Handbook of Hydrology, McGraw-Hill, USA.

Melaku Getnet, 2009. The impact of snail control on the prevalence and intensity of schistosomiasis mansoni in Finchaa and Wonjishoa sugar estates:Post-pilot control analysis. MSc thesis, Addis Ababa university , 1-74.

Mendoza, M., Bocco, G., Bravo, M., 2002. Spatial prediction in hydrology: status and implication in the estimation of hydrological processes for applied research. Progress in Physical Geography. 26(3), 319-338.

Mohamed, Y.A., Bastiaanssen, W.G.M., Savenije, H.H.G., 2004. Spatial variability of evaporation and moisture storage in the swamps of the upper Nile studied by remote sensing techniques. Journal of Hydrology 289 (2004) 145–164.

Molden, D., 2003. Pathways to improving productivity of water. p. 1-4. In Jinendradasa, S.S. (ed.) Issues of water management in agriculture: compilation of essays. International Water Management Institute, Colombo, Sri Lanka.

Monteith, J. L. (1965), Evaporation and environment. In: B.D. Fogg, (Ed.), The State and Movement of Water in Living Organism, Symposium of the society of experimental biology, 19, Cambridge University Press, Cambridge (1965), 205–234.

Moran, M. S. and Jackson, R. D., 1991. Assessing the spatial distribution of evapotranspiration using remotely sensed inputs. J. Envirnm. Qual. 20 725-737.

Moran, M.S., Rahman, A.F., Washburne, J.C., Goodrich, D.C., Weltz, M.A., Kustas, W.P., 1996. Combining the Penman–Monteith equation with measurements of surface temperature and reflectance to estimate evaporation rates of semiarid grassland. Agric. For. Meteorol. 80, 87–109.

Morse, A., Tasumi, M., Allen, R.G., Kramber, W.J., 2000. Application of the SEBAL Methodology for Estimating Consumptive Use of Water and Streamflow Depletion in the Bear River Basin of Idaho through Remote Sensing, Final Report. Idaho Department of Water Resources and University of Idaho, Idaho, 107 pp.

Mu, Q., Heinsch, F. A., Zhao, M., & Running, S. W. (2007). Development of a global evapotranspiration algorithm based on MODIS and global meteorology data. Remote Sensing of Environment, 111, 519−536.

Mu, Q., L. A. Jones, J. S. Kimball, K. C. McDonald and S. W. Running (2009) Satellite assessment of land surface evapotranspiration for the pan-Arctic domain. Water Resources Research 45, Number W09420 - 2009 (doi: 10.1029/2008WR007189).

Mu, Q., M. Zhao, S.W. Running (2011). Improvements to a MODIS Global Terrestrial Evapotranspiration Algorithm. Remote Sensing of Environment. (in press).

Mutiga,K,J.,Zu,Z.,andWoldai,T.,2008. Using satellite remote sensing to assess evapotranspiration: case study of the upper EWASO NG'IRO north basin Kenya. Remote Sensing and Spatial Information Sciences , 1457-1461.

Najjar, R.G. 1999. The water balance of the Susquehanna River Basin and its response to climate change. Journal of hydrology. 219, 7-19

Neilson, R.P., 1995. A model for predicting continental scale vegetation distribution and water balance. Ecological Application. 5(2), 362-385.

Oster, J.D., and Wichelns, D., 2003. Economic and agronomic strategies to achieve sustainable irrigation. Irrig. Sci. 22:107-120.

Qiu, G. Y., T. Yanob and K. Momiic, 1998. An improved methodology to measure evaporation from bare soil based on comparison of surface temperature with a dry soil surface. Journal of Hydrology 210 (1998) 93–105.

Qiu, G. Y., K. Miyamoto, S. Sase, and L. Okushima. 1999. Detection of crop transpiration and water stress by temperature related approach under field and greenhouse conditions. Tsukuba, Ibraki, Japan: Department of Land Improvement, National Research Institute of Agricultural Engineering.

Roerink, G.J., Su, Z., Menenti, M., 2000. S-SEBI: a simple remote sensing algorithm to estimate the surface energy balance. Phys. Chem. Earth 25, 147–157.

Sabins, F. F., 1997. Remote sensing principles and interpretation. New York: W. H. Freeman and Company.

Sadler, E.J., P.J. Bauer, W.J. Busscher, and A.J. Millen. 2000. Site-specific analysis of a droughted corn crop: Water use and stress. Agron. J. 92: 403-410.

Salomonson, V. V., 1983. Water resource assessment. In: Colwell, J., (eds.). Manual of remote sensing. Bethesda MD: American society of photogrammetery and remote sensing.

Schultz, G. A., and Engman, E. T., 2000. Remote Sensing in Hydrology and Water Management, Springer, Berlin, 1-14.

Seckler, D., 1996. New era of water resources management: From “dry” to “wet” water savings. IIMI Research Report 1 International Irrigation Management Institute. Colombo, Sri Lanka.

Senay, G. B., and J. Verdin. 2003. Characterization of yield reduction in Ethiopia using a GISbased crop water balance model. *Can. J. Remote Sensing* 29(6): 687-692.

Senay, G. B., M. Budde, J. P. Verdin, and A. M. Melesse. 2007. A coupled remote sensing and simplified surface energy balance approach (SSEB) to estimate actual evapotranspiration from irrigated fields. *Sensors* 7: 979-1000.

Senay, G.B, M.E. Budde and J.P. Verdin, 2011a. Enhancing the Simplified Surface Energy Balance (SSEB) Approach for Estimating Landscape ET: Validation with the METRIC model. Agricultural Water Management 98:606-618.

Senay, G.B, S. Bohms, R. Singh, P.H. Gowda, N. M. Velpuri, H. Alemu and J. Verdin, 2013. Operational evapotranspiration mapping using remote sensing and weather datasets: a new parameterization for the SSEB approach. Journal of American Water Resources Research. In Press.

Shaw, E.M., 1988. Hydrology in practice. Second edition, Chapman and Hall, New York, 539pp.

Shaw, E. M., 1994. Hydrology in practice. Chapman and Hall.

Shimelis Behailu, 2004. Stream flow simulation for the upper upper Awash basin. MSc. thesis,Addis Ababa university.

Siebert, S., Hoogeveen, J., and Frenken, K., 2006. Irrigation in Africa, Europe and Latin America. Update of the digital global map of irrigation areas to Version 4. Frankfurt Hydrology Paper 05. 135 p. University of Frankfurt, Institute of Physical Geography, Frankfurt am Main, Germany.

Sobrino, J. A., 1989. Desarrollo de un modelo teo´rico para implementar la medida de la temperatura realizada mediante teledeteccio´n. Aplicacio ´n a un campo de naranjos, PhD dissertation, University of Valencia, Valencia, Spain, 170 pp.

Sobrino, J. A., Caselles, V., & Becker, F., 1990. Significance of the remotely sensed thermal infrared measurements obtained over a citrus orchard. ISPRS Photogrammetric Engineering and Remote Sensing, 44, 343– 354.

Sobrino, J. A., & Raissouni, N., 2000. Toward remote sensing methods for land cover dynamic monitoring. Application to Morocco. International Journal of Remote Sensing, 21, 353– 366.

Sobrino, J. A., Raissouni, N., & Li, Z. -L., 2001. A comparative study of land surface emissivity retrieval from NOAA data. Remote Sensing of Environment, 75, 256– 266.

Su, Z. 2002. The surface energy balance system (SEBS) for estimation of turbulent heat fluxes. Hydrology and Earth system Sciences, 6(1):85-99.

Su, H., M. F. McCabe, E. F. Wood, Z. Su, and J. H. Prueger. 2005. Modeling evapotranspiration during SMACEX: Comparing Two approaches Local- and Regional-Scale prediction. J. Hydrometeor. 6(6): 910-922.

Tasumi, M., and Allen, R.G., 2007. Satellite-based ET mapping to assess variation in ET with timing of crop development. Agric. Water Manage. 88:54-62.

Tegegne Molla, 2009. Estimation of Evapotranspiration for Irrigation Performance Assessment Using Satellite Remote Sensing at Kobo Valley Irrigation Project, Northern Ethiopia.

Thenkabail, P.S., Biradar, C.M., Turral, H., Noojipady, P., Li, Y.J., Vithanage, J., Dheeravath, V., Velpuri, M., Schull M, Cai, X. L., Dutta, R., 2006. An Irrigated Area Map of the World (1999) derived from Remote Sensing. Research Report 105, International Water Management Institute (IWMI), Colombo, Sri Lanka.

Thorntwaite, C. W., J. R. Mather, 1957. Instructions and tables for computing potential evapotranspiration and the water balance. Publ. Climatol. 10(3).

Teshome Dechasa, 1999. Water balance and effect of irrigated agriculture on ground water quality in the Wonji Shoa area/ Ethiopian rift valley. MSc. Thesis,Addis Ababa university , 1-98.

UNCED, 2002. Conservation and management of resources for development. United Nations Conference on Environment and Development. Joahannesburg Summit, 26th Aug-04th Sep, Agenda 21, chap. 14- 18.

Valor, E., & Caselles, V.,1996. Mapping land surface emissivity from NDVI: application to European, African and South American areas. Remote Sensing of Environment, 57, 167–184.

Van de Griend, A. A., & Owe, M., 1993. On the relationship between thermal emissivity and the normalized difference vegetation index for natural surfaces. International Journal of Remote Sensing, 14(6), 1119–1131.

Wonji-Shoa Sugar Factory Working Manual, 2004. Addis Ababa. Unpub. 480 pp.